Title
THE ELECTRON PARAMAGNETIC RESONANCE OP IONS SUBSTITUTED IN PARAMAGNETIC TRANSITION METAL ION HOSTS

Author
St. John, Michael Robert.

Publication Date
1975-11-01

LBL-4185
c.1

THE ELECTRON PARAMAGNETIC RESONANCE OF IONS SUBSTITUTED IN PARAMAGNETIC TRANSITION METAL ION HOSTS

Michael Robert St. John
(Ph.D. thesis)

November 1975

Prepared for the U. S. Energy Research and Development Administration under Contract W-7405-ENG-48

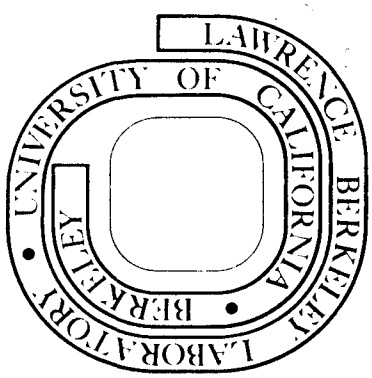

LBL-4185
c.1

DISCLAIMER

THE ELECTRON PARAMAGNETIC RESONANCE OF IONS SUBSTITUTED IN PARAMAGNETIC TRANSITION METAL ION HOSTS

Contents

THE ELECTRON PARAMAGNETIC RESONANCE OF IONS SUBSTITUTED IN PARAMAGNETIC TRANSITION METAL ION HOSTS

Michael Robert St. John

Inorganic Materials Research Division, Lawrence Berkeley Laboratory
and Department of Chemistry; University of California,
Berkeley, California 94720

ABSTRACT

The electron paramagnetic resonance (EPR) spectra of transition metal ions substituted as impurities into paramagnetic transition metal ion host lattices has been studied. Criteria for determining when reasonably sharp spectra are expected are presented. The literature of observed impurity spectra in various hosts is reviewed. A number of unexplained line width effects such as broadening on lowering the temperature, anisotropy, and field dependences have been observed in previous work. It is shown that these effects can be explained in terms of two process, (1) host spin-lattice relaxation narrowing and (2) spin quenching. Host spin-lattice relaxation narrowing produces sharp impurity lines when the host has a fast T_1 and the impurity has a T_1 slow enough not to broaden the lines. As an example, the impurity Mn^{2+} substituted into $(NH_4)_2Co(SO_4)_2 \cdot 6H_2O$ is discussed, and an approximate $T_1(Co^{2+})$ is calculated at 300°K to be 2×10^{-11} sec. Spin quenching produces sharp lines by a reduction of the individual magnetic moments of the host ions. This quenching occurs for non-Kramers ions in low symmetry crystal fields. The case of Mn^{2+} substituted into $K_2Ni(SO_4)_2 \cdot 6H_2O$ and $(NH_4)_2Ni(SO_4)_2 \cdot 6H_2O$ is qualitatively discussed.

Some systems may have their spin degeneracy only partially quenched. However, if a singlet state lies lowest, it may be exclusively populated

by thermal means thereby preventing dipolar fluctuations. Below 2°K the spectra of Cu^{2+}, Co^{2+}, Mn^{2+}, and V^{2+} substituted into the partially quenched α-$NiSO_4 \cdot 6H_2O$ and $NiSeO_4 \cdot 6H_2O$ lattices have been observed. Experiments on Cu^{2+} show that there are positive shifts of 0.2 to 0.8 unit in the g-value when α-$NiSO_4 \cdot 6H_2O$ is compared to the isostructural $ZnSeO_4 \cdot 6H_2O$ lattice. Two equivalent theories for the incorporation of the impurity spin Hamiltonian are presented. One of these theories is an extension of the standard perturbation techniques and the other utilizes a molecular field approach. These theories are applied in detail to the spectra of Cu^{2+} in the α-$NiSO_4 \cdot 6H_2O$ lattice. Both give similar results and indicate a nearest neighbor ferromagnetic Cu^{2+}-Ni^{2+} exchange with $-2J = -0.145 \pm 0.01$ cm^{-1}. The Co^{2+}-Ni^{2+} exchange is apparently slightly ferromagnetic, but the theories cannot give quantitative agreement with experiment. The Mn^{2+}-Ni^{2+} exchange is too small to be measured, and the V^{2+}-Ni^{2+} exchange indicates $-2J = +0.06 \pm 0.01$ cm^{-1}. All these exchange interactions are for hydrated ions and take place through hydrogen bonds. The trend of the exchange interaction between Ni^{2+} and the impurity, as the impurity electron configuration is varied, is discussed.

The impurity spectra in α-$NiSO_4 \cdot 6H_2O$ and $NiSeO_4 \cdot 6H_2O$ are observed to broaden very rapidly as the temperature is raised, becoming unobservable at 4.2°K. A mechanism for this rapid broadening is proposed which assumes that molecular field fluctuations at the impurity are produced by exiton motion of the excited state of the Ni^{2+}. Temperature data for Cu^{2+} substituted into α-$NiSO_4 \cdot 6H_2O$ and $NiSeO_4 \cdot 6H_2O$ are treated.

Appendix I lists impurity ions which have been observed and their host lattices, and Appendix II presents the spin Hamiltonian analysis for Mn^{2+} substituted into the diamagnetic $ZnSeO_4 \cdot 6D_2O$ (or H_2O). The spin Hamiltonian parameters for the deuterated host are $D = +600.0\times10^{-4}$ $cm^{-1}\pm0.4$, $E=+18.6\times10^{-4}\pm0.5$ cm^{-1}, $F=+34\times10^{-4}$ $cm^{-1}\pm2$, $a=-13\times10^{-4}$ $cm^{-1}\pm2$, $B=90\times10^{-4}$ $cm^{-1}\pm2$, $g_{\perp} = 1.997\pm0.003$. The zero-field splitting was observed to be a function of temperature, and small differences between the deuterated and hydrated salts were seen.

Appendix III deals with the Cu^{2+}-Cu^{2+} and Ni^{2+}-Ni^{2+} pair spectra in the $ZnSeO_4 \cdot 6H_2O$ lattice. Only a rough analysis is presented. It is believed that nearest neighbor and next nearest neighbor Cu^{2+}-Cu^{2+} pairs are observed. Data are presented on both pairs, and values of $-2J = +0.15\pm0.01$ cm^{-1} (nearest neighbor) and $|-2J| = 0.035\pm0.01$ cm^{-1} (next nearest neighbor) are found. Only nearest neighbor Ni^{2+}-Ni^{2+} pairs are thought to be observed, and a rough estimate of $-2J = -0.13\pm0.02$ cm^{-1} is made.

I. INTRODUCTION

The presence of chemically stable configurations containing unpaired electrons in transition metal ions provides a sensitive means of probing substances containing them. The electron's unpaired character and non s-orbital participation results in a magnetic moment originating from both spin and orbital angular momentum. This magnetic moment can be easily measured by various means. The technique that looks most closely at the properties of individual ions is electron paramagnetic resonance (EPR). This technique can really be considered as the Zeeman spectroscopy of the ground state.

Quite detailed magnetic and structual information can be obtained by the EPR method. The presence of the orbital angular momentum makes the net magnetic moment of the ions extremely sensitive to their electronic environment. This is because the orbital motion is effected directly, unlike the spin which may only feel the environment through spin-orbit coupling. Thus, EPR is able to distinguish the local symmetry of an ion's environment very precisely, and single crystal work allows the identification of ions with different orientations. Bond parameters between an ion and its ligands are also extractable from EPR data as well as simple properties like the ion's oxidation state. Interaction of the electronic moment with the nuclear moments of the ion and its ligands leads to coupling constants which reflect the nuclear spin values along with other properties already mentioned, i.e., symmetry, bonding, etc.

Abragam and Pryce (1951) formulated the interpretation of the EPR spectra in terms of a spin Hamiltonian where an effective spin is

used which correctly describes the degeneracy of the ground state. Though the spin Hamiltonian provides a convenient device for the interpretation of EPR spectra, it disguises the fact that orbital contributions are involved by incorporating them into experimentally determined parameters. This has often proved very confusing for workers not well acquainted with the field. A considerable amount of work has been done along the lines briefly outlined above, and the conprehensive treatise by Abragam and Bleaney (1970) provides an excellent review of the subject.

The observation of the properties mentioned is contingent on the ability to obtain well resolved spectra. It was discovered early that EPR in concentrated or pure magnetic materials resulted, at best, in broad ill-resolved spectra. For this reason concentrated magnetic materials have not been deemed to be suitable as host materials.

The principal cause of the line broadening in paramagnetic hosts is due to the classical interaction between magnetic dipoles, usually written in the form

$$\mathcal{H}_{\text{dipole}} = \frac{\underset{\sim}{\mu}_i \cdot \underset{\sim}{\mu}_j}{r^3} - 3\,\frac{(\underset{\sim}{\mu}_i \cdot \underset{\sim}{r})(\underset{\sim}{\mu}_j \cdot \underset{\sim}{r})}{r^5} = \underset{\sim}{\mu}_i \cdot \underset{\sim}{H}_{\text{dipole}} \qquad (1\text{-}1)$$

where $\underset{\sim}{r}$ is the vector joining the magnetic moments μ. As the last equality in Eq. (1-1) points out, the dipole interaction can be viewed as the energy of the magnetic dipole, i, in the field generated by the other, j. For typical distances encountered in crystalline solids, the dipole field from nearest neighbors usually amounts to a few hundred gauss. In concentrated materials the dipolar interaction must be summed over the entire lattice due to poor convergence of the

sum. This is because the volume of ions increases at the same rate as the interaction falls off. The net result of the sum of the dipolar fields is to produce a distribution of magnetic field strengths throughout the crystal. Different dipoles will then experience different magnetic fields resulting in different resonance conditions. This situation is known as inhomogeneous broadening and may give line widths as large as 1000 gauss.

A more dramatic effect occurs when the wavefunctions containing the unpaired spin are allowed to overlap. Here, wavefunction is defined as the actual wavefunction found when the bonding of the ion with its ligands is taken into account and not as a pure d or f orbital. When this occurs, the combined effects of the coulomb repulsion between the electrons and the antisymmetry of the wavefunctions required by the Pauli exclusion principle results in a coupling of the spins. This coupling of spins is the well known exchange interaction proposed by Dirac and Heisenberg in 1926. In its simplest form, the coupling is a scalar isotropic type written as

$$\mathcal{H}_{\text{exchange}} = -2J\underset{\sim}{S}_1 \cdot \underset{\sim}{S}_2 \quad . \tag{1-2}$$

This form is often referred to as Heisenberg exchange. A consequence of this coupling of the spins is that the problem can no longer be localized to a single ion plus ligands. It can become a many body problem involving cooperative interactions of the lattice as a whole. The spins may couple in such a way that no net magnetic moment remains resulting in antiferromagnetism. The most spectacular effect occurs when a magnet is formed. This occurs when the spins are coupled so as to be aligned all in the same direction, and this

type of coupling is known as ferromagnetism.

These interactions either destroy the EPR resonance or change the character of the problem to that of elemental excitations in the solid as a whole. Because of these problems, EPR in concentrated materials has not been as fruitful as might have been hoped. The standard procedure has been to eliminate the magnetic interactions by isolating the magnetic ions from one another. This may be accomplished by substituting small amounts of the ions into appropriate diamagnetic hosts, though in some instances this isolation may occur naturally, as for example in many biological systems. Nearly all EPR work to date has been done in magnetically dilute systems, these being the principal topic of the treatise by Abragam and Bleaney (1970).

Nonetheless, the EPR of ions substituted into paramagnetic lattices, if detectable, should contain the same information available in a diamagnetic lattice and in addition should also contain information relayed to it via the magnetic interactions about the interactions themselves and host ion properties. A number of impurity ions substituted into paramagnetic lattices have exhibited sharp spectra (Appendix I), and unusual behavior was often observed in their EPR spectra. It will be the purpose of what follows to elucidate exactly when sharp line spectra are attainable and how to extract the additional information relayed by the interactions from the observed spectra.

The problem divides itself up into two areas, spin dynamics and spin statics. The dynamic problem which is concerned with the impurity's relaxation and line width will be treated first for it is crucial in understanding under what circumstances sharp spectra will be observable.

The static problem then deals with anomalies associated with shifts in the spectral lines or equivalently changes in the spin Hamiltonian parameters caused by the magnetic interactions. The experimental emphasis will be placed on transition metal ion impurities doped into transition metal host lattices with lanthanide hosts being treated in a more casual way. In addition, a broadening mechanism will be proposed for the impurity ions that results from the motion of excitons through the lattice.

II. SPIN DYNAMICS

In recent years there has been a handful of papers reporting the EPR of transition or lanthanide metal ions doped into paramagnetic transition or lanthanide ion host lattices (Appendix I). In these papers several anomalous line width properties have been reported such as an increase of line width on decreasing the temperature, anisotropic line widths, and field dependent line widths. With the exception of one of these papers, Mitsuma (1962), little or no explanation of these effects were given. In the discussion of spin dynamics of impurity ions in paramagnetic hosts which follows, this data will be reviewed in the light of what is really some old ideas which seem to have been forgotten, and hopefully, it will be shown that it all fits very nicely into existing theory. Also, criteria for determining when sharp spectra of paramagnetic impurities in paramagnetic hosts are attainable should emerge from the discussion.

The principal cause of the line width of paramagnetic resonance lines in concentrated materials is the dipolar interaction, and in order for a resonance to be sharp, the effects of the dipolar interaction must be eliminated or at least reduced significantly. The reduction of the effective dipolar interaction can be accomplished either by motional effects or what has been called spin quenching. These two phenomena will be discussed separately in detail. Before specializing to cases of line widths of paramagnetic impurities in paramagnetic hosts, a brief account of motional narrowing theory along standard lines (Abragam, 1961; Anderson, 1954; Anderson and Weiss, 1953; Kubo and Tomita, 1954) will be given. This will allow the introduction

of results contained in the narrowing theory which are necessary in the discussion of effects in the paramagnetic hosts.

A. Motional Narrowing Theory

Motional narrowing is a well documented effect that reduces the effective magnitude of the dipolar interaction by rapid modulation of the interaction. Well known are the cases where the modulating motion is a result of coordinate motion or electron exchange (Bloembergen, Purcell and Pound, 1948; Anderson and Weiss, 1953).

First the Physical nature of the phenomena will be discussed. Only interactions of a magnetic nature, i.e., dipolar, spin-orbit, and hyperfine, are capable of effecting the magnetic moment of the spin directly and, therefore, are responsible for the time dependence of the magnetic moment which determines the line width. However, these interactions are subject to control by non-magnetic interactions which can not effect the magnetic moment directly, and it is this control which produces the narrowing. The control is brought about because the magnetic interactions are dependent on the positions of the electrons and atoms which in turn are controlled by the non-magnetic interactions since these are much larger than the magnetic ones. The magnetic interactions will then vary in time in a way controlled by the electronic or atomic motion resulting in time averaging of the magnetic interactions. When the motion is sufficiently rapid, the averaged effect may be much smaller than otherwise.

Next, the narrowing processes will be looked at from the more mathematical point of view, and the needed results will be derived. In dealing with narrowing problems, it is convenient to divide the Hamiltonian into three parts

$$\mathcal{H} = \mathcal{H}_o + \mathcal{H}_d + \mathcal{H}_m \tag{2-1}$$

The terms are defined as

$\mathcal{H}_o$ = Zeeman energy, single ion spin Hamiltonian

$\mathcal{H}_d$ = the time dependent perturbation, dipole interaction

$\mathcal{H}_m$ = the modulating Hamiltonian, unspecified as yet

Also, for narrowing to occur the following commutation relations must hold among the Hamiltonians

$$[\mathcal{H}_m, M] = 0 \; ; \; [\mathcal{H}_m, M] = 0 \; ; \; [\mathcal{H}_m, \mathcal{H}_d] \neq 0 \tag{2-2}$$

M is the magnetic moment of the resonant spins. In addition, it must be that $\mathcal{H}_d$ has no large matrix elements between the states determined by $\mathcal{H}_o$.

As the starting point for the determination of the line width, the line shape is taken to be given by the Fourier transform of the relaxation function, G(t), defined as (Abragam, 1961)

$$G(t) = \mathrm{Tr}\{M_x(t)\, M_x\} \tag{2-3}$$

The determination of G(t) reduces to the determination of $M_x(t)$ through the Heisenberg equation of motion

$$\frac{i\hbar dM_x(t)}{dt} = [\mathcal{H}, M_x] = [\mathcal{H}_o + \mathcal{H}_d, M_x] \tag{2-4}$$

where the last expression has made use of the special commutation relations. With Eq. (2-4) and the commutation relations, the effects of $\mathcal{H}_m$ are perceived to be that it has no effect on the line positions or line width directly, but since it does not commute with $\mathcal{H}_d$, it can

cause a time dependence of the dipolar term. The solution for $M_x(t)$ is aided by changing to the interaction picture which reduces Eq. (2-4) to the simpler form

$$-i\hbar \frac{dM_x^*}{dt} = \left[\mathcal{H}_d^*, M_x^*\right] \tag{2-5}$$

where the star indicates that the operator is in the interaction picture. In matrix notation with the eigenfunctions of $\mathcal{H}_o$ being used, the equation of motion becomes,

$$-i\hbar \frac{d\left(M_x^*\right)_{nn'}}{dt} = \sum_{n''} (\mathcal{H}_d)_{nn''} \left(M_x^*\right)_{n''n'} e^{i(E_{n''}-E_n)t/\hbar} - \left(M_x^*\right)_{nn''} (\mathcal{H}_d)_{n''n'} e^{-i(E_{n''}-E_n)t/\hbar} \tag{2-6}$$

Now the assumption is made that only terms in Eq. (2-6) where the exponential factor is zero contribute since the others oscillate so rapidly as to give no contribution when integrated over a time of sufficient length. This amounts to keeping only secular terms in the Hamiltonian, $\mathcal{H}_d$. Under this condition the equation of motion reduces to

$$-i\hbar \frac{d\left(M_x^*\right)_{nn'}}{dt} = \left[(\mathcal{H}_d)_{nn} - (\mathcal{H}_d)_{n'n'}\right] \left(M_x^*\right)_{nn'} = \hbar\Delta\omega(t)_{nn'}\left(M_x^*\right)_{nn'} \tag{2-7}$$

with the solution

$$\left(M_x^*\right)_{nn'} = (M_x)^{\circ}_{nn'} \exp\left[i\int_o^t \Delta\omega(t')_{nn'}dt'\right] \tag{2-8}$$

The quantity $\Delta\omega(t')_{nm'}$ is taken to be a random function of time and depends on the values of the diagonal elements of $\mathcal{H}_d$ which change in a random way at a rate governed by the motional Hamiltonian, $\mathcal{H}_m$, through the equation

$$i\hbar \frac{\partial \mathcal{H}_d}{dt} = [\mathcal{H}_m, \mathcal{H}_d] \neq 0 \tag{2-9}$$

The relaxation function now becomes

$$G(t) = \sum_{nn'} e^{i(E_n - E_{n'})t/\hbar} \left| \langle n|M_x|n'\rangle \right|^2 \exp\left[i \int_o^t \Delta\omega(t')_{nn'} dt \right] \tag{2-10}$$

Considering only a single line with $E_n - E_{n'} = \hbar\omega_o$ and observing that the $|\langle n|M_x|n'\rangle|^2$ can be considered as weighting functions for the exponential term, the relaxation function can be case in a form of an average of the exponential function.

$$G(t) = e^{i\omega_o t} \int_{-\infty}^{\infty} dx P(x)\, e^{iX(t)} = e^{i\omega_o t} \langle e^{iX(t)} \rangle \tag{2-11}$$

The following definitions have been used,

$$X(t) = \int_o^t \Delta\omega(t')_{nn'} dt'$$

$$P(x) = \text{probability distribution for } e^{iX(t)}$$

The problem becomes that of finding the distribution law P(x) for x(t) and then to calculate $\langle e^{iX(t)} \rangle$. The model chosen is that (1) the random function $\Delta\omega_{nn'}(t)$ is stationary and Gaussian and (2) the $\Delta\omega_{nn'}(t)$ mean square value $\langle \omega^2 \rangle$ has the same value as in the absence of motion. Thus with the Gaussian form of P(x) the relaxation function becomes

$$G(t) = e^{i\omega_o t}\, e^{-\langle x^2 \rangle/2} \tag{2-12}$$

which leaves only $\langle x^2 \rangle$ to be determined. The normalized correlation function of the local dipolar field fluctuations is given by

$$g_\omega(\tau) = \langle \Delta\omega_{nn'}(t)\ \Delta\omega_{nn'}(t+\tau) \rangle / \langle \omega^2 \rangle \tag{2-13}$$

where $\langle \omega^2 \rangle$ is the mean squared dipolar fluctuation given in terms of the fluctuating dipolar field by $\gamma^2\overline{\Delta H^2}$. With the definition in Eq. (2-13), $\langle x^2 \rangle$ becomes

$$\begin{aligned} \langle x^2 \rangle &= \left\langle \int_o^t dt' \int_o^{t'} dt'' \Delta\omega_{nn'}(t')\ \Delta\omega_{nn'}(t'')\ dt'' \right\rangle \\ &= \langle \omega^2 \rangle \int_o^t (t - \tau)\ g_\omega(\tau)\ d\tau \end{aligned} \tag{2-14}$$

The principal expression for the relaxation function can now be written with Eq. (2-12) and Eq. (2-14) as

$$G(t) = e^{i\omega_o t} \exp\left\{ -\langle \omega^2 \rangle \int_o^t (t - \tau)\ g_\omega(\tau)\ d\tau \right\} \tag{2-15}$$

With Eq. (2-15), the effects of the random modulation of $\Delta\omega_{nn'}(t)$ can be discovered. Two cases are easily handled, those of slow and fast motion.

Case 1. $\Delta\omega_{nn'}(t)$ varies slowly.

If $\Delta\omega_{nn'}(t)$ varies slowly the exponential term in Eq. (2-15) will drop to a very small value before $\Delta\omega_{nn'}(t)$ can change at all which implies that $g_\omega(\tau) = 1$. After intergration of the exponential factor in Eq. (2-15), the relaxation function can be written as

$$G(t) = e^{i\omega_o t} \; e^{-1/2\langle\omega^2\rangle t^2} \tag{2-16}$$

Equation (2-16) is recognized as the rigid lattice relaxation function and gives the first important result that in the absence of rapid motion the line shape is Gaussian with a line width given by

$$\Delta\omega = \sqrt{\langle\omega^2\rangle} \tag{2-17}$$

Case 2. $\Delta\omega_{nn}$,(t) varies rapidly.

In this case, the correlation function $g_\omega(\tau)$ falls rapidly to zero before the exponential has a chance to decay, and the integral in the exponential factor can be extended to infinity with the result

$$G(t) = e^{i\omega_o t} \exp\left\{-\langle\omega^2\rangle \; t \int_o^\infty g_\omega(\tau) \; d\tau\right\} \tag{2-18}$$

The integral over the correlation time is equal to some characteristic time related to how fast the correlation function falls off which is related to the inverse of the frequency of modulation of the dipolar interaction, ω_{nn},

$$\int_o^\infty g_\omega(\tau) \; d\tau = \frac{1}{\omega_m} \tag{2-19}$$

Using Eq. (2-19) the relaxation function under the narrowing condition of fast modulation becomes

$$G(t) = e^{i\omega_o t} \; e^{-\langle\omega^2\rangle t/\omega_m} \; . \tag{2-20}$$

This function describes a Lorentz line shape with the second important result that the line width in the presence of rapid motion is

$$\Delta\omega = \langle\omega^2\rangle/\omega_{nn} \qquad (2\text{-}21)$$

Equations (2-17) and (2-21) support the original assumption that the width is dependent on the size of the dipolar fluctuations since their mean squared value appears in both.

The treatment given here is necessarily simplified and requires at least one comment. When the modulating motion is very rapid, the neglect of non-secular terms in going from Eq. (2-6) to Eq. (2-7) is a poor assumption. The effect of the non-secular terms is to introduce the numerical factor 10/3 into Eq. (2-21) with the dipolar and modulating frequency dependence remaining unchanged (Kubo and Tomita, 1954). This so called 10/3's effect is only important when the modulating frequency is larger than the resonance frequency, i.e., $\omega_m >> \omega_o$. At this point specialization to paramagnetic hosts will take place.

B. Narrowing by Host Spin-Lattice Relaxation

The discussion of Section II-A points out that if an appropriate fast motion of some sort is present in the system the dipolar interaction may be greatly reduced. The question to be addressed now is whether or not any appropriate motional effects are operative for the observance of EPR of impurities in paramagnetic hosts.

The exchange interaction has been much discussed as a motional Hamiltonian with respect to pure and mixed materials (Anderson, 1954; Van Vleck, 1948). The case of exchange between unlike spins, which is of interest here, is much more complicated than for like spins. Unlike the case of like spins, exchange between unlike spins does not result in narrowing but contributes to broadening. This results

because the exchange Hamiltonian between unlike spins will no longer commute with the magnetic moment of the resonant spin thus contributing to its time dependence by Eq. (2-4). However, exchange among the host ions contributes to narrowing of the impurity resonance because it can modulate the impurity-host dipolar interaction and commutes with the magnetic moment of the impurity spin. It is obvious that the exchange effects are complicated, but they suggest that the rigid lattice width would contain a contribution from the impurity-host exchange. It should also be kept in mind that only isotropic exchange can cause narrowing, and thus anisotropy will contribute to broadening.

Another narrowing effect first proposed by Mitsuma (1962), which seems to have been overlooked by nearly all authors, is that fast spin-lattice relaxation of the host can randomly modulate the dipole and exchange interactions between the host and impurity. In other words, if the impurity is embedded in a host lattice which has a fast spin-lattice relaxation time and its own spin-lattice relaxation time is not so great as to broaden itself, the impurity ion will give a sharp spectra. A number of experimental reports, starting initially with the note by Bleaney, Elliot and Scovil (1951), have been given which conform to this criteria, host having a short T_1 and the impurity having a long T_1. Table I lists impurity ions which have been observed and their host lattice where the spin-lattice relaxation narrowing effect is expected to operate. The temperatures at which these spectra were observed were primarily room temperature with an occasional sample being reduced to liquid nitrogen temperature. At these relatively high temperatures, these samples are considered to

Table I. Observed paramagnetic impurities in paramagnetic hosts where hose spin-lattice relaxation narrowing is expected to occur.

Observed Impurity Ion	Host	Reference
	TRANSITION METALS	
Cu^{2+}	$K_2Co(SO_4)_2 \cdot 6H_2O$	Sastry and Sastry, 1973
Mn^{2+}	$(NH_4)_2Co(SO_4)_2 \cdot 6H_2O$	Upreti, 1973
Mn^{2+}	$(NH_4)_2Co_2(SO_4)_3$	Chowdari, 1969
Cr^{3+}	$K_3Fe(CN)_6$	Mitsuma, 1962
	LANTHANIDE METALS	
Gd^{3+}	$Ce(C_2H_5SO_4)_3 \cdot 9H_2O$	Bleaney, Elliot, and Scovil, 1951
Gd^{3+}	Pr^{3+}, Sm^{3+}, Nd^{3+}, Tb^{3+}, Dy^{3+}, Ho^{3+}, & Er^{3+} ethylsulfates	Gerkin and Thorsell, 1972
Gd^{3+}	$Nd(NO_3)_3 \cdot 6H_2O$	Singh and Verkarteswarlu, 1967
Gd^{3+}	$NdCl_3 \cdot 6H_2O$ and $PrCl_3 \cdot 7H_2O$	Singh, Upreti, and Verkarteswarlu, 1967

meet the criteria that the host has fast spin-lattice relaxation and the impurity has slow spin-lattice relaxation. From the table it may be observed that the well known slow relaxing S-state ions like Mn^{2+} and Gd^{3+} are primary candidates as impurity ions where this narrowing phenomena can be observed. In the lanthanide group all other 3+ ions are fast relaxers due to the Orbach mechanism and, therefore, may be used as hosts for Gd^{3+}. In the transition metal group more selectivity needs to be exercised. Here the fast relaxing hosts will be ones where the orbital angular momentum is not quenched, as for example Co^{2+}.

Since the host spin-lattice relaxation narrowing effect is not well known, it will be shown that the requirements stated in Section II-A for narrowing are met. The Hamiltonian given by Eq. (2-1) is broken down this way. $\mathcal{H}_o$ is the unperturbed spin Hamiltonian which gives rise to the positions of the spectral lines. $\mathcal{H}_d$ is again the time dependent perturbation taken to be the dipolar interaction. $\mathcal{H}_m$ is identified with the spin lattice coupling of the host, i.e., primarily host spin-orbit and orbit-lattice coupling. Since $\mathcal{H}_o$ and M contain only the impurity operators and $\mathcal{H}_m$ only host operators, the commutation relations (Eq. (2-2)) which need to be zero are fulfilled. $\mathcal{H}_m$ does not commute with $\mathcal{H}_d$ since it contains both host and impurity spin operators, and by Eq. (2-9), $\mathcal{H}_d$ will obtain a time dependence from $\mathcal{H}_m$. If the commutation relationships hold, it only remains to show that $\mathcal{H}_m$ can be much greater than $\mathcal{H}_d$ and that no large matrix elements of $\mathcal{H}_d$ connect states of $\mathcal{H}_o$. Typically $\mathcal{H}_d$ is around 0.01 cm^{-1} which corresponds to a frequency in the range 10^7-10^8 Hz which implies that the host spin-lattice relaxation should be faster than 10^{-9} sec

(10^9 Hz) for narrowing to occur. This certainly is true at higher temperatures, where the condition $\mathcal{H}_m >> \mathcal{H}_d$ can be fulfilled. Also with conventional spectrometers, the dipolar interaction is always smaller than the Zeeman splittings which meets the second condition. The varification of the conditions needed for narrowing is thus demonstrated for the case of host spin-lattice relaxation motional narrowing.

The host spin-lattice relaxation time should increase when the temperature is lowered and will then not be able to average the dipole interaction as effectively. This increase will result in a broadening of the impurity lines. The increase of line width on lowering the temperature, in contradiction to the usual decrease, is an identifying feature of the host spin-lattice relaxation narrowing effect. In those cases where temperature dependences have been done, such broadening has been observed. This observed temperature dependence is a good case against the narrowing being due to exchange since narrowing by this means is not expected to be temperature dependent. Sastry and Sastry (1973) observed the broadening of Cu^{2+} in $K_2Co(SO_4)_2 \cdot 6H_2O$ on decreasing the temperature and attributed it to "the superposition of a broad cobalt line on the spectrum of Cu^{2+}". Upreti (1973) observed Mn^{2+} lines in $(NH_4)_2Co(SO_4)_2 \cdot 6H_2O$ to increase from 12 gauss to 21 gauss on going from ~373°K to ~90°K, and he attributed this to "increased magnetic interactions". Also Gerkin and Thorsell (1972) observed increases in Gd^{3+} line widths for many of the lanthanide enthylsulfate hosts when the temperature was lowered from room to liquid nitrogen temperatures and indicated

that "these results are not presently understood". Mitsuma (1962) on the other hand did a thorough temperature study of Cr^{3+} in $K_3Fe(CN)_6$ and developed his results along the lines of the host spin-lattice relaxation narrowing theory presented earlier. It is believed that the narrowing theory gives the most plausible interpretation of the experimental data presented in this paragraph.

So far the analysis has led to two conclusions. The first is that impurity resonances will be sharp when the host spin-lattice relaxation time is fast compared to the dipolar energy in frequency units and the impurity spin-lattice relaxation time is long enough that it is not the source of the impurity's line broadening. Secondly, when the conditions for the narrowing are in effect, the impurity line width reflects the spin-lattice relaxation time of the host. Though no entirely rigorous formulation of the line shape in narrowing cases is available, a very satisfactory approximation for the line-width is given by Eq. (2-21) where it will be remembered that $\langle\omega^2\rangle$ is the mean squared width in the absence of narrowing, and ω_m is the average rate of change of the broadening interactions which is now the inverse of the host spin-lattice relaxation time. The use of an impurity probe to measure the extremely fast spin-lattice relaxation times at high temperature seems to be a technique which has not been exploited except for the single attempt by Mitsuma (1962). The main difficulty that arises is the determination of the mean squared width in the absence of narrowing, $\langle\omega^2\rangle$. As pointed out earlier the exchange between unlike ions adds to the broadening, and, therefore, the mean squared width in the absence of narrowing will be composed

of a contribution from the dipolar and exchange interaction, the latter being generally unknown. This fact was not recognized by Mitsuma (1962) who found that the rigid lattice dipolar width was too small for $\langle\omega^2\rangle$. He attributed this increased width without narrowing to anisotropic exchange on the basis of work by Bleaney and Ingram (1952) on the Fe^{3+} line width in $K_3Fe(CN)_6$. However, anisotropic exchange among the Fe^{3+} would only serve to cause exchange narrowing to be less effective, but exchange narrowing effects were assumed absent. Therefore, this can not be the reason for the increase in $\langle\omega^2\rangle$. In the end Mitsuma was forced to make a resonable guess based on his experimental data.

As an illustration of an order of magnitude calculation, the spin-lattice relaxation time of Mn^{2+} in $(NH_4)_2Co(SO_4)_2\cdot 6H_2O$ will be found from the data of Upreti (1973). As an approximation for H_d ($\sqrt{\langle\omega^2\rangle}$ in field units), the formula of Anderson and Weiss (1953) will be used

$$H_d^2 = 5.1\ (g\beta n)^2\ S(S+1) \qquad (2\text{-}22)$$

All terms pertain to the host, and n is the density of spins per cubic centimeter found from crystalographic data (Wyckoff, 1965). This value will be a lower limit since exchange terms have been neglected. Letting g for Co^{2+} be 4, H_d equals 203 guass. Mitsuma's formula for the spin-lattice relaxation time of the host is

$$T_1(\text{host}) = (h/g_{host}\beta)(3/20)\left[\Delta H_{1/2}(\text{impurity})/H_d^2\right] \qquad (2\text{-}23)$$

The non-secular terms are included in this equation by the factor 10/3. At 300°K the Mn^{2+} peak to peak line width in $(NH_4)_2Co(SO_4)_2 \cdot 6H_2O$ is 16 gauss. When this width is used in Eq. (2-23), the spin-lattice relaxation time for the Co^{2+} is $T_1(Co^{2+}) = 2\times10^{-11}$ sec. The actual value would be smaller since a lower limit on H_d was used. Nonetheless, this value is in good agreement with values of Co^{2+} spin-lattice relaxation times extrapolated to room temperature from low temperature solid state data. For example, extrapolating the data of Zverev and Petelina (1962) for the two cobalt sites in Al_2O_3 yield $T_1 = 3\times10^{-11}$ sec and $T_1 = 3\times10^{-12}$ sec. Similarly, the data of Pyrce (1965) for cobalt in MgO yields a value $T_1 = 1\times10^{-11}$ at room temperature. This agreement would indicate that at least up to room temperature no new relaxation effects become operative for octahedral Co^{2+} which are not operative at low temperatures.

C. Spin Quenching

In the case of spin quenching, the dipolar interaction is reduced by an actual decrease in the magnetic moments of the host ions. The line width is a function of the magnetic moment size with or without narrowing through Eqs. (2-17) and (2-21) which contain the mean squared dipolar fluctuation $\langle\omega^2\rangle$. The reduction of the magnetic moment results from the quenching of the spin by the crystal field and spin-orbit coupling. This is analogous to the quenching of orbital angular momentum by the crystal field where the orbital momentum effects are reduced to second order. Two experimental cases arise depending on whether or not the spin is completely or only partially quenched. Complete quenching arises when all the spin

degeneracy is broken by the crystal field and spin-orbit coupling. This situation occurs when the site symmetry of the host ion is very low, i.e., rhombic, and the host ions are non-Kramers ions. The result in these circumstances is that the magnetic moments of the host ions become entirely second order which causes an acute reduction of the mean squared dipolar interaction. At temperatures where kT is greater than the zero-field splittings, susceptibility measurements do not indicate whether or not the spin is quenched. This is because even though the magnetic moments of the ions are reduced, the increased splittings between energy levels has increased the population differences causing the susceptibility to be basically the same. The observation of sharp EPR spectra of an impurity ions in a paramagnetic sample is thus the only indication of spin quenching resulting from low site symmetry at high temperatures.

An example is illuminating and allows the explanation of some hitherto unexplained data. Ni^{2+} is a prime candidate for spin quenching being a commonly occurring non-Kramers ion, and the nickel ions in the compounds $K_2Ni(SO_4)_2 \cdot 6H_2O$ and $(NH_4)Ni(SO_4)_2 \cdot 6H_2O$ (nickel Tutton salts) are known to have rhombic site symmetry (Griffith and Owen, 1952) making them suitable for hosts. Indeed, Upreti (1974) has observed the spectra of Mn^{2+} in these two salts, and it is these spectra which shall be discussed.

The magnetic moment of an individual ion is defined by $\partial E_n/\partial H$ which is the derivative of the energy of state n with respect to the magnetic field. Using the energy levels given by Griffith and Owen (1952) the instantaneous magnetic moment of the Ni^{2+} can be cast in the following form,

$$\mu_{inst} = -\frac{\partial E_n}{\partial H} = \begin{cases} 0 \\ \text{or} \\ \dfrac{\pm g^2\beta^2 H}{[A^2 + G^2\beta^2 H^2]^{1/2}} \end{cases} \qquad (2\text{-}24)$$

The A term encompasses various combinations of zero-field parameters depending on the orientation of the magnetic field. Equation (2-24) specifies the magnetic moments between which the nickel ions fluctuate and which are responsible for the magnitude of the mean squared dipolar fluctuation, $\langle\omega^2\rangle$. When the zero-field term is large compared to the Zeeman energy, $A >> g\beta H$, the magnetic moment and thus the dipolar interaction will be reduced. This reduction may be easily seen by comparison with the case of an unquenched spin. In the unquenched case $\mu_{max}^{unquenched} \cong g\beta$ and in the quenched case $\mu_{max}^{quenched} < g^2\beta^2 H$. Letting $g = 2$ and $H = 3000$ gauss, the values for the moments become $\mu_{max}^{unquenched} \cong 1\times10^{-5}$ cm^{-1}/gauss and $\mu_{max}^{quenched} < 3\times10^{-8}$ cm^{-1}/gauss. This approximate calculation shows that the magnetic moment is reduced by a factor greater than 10^3 which is certainly a sizable reduction.

Next the line width properties of Mn^{2+} in $(NH_4)_2Ni(SO_4)_2\cdot6H_2O$ and $K_2Ni(SO_4)_2\cdot6H_2O$ will be listed and qualitatively explained in terms of the spin quenching ideas. First of all a large anisotropy of the manganese line width is observed for both salts. With H_o along the X axis of one of two ions in the unit cell, sharp spectra are observed while with H_o along the ion Z axis, the manganese lines are almost broadened entirely away. Figure 1 shows this effect. This observation is easily explained by realizing that with H_o along Z, one of the ions in the unit cell has A = E and that E is not much larger than the Zeeman energy, $g\beta H$. Under this circumstance, the magnetic moment increases

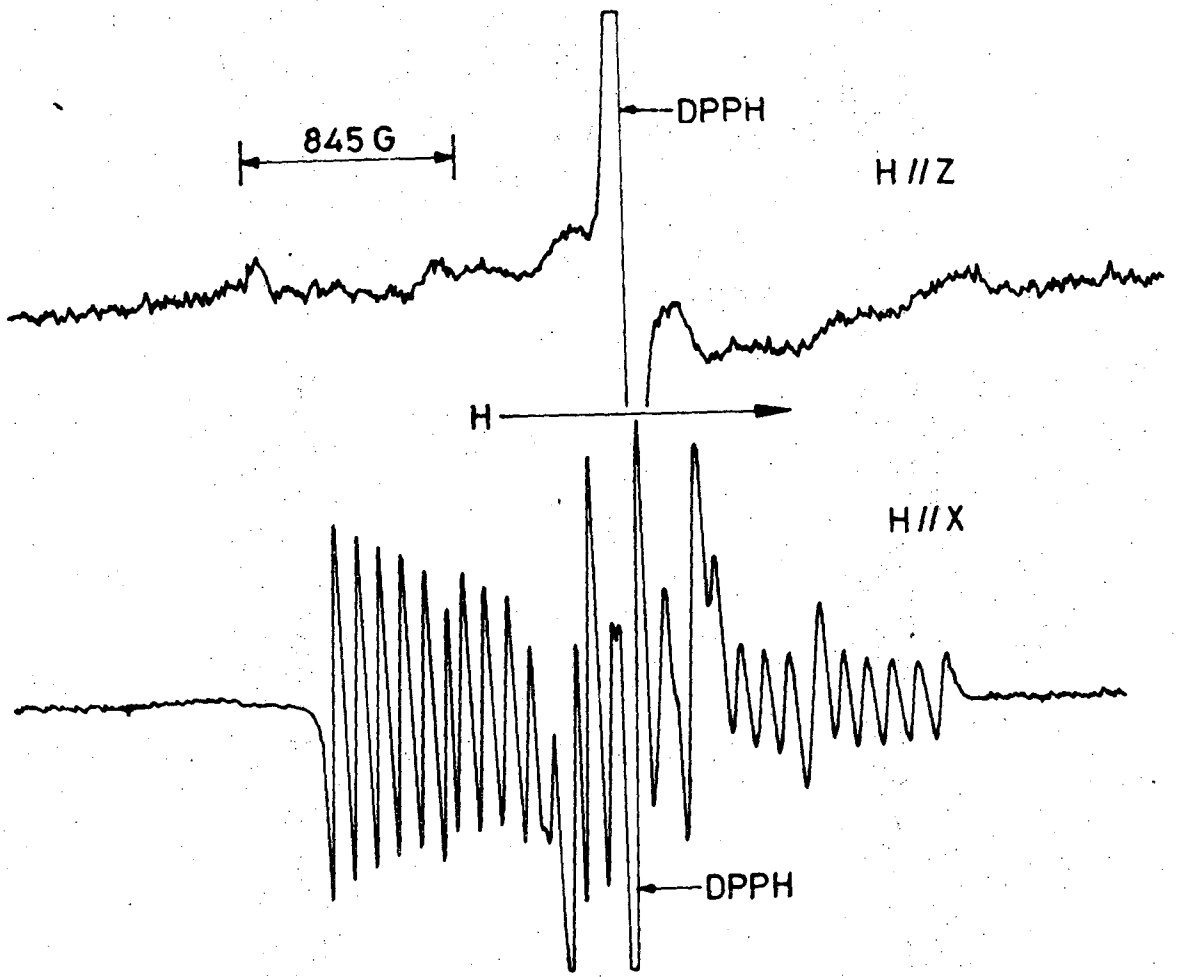

XBL 759-8358

Fig. 1a. The spectra of Mn^{2+} in $(NH_4)_2Ni(SO_4)\cdot 6H_2O$ at room temperature (~300°K) and X-band (~9.5 GHz) for H along the principal Z and X axes of one group for equivalent ions (taken from Upreti, 1974).

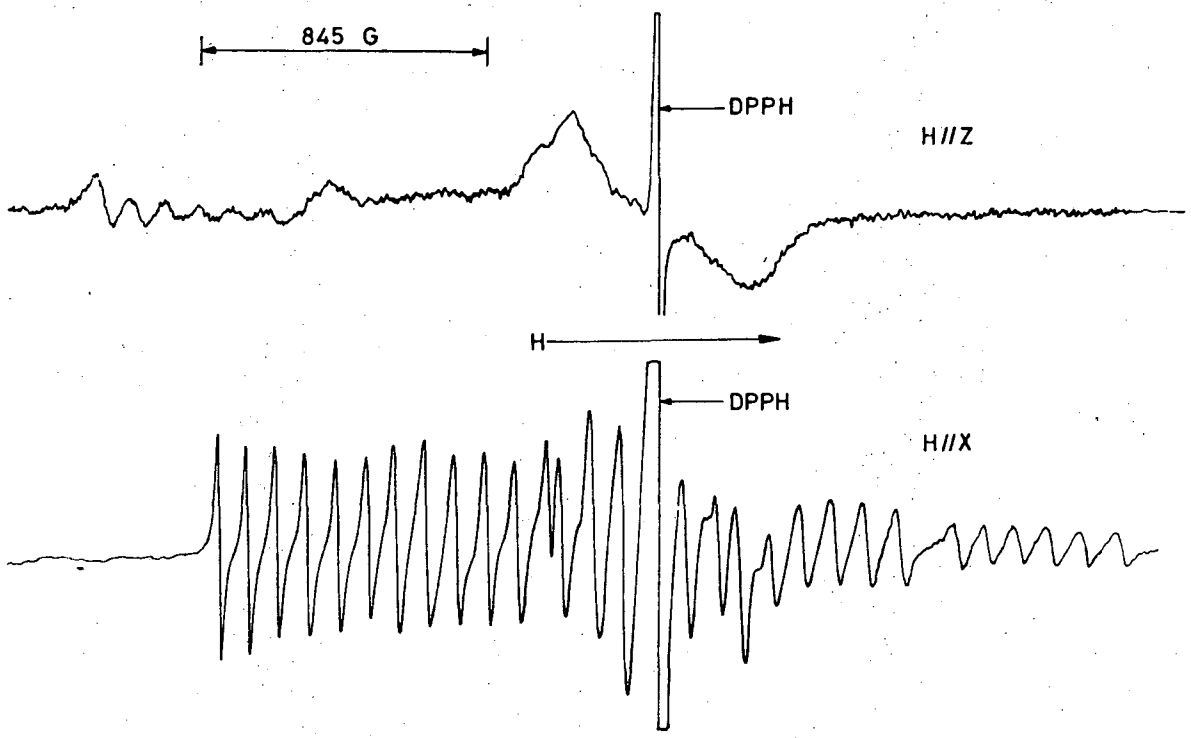

XBL 759-8359

Fig. 1b. The spectra of Mn^{2+} in $K_2Ni(SO_4)_2 \cdot 6H_2O$ at room temperature (~300°K) and X-band (~9.5 GHz) for H along the principal Z and X axes of one group of equivalent ions (taken from Upreti, 1974).

causing the increase in the line width. When H_o is along X, A = (D + E)/2 for one of the ions and the other has H_o nearly in the xy plane which gives an A value on the order of D. Both A's are much larger than the Zeeman energy, and the magnetic moment becomes entirely second order resulting in narrow lines. The line width anisotropy is seen to be a consequence of the magnetic moment functionality of field orientation. Secondly, the line width shows a field dependence. This is expected since the magnetic moment given in Eq. (2-24) is field dependent. Furthermore, coupling Eq. (2-24) with Eqs. (2-17) and (2-21) for the widths indicates a linear field dependence in the absence of narrowing and a quadratic field dependence with narrowing. Lastly, when H_o is along Z, the lines in $K_2Ni(SO_4)_2 \cdot 6H_2O$ are noticeably narrowing than in $(NH_4)_2Ni(SO_4)_2 \cdot 6H_2O$. As noted before, in this orientation A = E for one of the ions and upon consulting Eq. (2-24), the compound with the larger E value should have the narrower lines. Griffith and Owen (1952) give the following values for E at 290°K, E = -0.38 cm^{-1} for $(NH_4)_2Ni(SO_4)_2 \cdot 6H_2O$ and E = -0.51 for $K_2Ni(SO_4)_2 \cdot 6H_2O$ which varifies the prediction. All these line width effects seem to be qualitatively explained by this very simple approach.

Very little temperature dependence of the impurity line widths is expected until temperatures low enough to make kT comparable with the energy separations of the spin levels are reached. This absence of temperature dependence can be explained by observing that the instantaneous magnetic moments will not be changed, but their weights in the average for the mean squared fluctuation will change. However, for temperatures where kT is larger than the energy separations of the

spin levels, the weights will be effectively equal, but when kT is smaller, the average will depend on the statistical weights. Moriya and Obata (1958) have obtained the same results in a more mathematical way using Kubo and Tomita theory and provide a semi-quantitative approach to the problem.

Hosts containing Ni^{2+} probably provide some of the best lattices in which to observe the various line width variations due to the nominal size of D and E commonly encountered. If the zero-field splittings are too large, the magnetic moment will be reduced to the point where it is no longer responsible for the width of the impurity lines. Most observations to date have been made in nickel lattices, and Table II lists nickel salts in which Mn^{2+} has been observed. Similar effects as were found in the two nickel Tutton salts were also seen in the other nickel salts. Other ions should be equally well observable in these lattices provided that they are not broadened away by their own spin-lattice relaxation.

As noted earlier the field dependence of the line width is an indication whether or not a narrowing process is operative. The dependence is linear with no narrowing and quadratic with narrowing implying that if a quadratic dependence is observed, information about the narrowing process will be available. For some of the nickel salts listed, the nickel resonances at room temperature have been observed, and for this reason, their spin-lattice relaxation times would be too slow for the spin-lattice relaxation narrowing mechanism to be operative. Exchange interactions would then have to be responsible for any narrowing in these salts and might possibly

Table II. Nickel compounds in which Mn^{2+} has been observed and their zero-field splittings.*

Compound	D(cm^{-1})	E(cm^{-1})	Reference
$(NH)_4Ni_2(SO_4)_3$	---	---	Chowdari, 1969
$Ni(CH_3COO)_2 \cdot 4H_2O$	-5.61	-0.83	Janakiraman and Upreti, 1971a
$NiSO_4 \cdot 7H_2O$	3.56	1.5	Janakiraman and Upreti, 1971a and 1971b
$K_2Ni(SO_4)_2 \cdot 6H_2O$	-3.30	-0.51	Upreti, 1974
$(NH_4)_2Ni(SO_4)_2 \cdot 6H_2O$	-2.24	-0.38	Upreti, 1974

*All at room temperature.

be estimated from Eq. (2-21). Janakiraman and Upreti, 1971a fit the field dependence of Mn^{2+} in $Ni(CH_3COO)_2 \cdot 4H_2O$ and $NiSO_4 \cdot 7H_2O$ to both linear and quadratic forms and found that neither fit the data very well, implying that some intermediate case exists. Both salts seem to be more compatible with no narrowing. This is not surprising since the isotropic exchange in these salts is not expected to be large. In addition for ions which do not have the same axis of quantization, isotropic exchange will appear as anisotropic which would further reduce the narrowing effect of the exchange in these salts where the spin axes of the host are specified primarily by the zero-field terms. The extraction of exchange data from this data of this type certainly becomes difficult at best, and there seems to little promise in this regard.

The line width also reflects the zero-field splitting of the host, and anisotropy of the line width is a consequence of the changes in the energy level pattern of the host. In theory the zero-field parameters of the host could be determined from the angular dependence of the line width, but experimentally, factors like the extreme line broadening and the presence of more than one ion per unit cell would make their determination unreasonable, other methods being preferable. The conclusion to be drawn from this analysis is that even though many line width effects are observable, little quantitative information is easily extracted from them.

The only other transition metal lattices used where spin quenching is expected to be operative are those containing Fe^{2+}. Table III gives a list of these. The Fe^{2+} lattices have been kept separate

Table III. Iron(II) host lattices and observed impurities.

Impurity	Lattice	Reference
Mn^{2+}	$(NH_4)_2Fe(SO_4)_2 \cdot 6H_2O$	Janakiraman and Upreti, 1970
Cu^{2+}	$(NH_4)_2Fe(SO_4)_2 \cdot 6H_2O$	Gill and Ivey, 1974
Ni^{2+}	$FeSiF_6 \cdot 6H_2O$	Rubins, 1974

because the host spin-lattice relaxation narrowing mechanism will be operative along with spin quenching, Fe^{2+} having a fast T_1, and combination effects are expected. Fe^{2+} tends to have quite large zero-field splittings, and the magnetic moments will be very effectively quenched for this reason. The Fe^{2+} would then be expected to exert little or no influence on the impurity ion line width at any temperature, this is observed for the Mn^{2+} and Ni^{2+} impurities listed. The width of Cu^{2+} in $(NH_4)_2Fe(SO_4)_2 \cdot 6H_2O$ is observed to broaden on lowering the temperature, reaching a maximum at 13°K. This broadening will be commented on in Section IV.

Next the case of partial quenching will be considered. This situation arises when the spin degeneracy is not entirely lifted resulting from an increase of symmetry of the crystal field. Under the condition that a singlet lies lowest, it becomes possible to populate the singlet exclusively by thermal means with the result that the magnetic moment becomes entirely second order as in the completely quenched spin case. More important, however, is the fact that by thermal restriction to a single state fluctuations between the states have been removed, and thus no time dependence of the dipolar field remains. Again, a non-Kramers ion is required for a singlet to exist. Hosts of this sort have primarily centered around lanthanide ions having singlet ground states separated from the first excited states by energies of the order of the spin-orbit coupling, i.e., several hundred wave numbers. With this size energy separation, population of the singlet by thermal means is relatively easy and may only require temperatures in the liquid nitrogen range. Transition

Table IV. Cu^{2+} apparent g and A values in two hosts.*

Axis	α-$NiSO_4 \cdot 6H_2O$		$ZnSeO_4 \cdot 6H_2O$	
	g	A(gauss)	g	A(gauss)
a	2.68±.02	59.7±0.6	2.179±.002	69.9±.3
c	2.50	91.0	2.279	97.2
γ	2.85	74.6	2.260	90.8
z	2.91	93.8	2.429	115.7
x	2.50	10	2.097	15
	ϕ = 61.8°		ϕ = 43.3°	

*a and c refer to the crystal axes and z and x refer to the magnetic axes of the ions, (the z-axis here is defined as the maximum g in the γc plane.)

metal zero-field splittings are much smaller, typically in the range 0.1-20 cm^{-1}, which would, therefore, require liquid He temperatures to exclusively populate a singlet ground state.

Along these lines a number of transition metal ion impurities have been observed in α-$NiSO_4 \cdot 6H_2O$ and the isostructural $NiSeO_4 \cdot 6H_2O$. The spectra in these lattices will be discussed in Section III, and the line broadening in Section IV.

III. SPIN STATICS

Section II has described under what circumstances spectra of impurities are to be observed in paramagnetic hosts. The next natural step in the development of the spectroscopy of impurities in paramagnetic hosts is the description of the spectra when they are observed. In some cases anomalous g and zero-field parameters have been observed, and these are the observations to be explained. The simplest case and the one which has been most exploited is the case where a single state of the host can be exclusively populated. The advantage of this situation is that the statistical problem is greatly simplified since only one state of the host is involved. Also, the population of the excited states tends to reduce the magnitude of the shifts making exclusive population of the host singlet desirable. As mentioned previously, hosts of this type have revolved around lanthanide ions with ground states derived from a J = 0 free ion state with a separation from the first excited state usually on the order of 100 cm^{-1}, i.e., a Van Vleck paramagnet (Mehran, Stevens, Title, and Holtzberg, 1971; Birgeneau, Bucher, Rupp and Bierig, 1964; Rettori, Davidov, Grayevsky, and Walsch, 1975; Sugawara, Huang, and Cooper, 1975).

There are two modes of attack on the problem of incorporating the interaction into the impurity ion description. If the Hamiltonian is known or a reasonable guess can be made, it can be fit to the experimental data. Alternatively differences in the spectra of the impurity in a paramagnetic lattice and in an isostructual idamagnetic lattice can be singled out as arising from the interactions. This assumes that the Hamiltonian can be written as a sum of the single ion

Hamiltonian. The ideal host material would be one where the host-impurity interaction could be turned on and off by the experimenter. By such a means those features of the spectra due to the host-impurity interactions could be unequivocally isolated. An approximation of this situation can be contrived if the paramagnetic host lattice has a isostructural diamagnetic lattice. Differences between the spectra of the impurity in the paramagnetic lattice (interaction on) and the diamagnetic lattice (interaction off) should be due to the host-impurity interaction and be relatable to it. Both of these methods will be employed in the analysis of the data to be presented.

Transition metal ions with large zero-field splittings can also have a singlet ground state which can be exclustively populated, but no impurity spectra in transition metal hosts of this type have been reported. One such host is α-$NiSO_4 \cdot 6H_2O$ whose spin triplet is split in a tetragonal crystal field by spin-orbit coupling into a singlet and a doublet with the singlet lying lowest by 4.74 cm^{-1} (Fisher and Hornung, 1968). $ZnSeO_4 \cdot 6H_2O$ is an isostructural diamagnetic lattice which can be used as the reference lattice (Hajek and Cepelak, 1965). These two lattices provide a convenient system in which to investigate the magnetic interactions of paramagnetic impurities in α-$NiSO_4 \cdot 6H_2O$.

The rest of part III is organized as follows. Section A gives a theoretical discussion of the effects of magnetic interactions on the spectra of impurity ions in the low temperature limit when a single state of the host can be assumed populated. This is followed in Section B with a brief account of the necessary crystalographic data and experimental procedures in Section C. In Sections D through F

a detailed analysis of the g-value shifts of Cu^{2+} in α-$NiSO_4 \cdot 6H_2O$ is given by a spin Hamiltonian perturbation method and by an alternative molecular field method. Lastly, Section G presents data on Co^{2+}, Mn^{2+}, and V^{2+} doped into the α-$NiSO_4 \cdot 6H_2O$ lattice, and Section H discusses the trend in the exchange interaction as the number of d electrons of the impurity is reduced.

A. Theory

The principal theoretical problem in the interpretation of EPR spectra of ions substituted into paramagnetic hosts is the incorporation of the host-impurity interaction into the impurity ion's description. Since the spin Hamiltonian formalism has proved to be a convenient and useful method for describing ions in diamagnetic lattices, it would seem desirable to stay within its framework for ions in paramagnetic lattices. The following discussion presents two methods which describe how to incorporate the effects of the host-impurity interactions into the impurity ion's spin Hamiltonian parameters with emphasis on the g-value shifts. The first approach extends the conventional spin Hamiltonian perturbation theory scheme similar to that used by Hutchings, Windsor, and Wolf (1966), and the second approach utilizes molecular field theory.

1. Perturbation Method

The physical unit under consideration is defined to be the impurity ion plus a cluster of neighbors. The impurity ion is assumed to interact with each neighbor independently in a pair-wise manner. No direct account is taken of possible interaction effects of the neighbors with the other host ions. Since the neighbor-impurity

interactions are considered to be independent, the results for a pair can be developed and then summed over an appropriate number of neighbors. The perturbation Hamiltonian is taken to be

$$\mathcal{H} = \beta \underset{\sim}{H} \cdot (\underset{\sim}{L}_I + 2\underset{\sim}{S}_I) + \lambda_I \underset{\sim}{L}_I \cdot \underset{\sim}{S}_I + \beta \underset{\sim}{H} \cdot (\underset{\sim}{L}_N + \underset{\sim}{S}_N) + \lambda_N \underset{\sim}{L}_N \cdot \underset{\sim}{S}_N + \underset{\sim}{S}_I \cdot \underset{\sim}{K}_N \cdot \underset{\sim}{S}_N \qquad (3\text{-}1)$$

The subscripts I and N refer to the impurity and neighbor, respectively, and the interaction term has been taken as the general bilinear exchange form. The other terms have their usual meanings.

The aim of the spin Hamiltonian scheme is to evaluate parametrically, or in actuality, if possible, all operators except those of the spin under consideration. For the host-impurity pair, all the orbital operators and the host spin operators need to be evaluated in order to leave a Hamiltonian only in the impurity spin operator. Using product wavefunctions of the form $|\psi_I^\circ \psi_N^\circ \sigma_N^\circ\rangle$, where the ψ's refer to orbital functions and σ to the spin function, and considering only the case of orbital non-degenerate ions, the first-order spin Hamiltonian for the impurity ion is

$$\mathcal{H}^{(1)} = 2\beta \underset{\sim}{H} \cdot \underset{\sim}{S}_I + \underset{\sim}{S}_I \cdot \underset{\sim}{K}_N \cdot \langle \sigma_N^\circ | \underset{\sim}{S}_N | \sigma_N^\circ \rangle \quad . \qquad (3\text{-}2)$$

Carrying the development of the spin Hamiltonian to second-order requires the consideration of several types of excited state wavefunctions. The singly excited forms $|\psi_I^n \psi_N^\circ \sigma_N^\circ\rangle$ and $|\psi_I^\circ \psi_N^n \sigma_N^\circ\rangle$ contribute the normal second-order terms to the g-value and the zero-field splittings of the impurity and host ions, respectively, and add nothing new. The singly excited host spin state, $|\psi_I^\circ \psi_N^\circ \sigma_N^n\rangle$, adds a new term which involves the exchange interaction and is given by

$$\mathcal{H}^{(2)} = \sum_n \frac{|\langle \sigma_N^o | 2\beta \underset{\sim}{H} \cdot \underset{\sim}{S}_N + \underset{\sim}{S}_I \underset{\sim}{K}_N \cdot \underset{\sim}{S}_N | \sigma_N^n \rangle|^2}{E_o - E_n} \tag{3-3}$$

This second-order expression contributes two terms to the impurity ion spin Hamiltonian, one arises from the cross term of the exchange and host Zeeman energies and one from the square of the exchange energy. All multiple excited states yield no additional terms. The validity of this perturbation approach is specified by Eq. (3-3), where the condition that the exchange interaction be small compared to the separation of the host ground and excited states is implied.

Retaining only first-order exchange terms and neglecting zero-field terms, the impurity ion spin Hamiltonian becomes

$$\mathcal{H}_I = \beta \underset{\sim}{H} \cdot \underset{\sim}{g}_I \cdot \underset{\sim}{S}_I + \underset{\sim}{S}_I \cdot \sum_N \underset{\sim}{K}_N \cdot \langle \sigma_N^o | \underset{\sim}{S}_N | \sigma_N^o \rangle \quad , \tag{3-4}$$

where the sum is to be taken over an appropriate number of neighbors. To appreciate the effect of the exchange term, knowledge of the host wave-function is required. For pure singlet states, the host spin matrix elements are identically zero. However, the presence of a magnetic field generates Van Vleck paramagnetism which arises from the field mixing excited states into the singlet ground state. For low lying excited states the mixing can be appreciable, thus causing the host spin matrix elements to be significant. Since the mixing is done by the magnetic field, the matrix elements acquire a linear field dependence when the wave functions are taken to first-order in perturbation theory. Thus, for host ions with a singlet ground state, the first order exchange term contributes an additional Zeeman term or equivalently a g-value shift. Host ions that possess

paramagnetism in addition to the Van Vleck paramagnetism will contribute a zero-field term linear in the impurity spin. This case has not been observed yet and may not be since at temperatures where a single state could be populated, magnetic ordering will probably have already ensued.

The second-order terms also contribute linear field terms as well as higher powers in the field, and various zero-field terms are generated. Explicitly they are given by

$$\mathcal{H}^{(2)} = \sum_n \sum_N \left\{ \frac{\beta \langle \sigma_N^\circ | \underset{\sim}{H} \cdot \underset{\sim}{g}_N \cdot \underset{\sim}{S}_N | \sigma_N^n \rangle \langle \sigma_N^n | \underset{\sim}{S}_I \cdot \underset{\sim}{K}_N \cdot \underset{\sim}{S}_N | \sigma_N^\circ \rangle}{E_o - E_n} + \text{C.C.} \right\} \tag{3-5}$$

$$+ \sum_n \sum_N \frac{\langle \sigma_N^\circ | \underset{\sim}{S}_I \cdot \underset{\sim}{K}_N \cdot \underset{\sim}{S}_N | \sigma_N^n \rangle \langle \sigma_N^n | \underset{\sim}{S}_I \cdot \underset{\sim}{K}_N \cdot \underset{\sim}{S}_N | \sigma_N^\circ \rangle}{E_o - E_n}$$

where C.C. means complex conjugate. These higher order terms were not found necessary for the interpretation of the experimental data which follows and will not be considered in greater detail.

To summarize, this type of analysis finds the not too surprising fact that the exchange interaction should modify the observed g-values and zero-field splittings of the impurity ion. The importance of dipolar interaction will be discussed in Section D.

A few practical comments on the use of the equations seems in order. First of all, to evaluate the matrix elements of the host ion, a rather exact knowledge of the host wavefunction is necessary. There are two sources which may yield this information. Magnetic resonance of the pure host of the host in an isostructural diamagnetic lattice should be able to provide the wavefunctions. However, in the type of

lattice where spectra should be most easily observable, those with singlet ground states, the absorptions will be in the far infrared. Coupling this fact with possible line broadening problems in the pure host, yields the result that almost no experimental data of the spectroscopic kind is available. Probably a better source of wave-function data is rigorous magneto-thermodynamic work where the host energy level scheme has been determined (Fisher and Hornung, 1968). Also, the general bilinear form for the exchange interaction, which may be an asymmetric tensor, can introduce as many as nine additional parameters into the Hamiltonian. This can put a severe burden on the experimental data. However, the Hamiltonian was developed for the orbital singlet ground state case where isotropic exchange can be shown to be the dominate term in the exchange interaction (Moriya, 1963). Therefore, under those conditions where Eq. (3-4) would be expected to hold, isotropic exchange will be a very good approximation. On the other hand, ions with appreciable orbital angular momentum, for example Co^{2+}, isotopic exchange as well as Eq. (3-4) become questionable and in all probability cannot give an accurate interpretation of the experimental data.

2. Molecular Field Method

An alternative first-order theory will be presented which combines some ideas of molecular field theory into the impurity ion field Hamiltonian. The starting point will deal more directly with the impurity ion whose Hamiltonian will be assumed to be a sum of the single ion spin Hamiltonian plus pair-wise interactions with its neighbors,

$$\mathcal{H}_I = \beta \underset{\sim}{H} \cdot \underset{\sim}{g}_I \cdot \underset{\sim}{S}_I - 2J \sum_N \underset{\sim}{S}_N \cdot \underset{\sim}{S}_I \quad . \tag{3-6}$$

In Eq. (3-6), zero-field and hyperfine terms have been neglected, and isotropic exchange has already been assumed.

The problem to be addressed is how to replace the host ion spin by some known quantities in order to leave a Hamiltonian containing only the impurity spin operators. Moriya and Obata (1958) pointed out that the host spin can be divided into two parts, a thermal equilibrium or average value and a time dependent deviation, mathematically, $\underset{\sim}{S} = \langle \underset{\sim}{S} \rangle + \delta S(t)$. The time dependent part will cause the broadening of the spectra, and the static part will result in an exchange or molecular field at the impurity ion. Molecular field theory replaces the neighbor spin operators by this average spin. With z equivalent nearest neighbors, Eq. (3-6) becomes

$$\mathcal{H}_I = \beta \underset{\sim}{H} \cdot \underset{\sim}{g}_I \cdot \underset{\sim}{S}_I - 2zJ \langle \underset{\sim}{S}_N \rangle \cdot \underset{\sim}{S}_I \quad . \tag{3-7}$$

The average spin $\langle \underset{\sim}{S}_N \rangle$ is in general still a vector quantity since in an anistropic system spin components will be induced perpendicular as well as parallel to the magnetic field direction. The advantage of this replacement is that the average spin can be related to the macroscopic magnetization $\underset{\sim}{M}$ or the magnetization per atom m by the relation (Smart, 1966)

$$\langle \underset{\sim}{S}_N \rangle = - \frac{\underset{\sim}{M}}{N g_N \beta} = - \frac{\underset{\sim}{m}}{g_N \beta} \quad .$$

Replacement of the average spin by the magnetization implies that all the ions are energetically equivalent. Though this conditions is not

in general fulfilled, there are usually symmetry axes where it is. When the energy level scheme is available, the magnetization per ion may be calculated using the relation (White, 1970),

$$\underset{\sim}{m} = - \left\langle \frac{\delta E_N}{\delta H} \right\rangle \quad .$$

With the above considerations in mind, the exchange interaction becomes,

$$\mathcal{H}_{ex} = - \frac{2zJ}{g_N \beta} \left\langle \frac{\delta E_N}{\delta H} \right\rangle S_{zI} = \frac{2zJm_N}{g_N \beta} S_{zI} \quad ,$$

which is applicable when the impurity spin can be considered quantized along the magnetic field direction. Equation (7) now reduces to

$$\mathcal{H}_I = g_I \beta H_o S_{zI} - \frac{2zJ}{g_N \beta} \left\langle \frac{\delta E_N}{\delta H} \right\rangle S_{zI} \quad , \qquad (3\text{-}8)$$

where for axial symmetry $g_I^2 = g_\parallel^2 \cos^2\theta + g_\perp^2 \sin^2\theta$ in the usual way.

In the true molecular field approach, the two terms of Eq. (3-8) would be combined by incorporating the exchange part into an effective field. In the case under consideration, it is also possible to incorporate the exchange part into an effective g-value by factoring Eq. (3-8) in the following way,

$$\mathcal{H}_I = \left[g_I - \frac{2zJ}{g_N \beta^2} \left\langle \frac{\delta E_N}{\delta H} \right\rangle \frac{1}{H_o} \right] \beta H_o S_{zI} = g_I' \beta H_o S_{zI} \quad . \qquad (3\text{-}9)$$

Here, as in the perturbation method, the exchange interaction results in a g-value shift for host ions with a singlet ground state. In this case, the host ion energy is principally second-order and thus, quadratic in the field. The derivative of the energy with respect to

the field is then nearly linear in field, and the field term in the denominator will be cancelled resulting in a constant g-value shift.

B. Crystal Structure of α-$NiSO_4 \cdot 6H_2O$

X-ray and neutron diffraction studies have determined the complete crystal structure of α-$NiSO_4 \cdot 6H_2O$ (beevers and Lipson, 1932) and α-$NiSO_4 \cdot 6D_2O$ (O'Connor and Dale, 1966), respectively. The crystal is tetragonal with space group $P4_12_12$ or $P4_32_12$ depending on the enantiomorphic form. Analysis shows that the unit cell has dimensions $a = 6.790 \pm 0.003\text{Å}$ and $c = 18.305 \pm 0.004\text{Å}$ and contains four $Ni(H_2O)_6^{2+}$ complexes.

The spatial symmetry of the ligands around the nickels is not measurably different from octahedral. EPR of the α-$NiSO_4 \cdot 6H_2O$ and Ni^{2+} doped into the isomorphous $ZnSeO_4 \cdot 6H_2O$ reveal a substantial tetragonal distortion of the Ni^{2+} site. This distortion has been attributed to increased hydrogen bonding of two of the water molecules which reduces the crystal field in their directions (Jindo and Myers, 1972). The four ions in the unit cell are equivalent except for the orientation of their tetragonal axes. Each of the ion's tetragonal axes is tilted by an angle ϕ from the cyrstal c axis in a plane defined by the c axis and the ab bisector (hereafter called the γ axis). There are two γc planes, and each contains the axes of two ions with the tilt of ϕ being opposite for these ions. Figure 2 shows four unit cells illustrating the orientation of the ions and Fig. 3 shows the projections of the ion axes on the two γc planes.

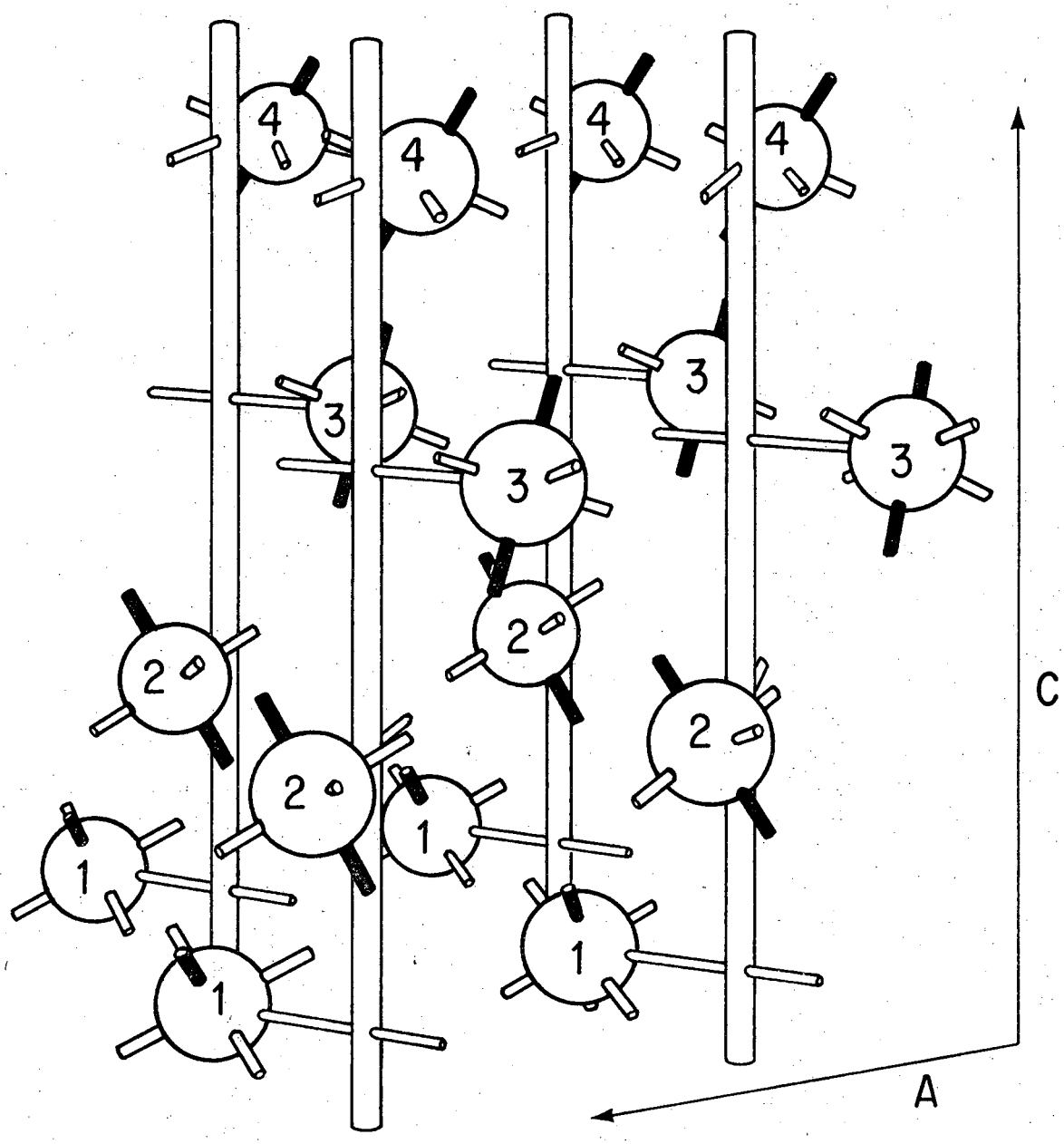

Ni^{2+} for α-$NiSO_4 \cdot 6H_2O$

XBL 758-6926

Fig. 2. The positions and orientations of the nickel ions in α-$NiSO_4 \cdot 6H_2O$ are illustrated. Four unit cells are shown. Each unit cell is shown as composed of four nickel ions attached to the vertical rods. The unique axis of the spin Hamiltonian is darkened.

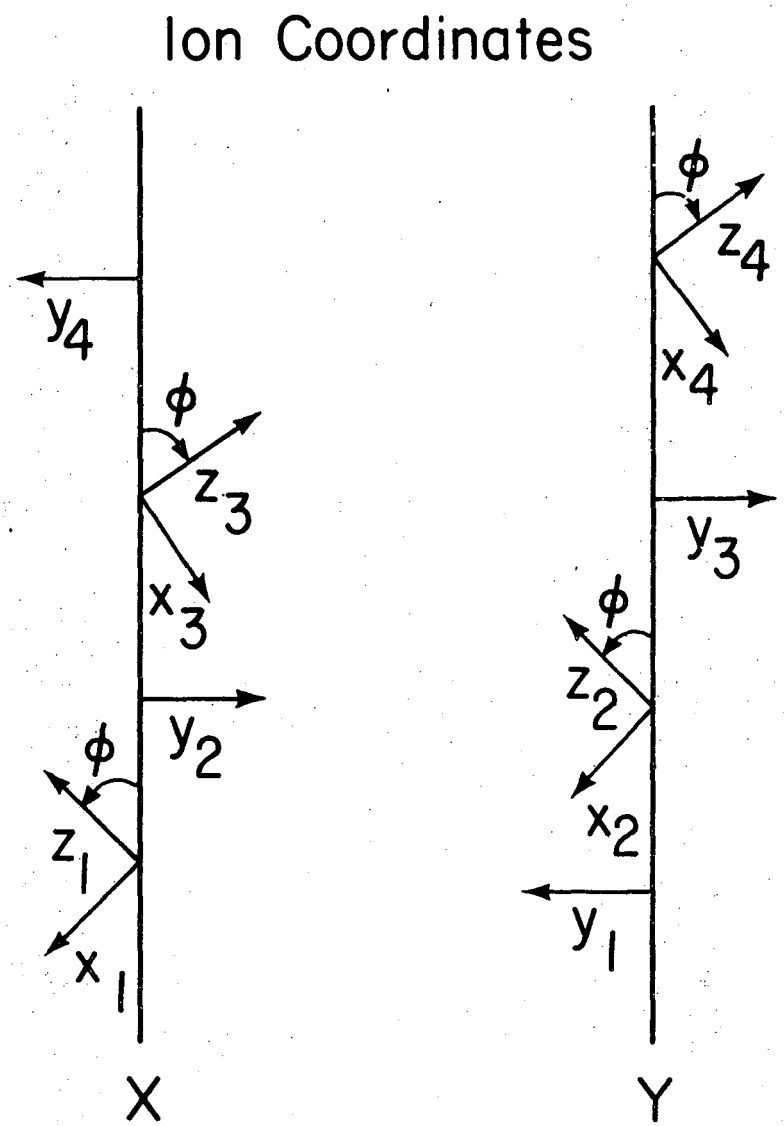

Fig. 3. The projections of the magnetic axes of the ions in the α-$NiSO_4 \cdot 6H_2O$ lattice on the two γc planes are shown. The angle ϕ is the angle between the ion's unique axis and the crystal c axis.

Another important feature to be noted is the neighbor arrangement. Referring to Fig. 2, an ion located in site 2 is surrounded by four nearest neighbors at sites 1 and 3 in a tetrahedral fashion and at a distance of 5.72Å. There are four more next nearest neighbors located in the plane defined by all ions of type 2. These neighbors are related by a lattice translation along a and are, therefore, located 6.79Å away. Further neighbors will not be considered due to their distance. The nearest neighbors ions would appear to have an obvious superexchange pathway through the hydrogen bonding of water molecules in the coordination sphere of the two metal ions. Next nearest neighbors have no such obvious pathway and presumably would have to involve an SO_4^{2-} ion between the waters. For this reason, along with the spectral data to be presented, the nearest neighbor interactions are considered to be dominate.

The diamagnetic reference lattice used was $ZnSeO_4 \cdot 6H_2O$. Klein (1940) found that it was isomorphous with α-$NiSO_4 \cdot 6H_2O$, and EPR spectra of various ions in this lattice by Jindo and Myers (1972) has verified this. The lattice ratio is given by Klein to be $\sqrt{2}a:c = 1:1.8949$ which is to be compared with the α-$NiSO_4 \cdot 6H_2O$ ratio $\sqrt{2}a:c = 1:1.912$ indicating a slight relative expansion in the a direction. X-ray cyrstallographic data on $ZnSeO_4 \cdot 6H_2O$ is given by Hajek and Cepelak (1965).

A more accurate analysis of the data to be presented could have been obtained if a tetragonal form of $ZnSO_4 \cdot 6H_2O$ was available. However, no such structure has been reported, the monoclinic form being the only hexahydrate. The monoclinic $ZnSO_4 \cdot 6H_2O$ is well

established (Gmelins, 1956), but a tetrogonal form reported in Gmelin system No. 32, p. 226 (1924) appears to be in error since it is not included in the newer addition.

C. Experimental Techniques

1. The Spectrometers

The X-band EPR spectrometer used was one that has been built up and modified through the years by previous students in this laboratory (Pratt, 1967; Batchelder, 1970; Jindo, 1971). Detailed description of the spectrometer can be found in their theses, especially that of Pratt, and only a brief account of the apparatus will be presented with emphasis on modifications that were made.

The basic electronics consisted of a Varian V4502 EPR spectrometer with a Varian 9 in. magnet. In order to field modulate samples immersed in the liquid He double dewar used in the low temperature work, modulation coils were wound on the pole pieces of the magnet for the production of low frequency modulation capable of penetration to the sample. The coils were driven either by the Varian V4200B sweep unit or the signal generator of a PAR 124A lock-in amplifier in the range 100 to 800 Hz with amplification by a Dynaco audio amplifier. A variable capacitor arrangement was included to insure that the coils remained resonant. Higher frequencies than 800 Hz were not practical due to the excessive power loss from eddy currents in the pole pieces. Though the microphonic noise spectrum varied from run to run, frequencies around 100 Hz gave, in general, the best signal to noise ratio presumably due to the fact that greater modulation amplitude could be produced because of the larger skin depth and less eddy losses at this frequency.

The mechanical chopper low frequency phase detector unit in the Varian spectrometer is of poor quality, and the PAR 124A lock-in amplifier with the PAR 117 differential preamplifier was used in its place. Another simple modification was the incorporation of a Watkin-Johnston low noise TWT amplifier, tube type WJ-297-5, into the microwave bridge for working at low power levels.

The variable coupler incorporated by Jindo was removed because it introduced considerable microphonic noise. Fixed coupling was, therefore, employed with coupling adjustment being made with a HP 8690A sweep oscillator before the probe was inserted into the dewar system.

A variable frequency circular cavity was made which operated in the TE 011 mode and covered the range of the klystron. It was made of silver plated, solid brass tubing with no precautions taken for mode supression. Extraneous modes were not a problem at most frequencies. The frequency of the cavity was made variable by having a movable bottom and adjusting the amount of teflon packing. The teflon packing played three roles. The first was to make the cavity dimensions smaller in order to allow the cavity to fit in the double dewar. The second was to allow for variability of the frequency, and the third was to provide a solid support for the sample. Teflon has the disadvantage that it shrinks considerably more than the brass tubing on cooling, and even at liquid nitrogen temperatures the teflon packing becomes free to jiggle around. In order to reduce this jiggling, the cavity was fitted with brass spring to squeeze the packing together. Figure 4 shows a cross section of the cavity with a packing arrangement which would give a frequency of approximately

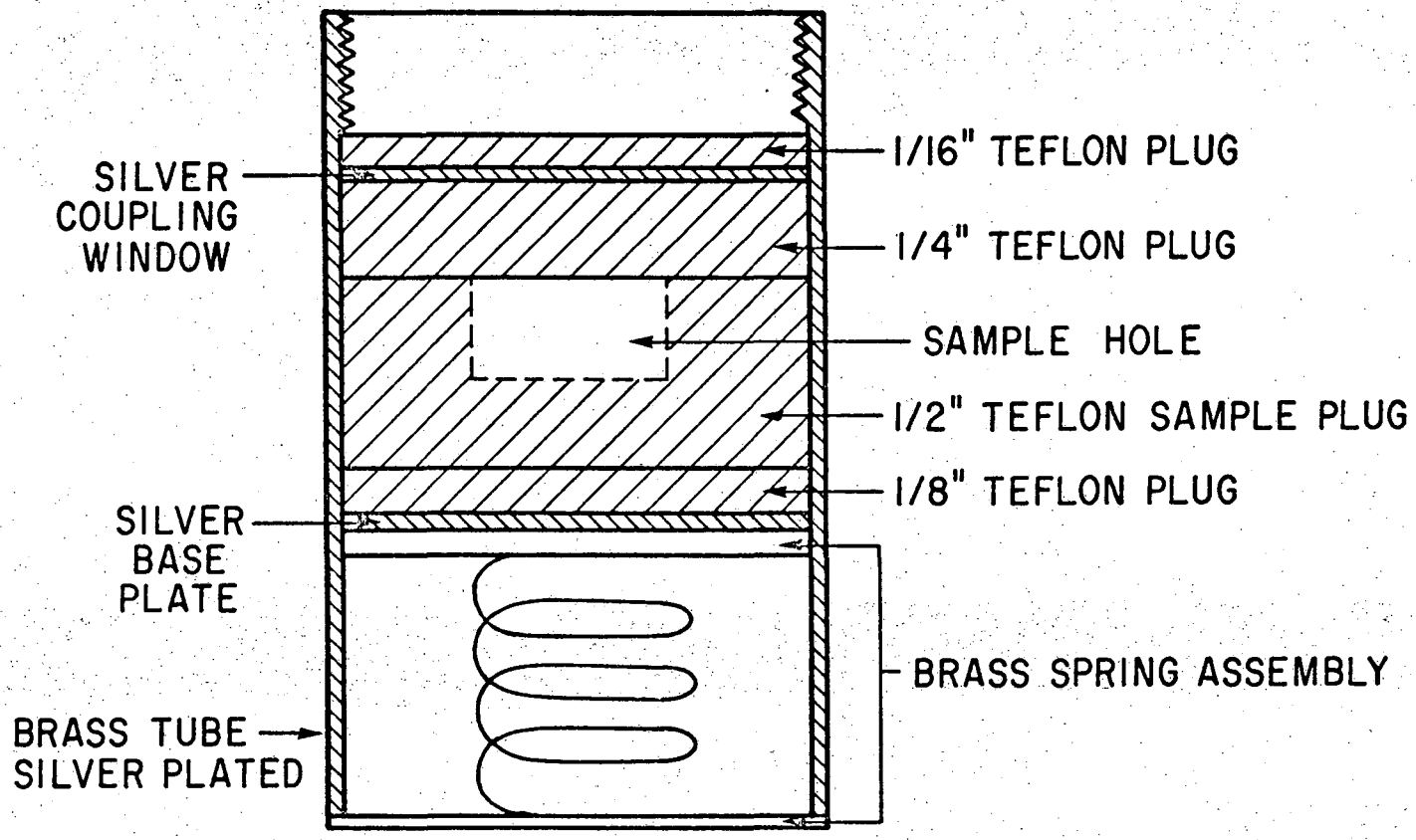

XBL 759-7262

Fig. 4. A cross section of the cylindrical X-band cavity operating in the TE011 mode and packed with teflon to make it resonant at ~9.4 GHz.

9.4 GHz. The bottom plate was held on by masking tape which retains its adhesive properties even down to liquid He temperatures.

Crystal orientation was accomplished by the use of various teflon plugs with appropriate slots cut in them. Figure 5 shows the three main plugs used. The magnet could then be rotated to obtain any orientation in a given plane. Since the sample's orientation was fixed in the cavity, its orientation with respect to the external magnetic field was dependent on the accuracy of the dewar and probe alignment with respect to the magnetic field. Because of this, the misalignment of the crystal was extimated to be 1 to 2 degrees. This misalignment was found to account for the doubling of lines which Jindo (1971) and Jindo and Myers (1972) observed in certain planes of the crystals studied. Carter's rubber cement was used to hold the crystals on the teflon plugs. The adhesive properties were good at temperatures from 300°K to 1.3°K, and only a very small broad signal near g = 2 was produced by it.

The cryogenic equipment consisted of a pyrex double dewar connected to a Welch Duo Seal pump, model 1398, for fast pumping. Temperatures down to 1.3°K could be reached with this arrangement. Temperature was determined by measuring the He vapor pressure at the top of the dewar with an NRC Alphatron vacuum gauge. The pressure could then be converted to temperature using the calibration work of Dijk, Durieux, Clement and Logan (1958).

The K-band spectrometer was designed by Professor Rollie Myers and built principally by Mrs. Joyce Yarnell. No discription of the spectrometer has been presented previously, and so a brief one will

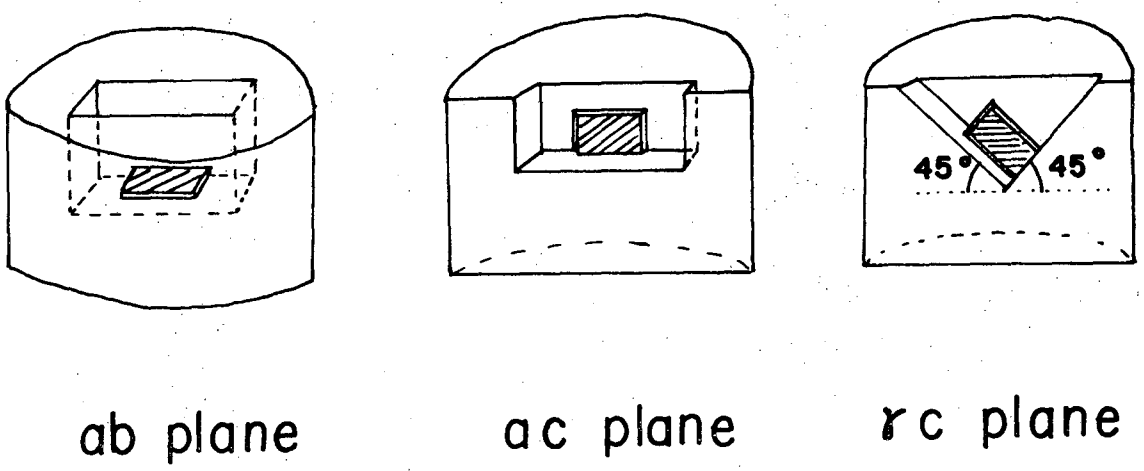

XBL 7012-7294a

Fig. 5. The three teflon crystal mounts and their planes of operation for low temperature X-band (~9 GHz) work. Similar mounts were used at K-band (~24 GHz).

be given here. Figure 6 shows a schematic representation of the spectrometer. The microwave supply was an Oki 24V10 klystron for which a water cooled copper jacket was constructed and which was powered by an FXR Z817A microwave power supply. It provided microwaves from 20-26 GHz. The microwaves were split into two parts. The first part was sent to the cavity and the second to a crystal mixer or wavemeter for frequency measurement. Accurate frequency measurement was obtained by observing the beat of the microwaves with a harmonic produced by a Polarad microwave source, model 128, operating in the frequency range 3.8-8.2 GHz, whose frequency could be accurately measured by an HP electronic counter. A portion of the microwave signal returning from the cavity was extracted by a 10 db directional coupler and was used to lock the klystron on to the cavity. Most often, the lock signal was generated by applying a 6 KHz signal from an HP 200CD oscillator to the FXR reflector circuit which was then phase detected by the Ithaco phase-lock amplifier, model 353. The signal was run into the Varian V4500-10A EPR control unit where the crystal current could be monitered and preamplification took place. For low temperature work, the field modulation and signal phase detection was identical to the X-band spectrometer.

A variable frequency cavity similar to the X-band cavity previously described was constructed for the K-band spectrometer. The cavity was designed to operate in the TE013 mode. Again no precautions for mode supression were taken, and extraneous modes were a problem. Coupling was fixed as with the X-band cavity. At room temperature a cavity made by Mrs. Joyce Yarnell was employed

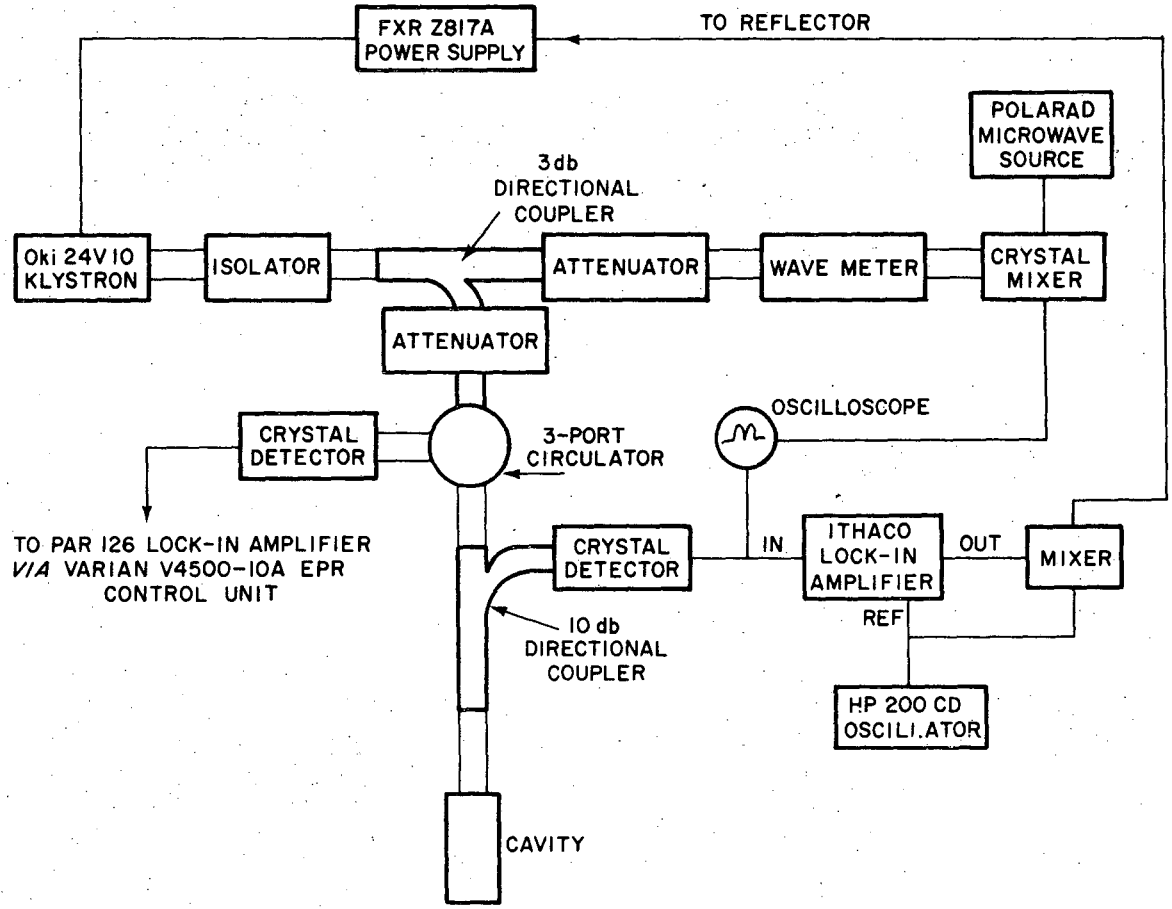

XBL 758-6931

Fig. 6. A schematic representation of the K-band (~24 GHz) spectrometer used.

which operated in the TE012 mode, had a wire wound section for mode supression, and an inductive loop variable coupler.

2. Crystal Preparation

Three host lattices were employed, $ZnSeO_4 \cdot 6H_2O$, $NiSeO_4 \cdot 6H_2O$, and α-$NiSO_4 \cdot 6H_2O$. In all cases, single crystals were grown by evaporation of saturated aqueous solutions. This was usually done by tying a seed crystal to a hair and suspending it in the solution. It was found that crystals grown suspended from hairs had a narrower line width than those grown on the bottom of beakers by approximately a factor of two. Apparently crystal defects are created when bottom-grown which inhomogeneously broadens the lines. Large crystals, e.g., 1.5×0.75×0.75 cm, can be grown of all the hosts in 5 to 21 days. Suitable samples can be obtained by cleaving of pieces from the large crystals along the easy cleavage plane in the ab plane. All the crystals grown with the same habit which has an easily recognizable nearly square ab plane. Figure 7 shows a whole crystal and a typical cleaved section with the axes labled. Having given those features common to all the hosts, each one will now be considered individually.

a. α-$NiSO_4 \cdot 6H_2O$. The tetragonal form α-$NiSO_4 \cdot 6H_2O$ is only obtainable from aqueous solution in the temperature range 30.7°-53.8°C (Gmelin, 1966), the heptahydrate being the stable room temperature form. For this reason, these crystals were grown in beakers immersed in a water bath maintained at 39°C. Normal reagent grade nickel salts were found to contain appreciable amounts of cobalt as well as lesser amounts of copper and manganeses all of which were easily detectable by EPR. "Ultra-pure" $NiSO_4 \cdot 6H_2O$ obtainable from Alfa Inorganics proved to be magnetic impurity free, and all crystals

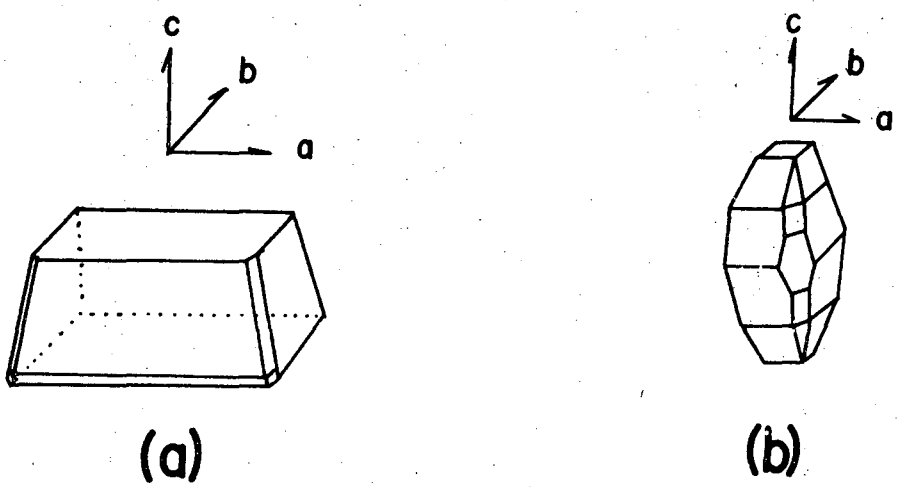

XBL 7012-7294b

Fig. 7. (a) A typical cleaved section of any of the hosts ($ZnSeO_4 \cdot 6H_2O$, $NiSeO_4 \cdot 6H_2O$, α-$NiSO_4 \cdot 6H_2O$) used for experiments with the axes indicated. (b) The morphology of a large crystal showing the crystal axes system.

were crystallized from mother liquors containing ≤1 at.% of the dopant, which consisted of the appropriate metal sulfate. Special procedures were necessary for the preparation of the α-$NiSO_4 \cdot 6H_2O$ crystal doped with V^{2+} due to its air sensitivity. The V^{2+} doping solution was generated from $VOSO_4$ by reacting it with Zn metal in sulfuric acid solution under a nitrogen atmosphere. This procedure obviously introduced Zn^{2+} ions into the crystal but only at a low doping concentration, and no ill effects were noticed from them. The V^{2+} solution was introduced to the crystal growing flask by a hypodermic needle. The crystal growing flask consisted of a three necked flask with nitrogen entering one neck and exiting through another. The center neck was fitted with a rubber stopper to which the hair with the seed crystal could be fastened. The nitrogen flow served both to keep oxygen out and to evaporate the solution.

b. $\underline{ZnSeO_4 \cdot 6H_2O}$. The $ZnSeO_4 \cdot 6H_2O$ host was prepared by addition of excess $ZnCO_3$ to selenic acid, followed by filtration of residual $ZnCO_3$. It was found that a solution of 40% selenic acid became reduced to selenous acid on standing over a period of months and that purchased 40% solutions contained varying amounts of selenous acid. Ampules of 96% selenic acid obtained from BDH Laboratory Chemicals was found to be very pure. The divalent transition metal selenites are quite insoluble and, therefore, do not really cause too great a problem when in small quantities since they are precipitated out and filtered with the excess $ZnCO_3$. Saturated solutions of the dopant selenates were prepared in the same manner as the $ZnSeO_4 \cdot 6H_2O$ from their carbonates. The doped crystals were prepared by addition of ≤1 at.% of the dopant

to the saturated $ZnSeO_4$ solution. Since the solubilities of the selenates of Mn through Ni are nearly the same (Klein, 1940), the crystal concentrations were very nearly the same as the mother liquor. This was substantiated by optical analysis of Ni as the tetracyano complex (Scoggins, 1970) for various crystals grown from various mother liquors. Efforts were expended to make a $ZnSeO_4 \cdot 6H_2O$ crystal doped with V^{2+}. However, the reducing power of V^{2+} is so great that all efforts resulted in reduction of SeO_4^{2-} to Se. At room temperatures crystals of $ZnSeO_4 \cdot 6H_2O$ dehydrate, but if kept in a refrigerator at 5°C, no loss of water occurs.

c. $\underline{NiSeO_4 \cdot 6H_2O}$. Crystals of doped $NiSeO_4 \cdot 6H_2O$ were usually grown prior to growing an α-$NiSO_4 \cdot 6H_2O$ crystal because of the relative ease of growing the selenate over the sulfate, the selenate being growable in the tetragonal form at room temperature. Since no ultra pure $NiSeO_4 \cdot 6H_2O$ was available and all regular reagent grade salts contained magnetic impurities, as previously noted, it was necessary to prepare the $NiSeO_4 \cdot 6H_2O$ from the "ultra pure" $NiSO_4$. This was accomplished by preparing the $NiCO_3$ from the "ultra pure" $NiSO_4$ via a method in Brauer (1963), and then reacting the carbonate with selenic acid.

D. Experimental Results Cu^{2+}: α-$NiSO_4 \cdot 6H_2O$

The general qualitative features of the Cu^{2+} spectra in the paramagnetic host α-$NiSO_4 \cdot 6H_2O$ are similar to the diamagnetic host $ZnSeO_4 \cdot 6H_2O$. The ions exhibit tetragonal symmetry. Four copper spectra are obtained for an arbitrary direction of the magnetic field corresponding to the four ions per unit cell. With the magnetic field

along the a and c axes, all spectra coalesce into a single one. Rotation of the field in the ac or ab planes results in two spectra for all directions (ions 1 and 3 being equivalent and 2 and 4 being equivalent). Rotation of the magnetic field in the γc plane results in three spectra which coalesce into two along the γ axis (ions 1 and 3 being equivalent at all angles). Details of the angular dependences can be found in Jindo and Myers (1972). They found a slight doubling of the spectra for arbitrary orientations of the field and attributed this to a tilt of the x-axis of the copper ions away from the γc plane. It was discovered that this doubling could be attributed in inaccurate crystal alignment on the order of 1°, as mentioned in Section C. For this reason their x-axis tilt is incorrect.

Several deviations from the diamagnetic host lattice spectra are observed. First, the apparent g-values are abnormally large, being 0.2 to 0.6 units higher in the nickel lattice. The value of ϕ is also observed to increase, where ϕ here is defined as the angle between the c axis and the maximum g-value found in the γc plane. Two other changes are a decrease in the hyperfine splittings and an increase in the linewidth. Table IV compares the g-values and hyperfine values for the external field along the principal magnetic and crystallographic axes.

Jindo (1971) attempted to fit the Cu^{2+} spectra to a conventional spin Hamiltonian, but he was unable to obtain a satisfactory fit. Figure 8 shows a comparison of the calculated and observed uncorrected g-values as a function of angle in the ab plane. These observations indicate that the copper-nickel interactions must be playing a

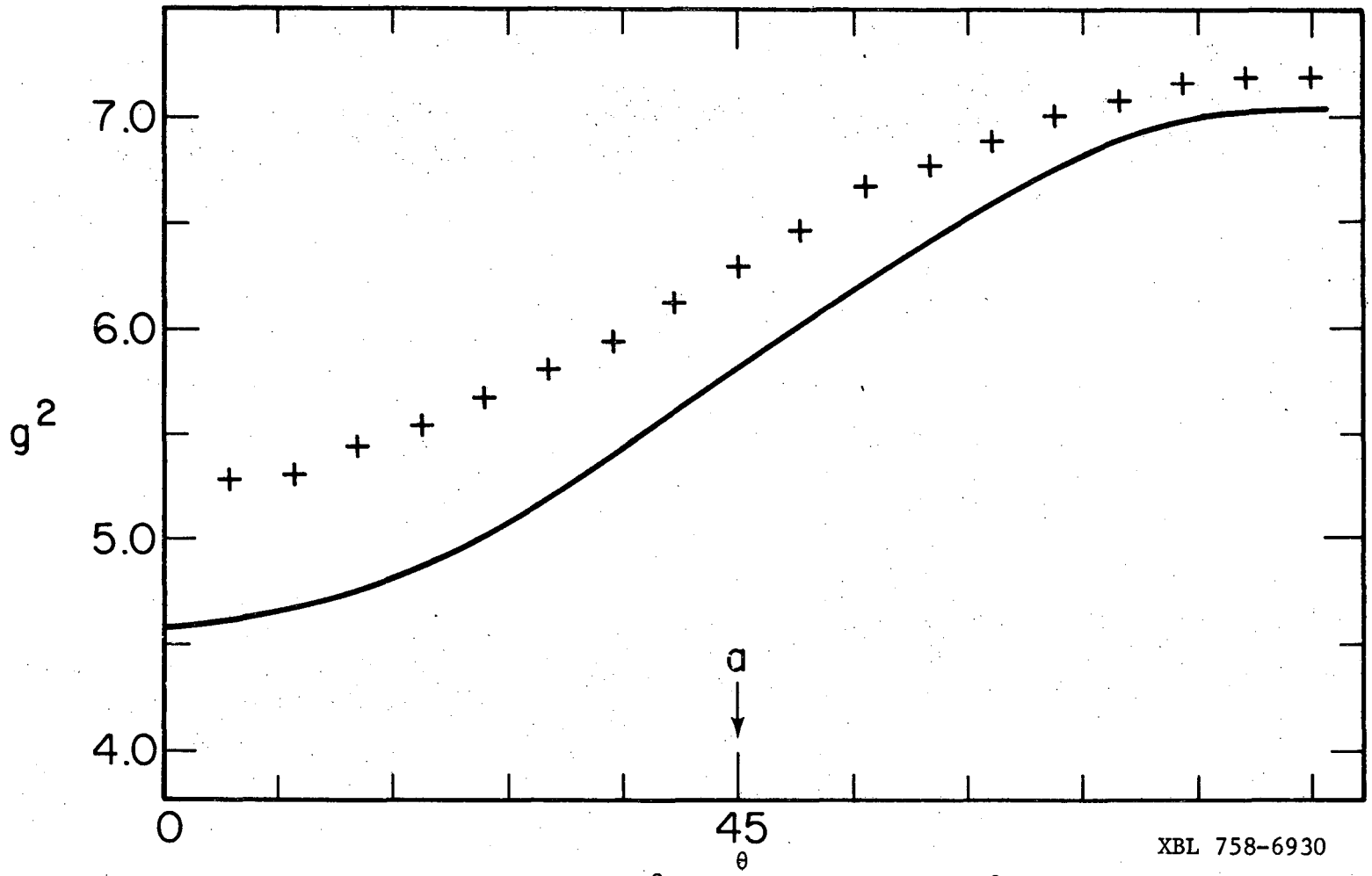

Fig. 8. The experimental angular dependence of g^2 in the ab plane for Cu^{2+} in α-$NiSO_4 \cdot 6H_2O$ is compared with the dependence calculated from the apparent spin Hamiltonian parameters. (+) indicates experimental points, and the line is calculated.

significant role in the spectra of the Cu^{2+}.

Svare and Seidell (1964) have pointed out that at low temperatures when it is possible to populate a single state, a paramagnetic sample will show a shape effect similar to that encountered in ferromagnetic resonance. Nearly all the samples used were of prismatic shape, and since it is not practical to calculate the effect for irregular shapes, an unknown error was introduced into the data. The shape effect for α-$NiSO_4 \cdot 6H_2O$ would be expected to be small because it is proportional to the magnetization which is entirely second-order at the temperatures of the experiments. The smallness was verified by spectra of Co^{2+} substituted into α-$NiSO_4 \cdot 6H_2O$ taken by Batchelder (1970) for samples of varying shapes at 1.3K. Table V gives representative g-values of Co^{2+} in samples of different shapes along two crystal axes. The spherical samples should have no shape effect while the plate should show the largest effect (Kittel, 1971). As can be seen the shape effect is not negligible, but it is believed that an upper limit of 0.02 may be set on the prismatic shapes of α-$NiSO_4 \cdot 6H_2O$. The differences in the uncorrected g-values between paramagnetic and diamagnetic hosts cannot be ascribed to the shape effect alone, but it is considered to be the limiting source of error in the g-value measurements in α-$NiSO_4 \cdot 6H_2O$.

At 1.3K the Cu^{2+} spectra in α-$NiSO_4 \cdot 6H_2O$ were, for the most part, well resolved into the characteristic four-line hyperfine pattern with the derivative peak-to-peak line widths of each hyperfine component about 20 gauss. Natural isotope abundances of Cu^{2+} were used, and the line width is the combined width of the two isotopes.

Table V. Co^{2+}: α-$NiSO_4 \cdot 6H_2O$

Axis	Sample Shape	g(uncorr.)
c	plate	4.282
	sphere	4.301
a	plate	4.744
	sphere	4.688

A typical absorption spectra is given in Fig. 9. The line width in $ZnSeO_4 \cdot 6H_2O$ is close to 10 gauss, and the two isotopes could be resolved in the outer hyperfine lines. The line broadening of the Cu^{2+} will be discussed in detail in Section IV.

E. Application of the Perturbation Method to Cu^{2+}

Equation (3-4) of Section A reduces to

$$\mathcal{H} = g\beta H_o S_{zI} - 2J\underset{\sim}{S}_I \cdot \sum_N \langle \sigma_N^\circ | \underset{\sim}{S}_N | \sigma_N^\circ \rangle \quad , \tag{3-10}$$

with $g_I^2 = g_\parallel^2 \cos^2\theta + g_\perp^2 \sin^2\theta$ when the impurity ion is axial symmetric and isotropic exchange has been assumed. The summation will be restricted to nearest neighbors only and hyperfine terms are neglected. The following assumptions are made about axes of quantization. The copper spins are taken as quantized along the external field, and the nickel spins are taken as quantized along their crystal field axes. The nickel coordinate systems used are those given in Fig. 3. These assumptions allow the simplest coordinates for the calculation of the interaction term.

To evaluate the nickel matrix elements in the exchange term, the scalar spin product is written in the coordinate system of the copper ion, and the nickel spin operators are rotated into their crystal field coordinates where their wavefunctions and matrix elements can be determined. The wavefunctions can then be obtained by diagonalization of the single ion axial Hamiltonian

$$\mathcal{H}(Ni) = DS_z^2 + g_\parallel \beta H_z S_z + g_\perp \beta (H_x S_x + H_y S_y)$$

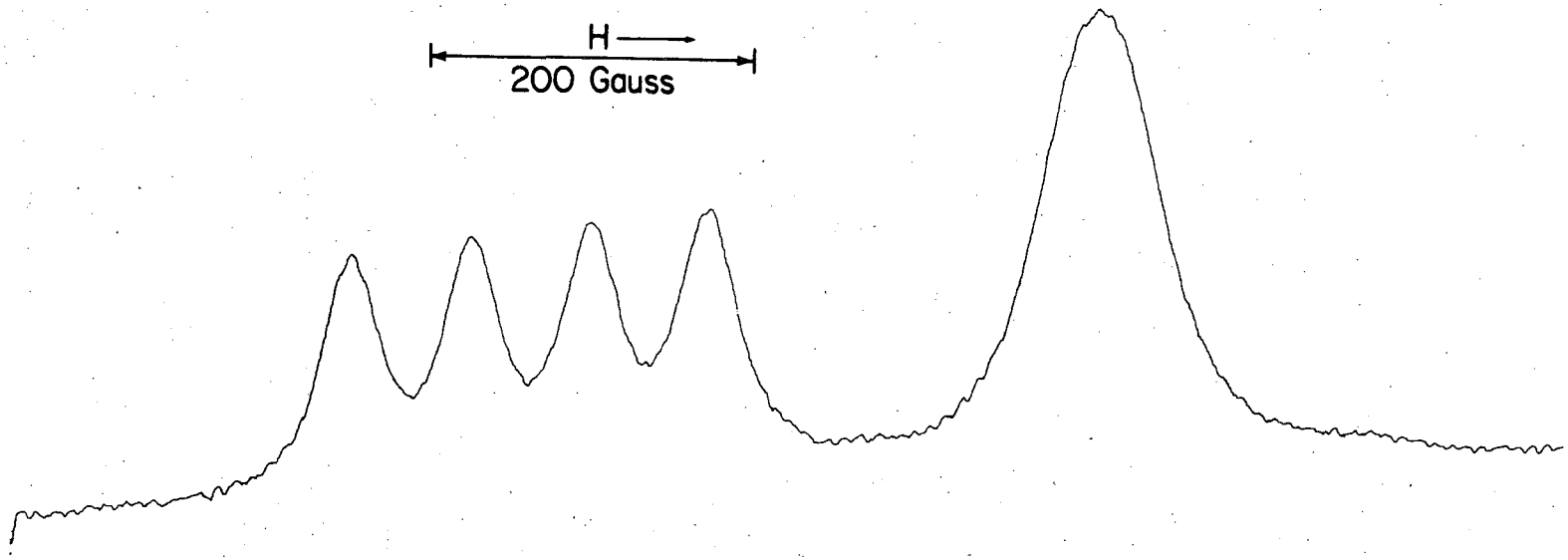

XBL 758-6927

Fig. 9. A typical absorption spectra of Cu^{2+} in α-$NiSO_4 \cdot 6H_2O$ is depicted when the field is along a γ axis showing two sets of Cu^{2+} spectra. Ions 1 and 3 are equivalent as are 2 and 4 in this direction. The hyperfine pattern is absent in the high field absorption due to the small value of $A_\perp$. The tip of the arrow on the right side of the 200 gauss marker is at 2550 gauss. T = 1.3 K and ν = 9.4533 GHz.

which is in general an imaginary matrix. The nickel spin Hamiltonian parameters were obtained from Fisher and Hornung (1968), Jindo (1971), and Myers (1973). The magnitude of the magnetic field at a nickel ion was taken as $H_{total} = H_{ext} + \gamma M$, where H_{ext} is the external field at which a given copper ion resonance took place, γ the molecular field parameter determined by Fisher and Hornung (1968), and M the magnetization. The inclusion of the molecular field improved the calculated results and indicate that nickel-nickel interactions have an effect on the impurity ion which can be taken into account in this way.

With H_{ext} along the a, c, and γ axes of the crystal, only components of the exchange in S_{zI} remain. After the nickel matrix elements are computed, the resulting Hamiltonian is of the form

$$\mathcal{H} = g\beta H_o S_{zI} + CJS_{zI} \quad , \tag{3-11}$$

where C is a combination of matrix elements and angular factors dependent on the field orientation. For arbitrary directions of the field, spin components in S_x and S_y are introduced. That the coefficient C is basically linear in the field H_o to first-order may be seen by inspecting the nickel ground state wavefunction. To first-order it is principally $|0\rangle$ with $|\pm 1\rangle$ states mixed in by the off diagonal Zeeman terms, i.e.,

$$|\sigma_N^\circ\rangle = |0\rangle + \sum_n \frac{\langle 0|g_\perp \beta(H_x S_x + H_y S_y|n\rangle}{E_o - E_n} |n\rangle \quad .$$

The largest matrix elements which contribute to C are those of the form which include a field term in their coefficients resulting in the linear field dependence.

An effective spin Hamiltonian can be written from Eq. (3-11) as

$$\mathcal{H} = [g_{dia} + CJ/\beta H_o]\ \beta H_o S_{zI} = g'\beta H_o S_{zI} \qquad (3\text{-}12)$$

with the effective g-value given explicitly by,

$$g_{obs} = g_{dia} + CJ/\beta H_o = \left[g_{\parallel}^2 \cos^2\theta + g_{\perp}^2 \sin^2\theta\right] + CJ/\beta H_o \ . \qquad (3\text{-}13)$$

Theoretically, the observation of four g-values at different orientations where Eq. (3-13) holds would serve to fix the four unknowns $g_{\parallel}$, $g_{\perp}$, J, and ϕ, and the impurity ion spectra could be solved without recourse to a diamagnetic lattice. Solutions for $g_{\parallel}$, $g_{\perp}$, and ϕ should be expected to correspond closely to the diamagnetic values. For the Cu^{2+} in α-$NiSO_4 \cdot 6H_2O$ four good and simple measurements are available. These are the two g-values along the γ axis and one each from the a and c axes. These four measurements turned out to be linearly dependent. Independent determination of the geometrical factor ϕ was not possible though in other cases it may be, e.g., from the hyperfine tensor. The angle ϕ was, therefore, taken as an adjustable geometrical parameter and varied until $g_{\parallel}$ and $g_{\perp}$ most closely matched the diamagnetic values. The best values are given in Table VI. Good agreement is obtained considering the assumptions employed.

Attacking the problem by relating the differences of the observed g-values in the paramagnetic and diamagnetic hosts yields the following equation for the exchange

$$J = \frac{(g_{obs} - g_{dia})\ \beta H_o}{C} \ . \qquad (3\text{-}14)$$

Table VI. Comparison of corrected g and ϕ values of Cu^{2+} in α-$NiSO_4 \cdot 6H_2O$ with those in diamagnetic $ZnSeO_4 \cdot 6H_2O$.

Lattice (method)	ϕ	$g_{\parallel}$	$g_{\perp}$	$-2J(cm^{-1})$
$ZnSeO_4 \cdot 6H_2O$	43.3°	2.4295	2.0965	---
$NiSO_4 \cdot 6H_2O$ (perturbation)	45°	2.40	2.12	-0.146
$NiSO_4 \cdot 6H_2O$ (molecular field)	45°	2.44	2.05	-0.152

Table VII lists the -2J values calculated for different orientations of the magnetic field providing a further check on the method.

One can see that the differences in the g-values of Cu^{2+} doped into the paramagnetic α-$NiSO_4 \cdot 6H_2O$ lattice from those in the isostructural $ZnSeO_4 \cdot 6H_2O$ lattice can be satisfactorially explained by the preceding theory. It requires an isotropic ferromagnetic exchange interaction between the Cu^{2+} and Ni^{2+} with $-2J = -0.146 \pm 0.007$ cm^{-1}.

F. Application of the Molecular Field Method

From Eq. (3-9) in Section A the g-value in the molecular field approximation is given by

$$g_{obs} = \left[g_{\parallel}^2 \cos^2\theta + g_{\perp}^2 \sin^2\theta\right] - \frac{2zJ}{g(Ni)\beta^2} \left\langle \frac{\delta E(Ni)}{\delta H} \right\rangle \frac{1}{H_o} \qquad (3\text{-}15)$$

where $g_{\parallel}$ and $g_{\perp}$ are the values which would be obtained in the absence of exchange. The value of $\left\langle \frac{\delta E(Ni)}{\delta H} \right\rangle$ was calculated by finding the slope of the energy vs field plot of the ground state at the field present at the nickel ions, which was again taken to be $H_{total} = H_{ext} + \gamma M$. The use of H_{total} reproduces the measured magnetization found by Fisher and Hornung (1968), and along the a and c a es $\left\langle \frac{\delta E(Ni)}{\delta H} \right\rangle \frac{1}{H_o}$ may be replaced by the measured magnetization per atom. Since the ground state's Zeeman energy is principally second order, the derivative is almost linear in the field and over the range of fields used, the g-value correction can be considered constant.

As before only three independent measurements were obtained, and the angle ϕ was again taken as an adjustable parameter. Table VI gives the results which most closely match the diamagnetic g-values when ϕ is varied. The values of -2J calculated from the paramagnetic-

Table VII. Cu^{2+}-Ni^{2+} isotropic exchange values along crystal axes from perturbation method

Axis	$-2J(cm^{-1})$
a	-0.139
c	-0.151
$\gamma(\gamma)$	-0.139
$\gamma(\perp)$	-0.156
Ave.	-0.146±.007

diamagnetic g-value differences along the various crystal axes are tabulated in Table VIII. The value J is calculated from the formula

$$J = \frac{(g_{obs} - g_{dia})\, g(Ni)\, \beta^2 H_o}{-8\langle \delta E(Ni)/\delta H \rangle} \qquad (3\text{-}16)$$

This simple molecular field approach also gives satisfactory agreement and yields a ferromagnetic copper-nickel isotropic exchange interaction of $-2J = -0.144 \pm 0.008$ cm^{-1}.

G. Other Impurity Ions in α-$NiSO_4 \cdot 6H_2O$

1. Co^{2+}

The qualitative features of Co^{2+} in α-$NiSO_4 \cdot 6H_2O$ were also found to be similar to the diamagnetic $ZnSeO_4 \cdot 6H_2O$ lattice. However, the data give unreasonable results when the previous theories are applied. Table IX lists the observed g-value of cobalt in the two lattices along the principal crystal axes.

The most disturbing observation about the data is the change in sign of the difference g(Ni) - g(Zn) which can only be explained with the present theory if the exchange constant J changes sign. Several reasons can be put forward of why the cobalt should not be satisfactorily explained by the theory. As is well known, the large orbital contribution to the g-tensor makes it extremely sensitive to changes in the crystal field. The initial assumption of the theory was that a suitable diamagnetic host was available for comparison, where suitable here means as much like a fictitous diamagnetic α-$NiSO_4 \cdot 6H_2O$ as possible. Ions like Cu^{2+} which do not possess large orbital moment contributions to their g-values are relatively insensitive to crystal field effects, and $ZnSeO_4 \cdot 6H_2O$ provides a suitable comparison lattice. For Co^{2+},

Table VIII. Cu^{2+}-Ni^{2+} isotropic exchange values along crystal axes from molecular field method.

Axis	$-2J\ (cm^{-1})$
a	-0.146
c	-0.138
$\gamma(\gamma)$	-0.157
$\gamma(\perp)$	-0.136
Ave.	-0.144±.008

Table IX. Co^{2+} apparent g-values.

Axis	α-$NiSO_4 \cdot 6H_2O$	$ZnSeO_4 \cdot 6H_2O$
a	4.69	4.453
c	4.30	4.315
$\gamma(\gamma)$	5.94	5.410
$\gamma(\perp)$	3.12	3.27

$ZnSeO_4 \cdot 6H_2O$ may no longer be a suitable lattice, and exchange effects cannot be unraveled from changes in the crystal field. Support for this can be found in the Tutton salts (Landolt-Bornstein, 1966) and isostructural lanthanum magnesium nitrate crystals (Culvahouse and Schinke, 1969). In these crystals changes of similar ions, e.g., K^+, Rb^+, or NH_4^+ in the Zn Tutton salt, causes changes of 0.2-0.3 of a g-value unit which is the same order of magnitude as the observed g shifts in the present experiments. The orbital moment should also complicate the exchange interaction. It would be unlikely for isotropic exchange to closely represent the cobalt-nickel interaction (Baker, 1971). As noted in Section A the theory was derived for the orbital singlet case which is not the case for Co^{2+} in an octahedral field. On the basis that the general trend seems to show g(Ni) larger than g(Zn), one would conclude from the molecular field theory that the cobalt-nickel exchange is probably slightly ferromagnetic.

2. Mn^{2+}

The spectra of Mn^{2+} was observed in $ZnSeO_4 \cdot 6H_2O$, $ZnSeO_4 \cdot 6D_2O$ and $NiSeO_4 \cdot 6H_2O$. A comparison was then made between the g-values found in the paramagnetic $NiSeO_4 \cdot 6H_2O$ and the two diamagnetic hosts. Jindo (1971) showed that the g-value shifts for ions in $NiSeO_4 \cdot 6H_2O$ were similar to those observed in α-$NiSO_4 \cdot 6H_2O$, and since the $NiSeO_4 \cdot 6H_2O$ is easily grown at room temperature, preliminary experiments were always done in it. Divalent manganese gave a very complex spectra in $ZnSeO_4 \cdot 6H_2O$ (or $6D_2O$) and $NiSeO_4 \cdot 6H_2O$. The normal complexity was increased in these lattices by the four ions per unit cell and by "forbidden" transitions which gained appreciable intensity due to the

break-down of selection rules by a large zero-field splitting. When the external field was perpendicular to the crystal field axes of two of the ions along the γ axis, the full set of five sextets from these ions could be distinguished and $g_\perp$ measured for the Ms = 1/2 to -1/2 transition. With H_o parallel the z crystal field axis, the spectra had the maximum spread, and all but the Ms = 1/2 to -1/2 sextet could be completely resolved. From the sextet splittings the zero-field splitting was determined. Table X gives $g_\perp$ and D in two lattices.

The largeness of the zero-field splitting made it necessary to use K-band frequencies in order to increase the validity of the second-order Hamiltonian (Abragam and Cleaney, 1970). The point to focus on here is that the overall exchange interaction is very close to zero since the g-values are very nearly identical in the two lattices. For this reason a more detailed analysis of the Mn^{2+} was not conducted. There are exchange contributions to the zero-field splitting, but the difference observed in Table X may be due to crystal field effects or temperature effects. Details of the experimental procedures for the Mn^{2+} spectroscopy may be found in Appendix II.

Table X. Mn^{2+} apparent $g_\perp$ and D values in two hosts.

Parameter	$NiSeO_4 \cdot 6H_2O$*	$ZnSeO_4 \cdot 6H_2O$**
$g_\perp$	2.02 0.02	1.997 0.003
D (gauss)	+624 10	+637 10

*At 1.3°K.
**At 77°K.

3. V^{2+}

The ion V^{2+} is good choice for study, since it has very little orbital angular momentum and represents a case where only t_{2g} electrons are involved in the exchange. However, it is a fairly strong reducing agent, and attempts to prepare $ZnSeO_4 \cdot 6H_2O$ crystals doped with V^{2+} resulted in reduction of the SeO_4^{2-} to Se. The SO_4^{2-} ion is less susceptible to reduction, and single crystals of α-$NiSO_4 \cdot 6H_2O$ doped with V^{2+} could be prepared. Even though a diamagnetic reference lattice was not available, large deviations of the g-value should be disernible since the small orbital contribution to the V^{2+} g-values makes them very close to 2.0. A sampling of V^{2+} g-values shows that they lie between 1.96 and 2.00 for known octahedral complexes (McGarvey, 1966).

Following the previous work, an axial spin Hamiltonian was assumed and is given by the standard form (Abragam and Bleaney, 1970)

$$\mathcal{H} = \beta \underset{\sim}{H} \cdot \underset{\sim}{g} \cdot \underset{\sim}{S} + D\left[S_z^2 - 1/3\ S(S+1)\right] \quad . \tag{3-17}$$

Then with S = 3/2, the spectra consisted of the expected three octets per ion. The octet arises from the vanadium nuclear spin of 7/2. With H_o along the γ axis, which is perpendicular to the crystal field axes of two of the ions in the unit cell, a set of three octets were easily resolved, and $g_\perp$ was determined from the center octet. Taking perturbation theory to second order, results in the following three field positions when the magnetic field is perpendicular to the crystal field axis,

$$H1 = H_o + D \tag{3-18a}$$

$$H2 = H_o - 9D^2/8H_o \tag{3-18b}$$

$$H3 = H_o - D \tag{3-18c}$$

where

$$H_o = h\nu/g_\perp \beta \quad .$$

The value of $g_\perp$ is defined as

$$g_\perp = \frac{h\nu}{\beta H2} - \frac{9D^2}{8h\nu\beta H2} \quad . \tag{3-19}$$

The splitting between the center of the high field octet and the low field octet is 2D, and, therefore,

$$|D| = \frac{|H1 - H3|}{2} \tag{3-20}$$

The first-order $g_\perp$ was found to be 1.836 neglecting the second-order shift which would make it even smaller, and with g = 2.0 the zero-field splitting was found to be 0.133 cm^{-1}. Thus, the observed $g_\perp$ value is considerably outside the range previously observed for V^{2+}. Since the observed $g_\perp$ for V^{2+} is smaller than expected for diamagnetic lattices, the implication from Eq. (3-14) or Eq. (3-16) is that the vanadium-nickel exchange interaction is antiferromagnetic. Estimating g_{dia} as 2.00 one obtains $-2J = +0.06$ cm^{-1} using the molecular field method.

H. Discussion

Table XI summarizes the different types of interacting pairs and the exchange interaction that were obtained. It is believed that the most advantageous superexchange pathway is through a hydrogen bond linking the waters of an ion with its nearest neighbor. Figure 10 illustrates this hydrogen bonding arrangement between the nearest neighbors. All other hydrogen bonded pathways have at least a sulfate oxygen as an intermediate between two water molecules. Two types of nearest neighbors are possible. The first involves the bonding of an equatorial water of the impurity and an axial water of the nickel. Choosing complex 3 on Fig. 10 as the impurity, the first pathway would be from complex 3 to complex 1. The other pathway involves bonding of an axial water of the impurity with an equatorial water of a nickel. Again, with complex 3 as the impurity, this situation uses complexes 3 and 2. For Cu^{2+} whose equatorial ($d_{x^2-y^2}$) and axial (d_{z^2}) orbitals are half-filled and filled, respectively, the exchange between the two types of neighbors may differ significantly, and the value of the exchange interaction calculated in the previous sections is really an average of these two exchange interactions. For ions with half-filled configurations (t_{2g}^3-V^{2+}, $t_{2g}^3 e_g^2$-Mn^{2+}, e_g^2-Ni^{2+}), both types of neighbors should have more nearly identical exchange.

Regardless of this problem, the obvious trend observed in Table XI is the gradual change in sign of the exchange interaction with impurity configuration on going across the periodic table from copper to vanadium. The implication is that e_g - e_g orbital interactions are ferromagnetic and t_{2g} - e_g interactions are antiferromagnetic.

Table XI. Summary of observed exchange interactions.

Pair	Configuration	Interaction	$-2J$ (cm^{-1})
Cu^{2+}-Ni^{2+}	e_g-$(e_g)^2$	Ferromagnetic	-0.144
Co^{2+}-Ni^{2+}	t_{2_g} $(e_g)^2$-$(e_g)^2$	Slightly Ferromagnetic	----
Mn^{2+}-Ni^{2+}	$(t_{2_g})^3(e_g)^2$-$(e_g)^2$	----	~0
V^{2+}-Ni^{2+}	$(t_{2_g})^3$-$(e_g)^2$	Antiferromagnetic	+0.06

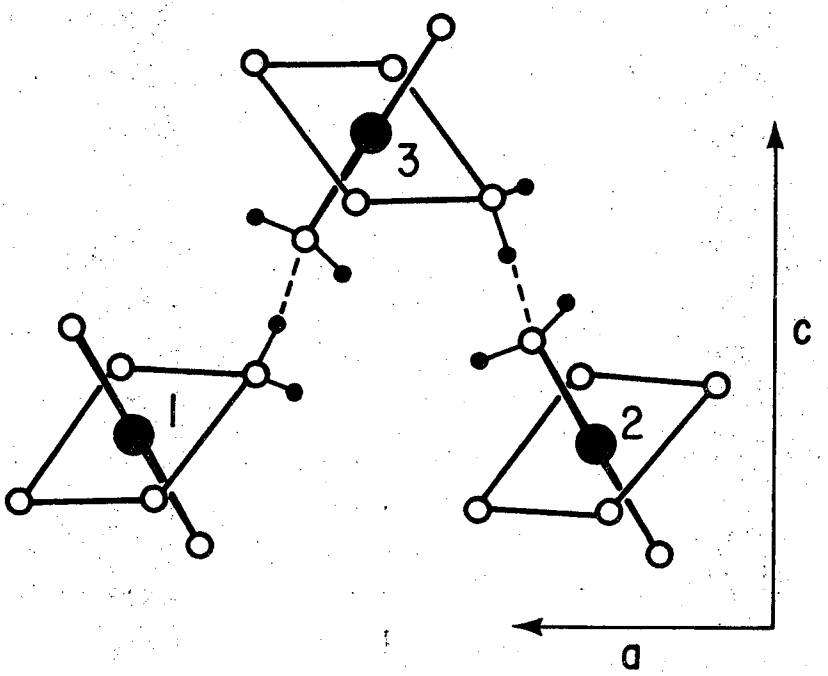

XBL 759-7208

Fig. 10. Three $Ni(H_2O)_6^{2+}$ complexes are illustrated showing the proposed nearest neighbor superexchange pathway via the hydrogen bonding between complexes. The figure is adapted from O'Conner and Dale (1966).

This observed trend conforms to the Kanamori-Goodenough rules (Goodenough, 1963; Kanamori, 1959) for ions coupled via a 90° interaction. However, the very complex geometry of the proposed hydrogen bonded superexchange pathway precludes any correlation along these lines.

It is interesting to note that in other hydrogen bond systems similar results have been obtained. Pair spectra in the hydrogen bonded double nitrate systems also indicated that $e_g - e_g$ interactions were ferromagnetic and $t_{2_g} - e_g$ interactions were antiferromagnetic (Culvahouse and Schinke, 1969; Dixon and Culvahouse, 1971). Two other reports in hydrated systems yield results conforming to the observed trend, Cu^{2+} pairs in $K_2Zn(SO_4)_2 \cdot 6H_2O$ were ferromagnetic ($e_g - e_g$) (Meredith and Gill, 1967) and Ni^{2+} pairs in $ZnSiF_6 \cdot 6H_2O$ were ferromagnetic ($e_g - e_g$) (Altshuler and Valishev, 1965). In these hydrogen bonded lattices the magnitude of 2J runs from 0.025 cm^{-1} to about 0.1 cm^{-1} unless cancellation of the mixed ($t_{2_g} - e_g$) type occurs.

IV. EXCITON RELAXATION OF Cu^{2+} in α-$NiSO_4 \cdot 6H_2O$ AND $NiSeO_4 \cdot 6H_2O$

A. Introduction

For the partially quenched ions, it has been observed that the temperature dependence of the impurity ion's line width corresponds closely with the populating of the excited states. The width should then be some function of the excited state population which in turn depends upon the splittings of the levels. Therefore, the possibility of determining the host's zero-field splittings exists, and in fact, very recently Davidov and Baberscke (1975) have applied this idea to determine the excited state crystalline field energy of Tm^{3+} by observing the temperature dependence of the Gd^{3+} line width in TmSb. The relaxation mechanism that they proposed for the substituted Gd^{3+} was one where the Gd^{3+} width was due to spin-lattice relaxation brought about by oscillations between the energy levels of the excited state manifold at the Gd^{3+} resonance frequency.

As reported in Section III, a number of transition metal ions have been observed in the α-$NiSO_4 \cdot 6H_2O$ and $NiSeO_4 \cdot 6H_2O$ lattices. As previously noted the nickel ions in these lattices have a singlet ground state separated from a doublet excited state by several wave numbers, e.g., 4.74 cm^{-1} in α-$NiSO_4 \cdot 6H_2O$. The line width observation for the impurity ions is that at 4.2°K the widths are so large as to make the resonances undetectable, but on lowering the temperature to 1.3°K the resonances are reasonably sharp. This rapid broadening does not occur in the isostructural diamagnetic host $ZnSeO_4 \cdot 6H_2O$ which

implies, not unexpectedly, that the nickel ions are connected with the broadening. The temperature range over which the impurity resonances broaden also corresponds to the range in which the excited states of the nickel becomes populated. At 1.3°K the nickel ion excited state population is approximately 1%, and at 4.2°K it is approximately equal to 28% for a zero-field splitting of 4.74 cm^{-1}. With these considerations in mind a study of the line width temperature dependence of Cu^{2+} in α-$NiSO_4 \cdot 6H_2O$ and $NiSeO_4 \cdot 6H_2O$ was undertaken.

B. Adaptation of Chemical Exchange Equations

It is proposed here that the line broadening of the Cu^{2+} in α-$NiSO_4 \cdot 6H_2O$ and $NiSeO_4 \cdot 6H_2O$ is the result of diffusion of the excited state of the nickel through the lattice, i.e., a Frenkel exciton. For low exciton concentrations, the Cu^{2+} ions find themselves in environments with different exchange fields depending on whether the exciton resides on a Cu^{2+} neighbor or not. Since the exciton is mobile, the Cu^{2+} fluctuates between different environments. This type of behavior is very reminiscent of chemical exchange problems in magnetic resonance where a spin is subject to environmental changes. The nuclear magnetic resonance of O^{17} in solutions containing paramagnetic ions where the O^{17} spin jumps back and forth between bulk water and coordination sphere water has been developed by Swift and Connick (1962), and the mathematical formalism should be adaptable to the Cu^{2+} resonance under discussion after an appropriate identification of terms is made.

As noted in Section III, the Cu^{2+} ions in these two nickel lattices are exchange coupled with four nearest neighbors which surround the

Cu^{2+} in a tetrahedral fashion. Considering this arrangement, the Cu^{2+} can exist in three environments for low exciton concentrations since the excited state has two possibilities. For clarity the various environments will be labeled and enumerated,

Environment A--Cu^{2+} surrounded by 4 Ni^{2+} neighbors in their ground states

Environment B--Cu^{2+} surrounded by 3 Ni^{2+} neighbors in their ground states and a fourth in the excited state $|+1\rangle$

Environment C--Cu^{2+} surrounded by 3 Ni^{2+} neighbors in their ground states and a fourth in the excited state $|-1\rangle$

The equations derived by Swift and Connick (1962) require that one of the species be dominant and that the exchange of environments occur only from A to B or C and not between B and C, which really is a consequence of A being the dominant species. Over the temperature range studied, environment A decreases from 99% to 92% in α-$NiSO_4 \cdot 6H_2O$, and the condition that A be the dominant species is reasonably fulfilled. Under these approximations the experimental half-width at half-height of the Cu^{2+} resonance is given by,

$$\frac{1}{T_2} = \frac{1}{T_{2A}} + \frac{P_B}{T_B}\left[\frac{(1/T_{2B})(1/T_{2B} + 1/T_B) + \Delta\omega_B^2}{(1/T_{2B} + 1/T_B)^2 + \Delta\omega_B^2}\right] + \frac{P_c}{T_c}\left[\frac{(1/T_{2C})(1/T_{2C} + 1/T_C) + \Delta\omega_C^2}{(1/T_{2C} + 1/T_C)^2 + \Delta\omega_C^2}\right] \qquad (4\text{-}1)$$

where the symbols have the following meanings,

T_{2A} is the transverse relaxation time of the Cu^{2+} when all of the nickels are in their ground states, i.e., at T = 0°K.

$T_{2B,C}$ are the transverse relaxation times of the Cu^{2+} in environments B or c.

$T_{B,C}$ are the lifetimes of environments B or C.

$\Delta\omega_{B,C}$ are the differences between the resonance frequency of Cu^{2+} in environments B or C and the observed frequency.

$P_{B,C}$ are the fractions of Cu^{2+} ions in environments B or C.

At the magnetic fields employed to observe the Cu^{2+} resonances, the energy difference between the two excited states of the Ni^{2+} ions is small compared to the zero-field splitting, and the two states can be considered to be approximately degenerate. Under this condition $P_B = P_C$, and the fractional population of environment B is given by the product of the fraction of Ni^{2+} ions in the excited state times the concentration of neighbors, which is four times the copper concentration, divided by the concentration of copper ions,

$$P_B = \frac{4e^{-D/kT}}{[1 + 2e^{-D/kT}]} \qquad (4\text{-}2)$$

Also, the transverse relaxation times T_{2B} and T_{2C} are expected to be the same and are probably not too much different than T_{2A}. If different, they will be shorter than T_{2A}. The shifts $\Delta\omega_B$ and $\Delta\omega_C$, though they may be opposite sign, should have similar magnitudes. The lifetimes of the environments B and C should be controlled by the exchange interaction between nickel ions. Since the Ni^{2+} excitation can not jump to the Cu^{2+} due to energy conservation, it may jump to any three of the nearest neighbor nickel ions, and since the exchange

is largest among these, the probability of jumping to other neighbors can be assumed negligible. Because the jumping rate for both B and C environments are controlled by the same exchange interaction, T_B will be the same as T_c and may be defined as

$$T_B = \hbar/3J \tag{4-3}$$

Under the above assumptions, the two sites B and C are identical, and the problem collapses to a two site problem with the width now being given by

$$\frac{1}{T_2} = \frac{1}{T_{2A}} + \frac{2P_B}{T_B}\left[\frac{(1/T_{2B})(1/T_{2B} + 1/T_B) + \Delta\omega_B^2}{(1/T_{2B} + 1/T_B)^2 + \Delta\omega_B^2}\right] \tag{4-4}$$

A number of limiting cases exist depending on the relative magnitudes of the terms in Eq. (4-4), i.e., the relative rates of the various processes. Swift and Connick (1962) list the following situations.

1. $$\Delta\omega_B^2 >> \frac{1}{T_{2B}^2} \quad , \quad \frac{1}{\tau_B^2} \quad ; \quad \frac{1}{T_2} - \frac{1}{T_{2A}} = \frac{2P_B}{\tau_B}$$

The exchange of environments is relatively slow and can not average the two environments effectively. Two resonances, one from each environment, may be detectable. Their widths are dependent on the speed of environmental exchange and result from a change in precessional frequency.

2. $$\frac{1}{\tau_B^2} >> \Delta\omega_B^2 >> \frac{1}{(T_{2B}\tau_B)} \quad ; \quad \frac{1}{T_2} - \frac{1}{T_{2A}} = 2P_B\tau_B\Delta\omega_B^2$$

Here the environmental exchange is of an intermediate value capable of averaging the two sites. Its frequency is larger than the difference in precessional frequency but not so large as to make the second inequality hold. The width depends on how effectively T_B can average the two sites and is a function both of exchange time and the frequency difference.

3. $$\frac{1}{T_{2B}^2} >> \Delta\omega_B^2 \ , \ \frac{1}{\tau_B^2} \ ; \ \frac{1}{T_2} - \frac{1}{T_{2A}} = \frac{2P_B}{\tau_B}$$

The trasverse relaxation time of site B is very effective in causing relaxation, and the width depends on how long the species is subject to environment B.

4. $$\frac{1}{(T_{2B}\tau_B)} >> \frac{1}{T_{2B}^2} \ , \ \Delta\omega_B^2 \ ; \ \frac{1}{T_2} - \frac{1}{T_{2A}} = \frac{2P_B}{T_{2B}}$$

The environmental exchange is the dominate process being very fast. The width becomes dependent on the transverse relaxation time in environment B.

The relevant quantities which might be determined from the data, depending on which case holds, are τ_B which contains the exchange value between host ions and zero-field splittings contained in P_B. The next section investigates the propriety of the various situations listed to the Cu^{2+} line width in α-$NiSO_4 \cdot 6H_2O$ and $NiSeO_4 \cdot 6H_2O$.

Table XII. Temperature dependence of Cu^{2+} peak-to-peak line width in α-$NiSO_4 \cdot 6H_2O$ and $NiSeO_4 \cdot 6H_2O$.

α-$NiSO_4 \cdot 6H_2O$

T(°K)	LW (gauss)	$(LW)-(LW)_o$ (gauss)
1.34±0.01	50.7±0.06	7.7±5
1.56	58.3	15.3
1.75	74.0	31.0
1.92	92.8	49.8
2.02	107.7	64.7
2.18	130.0	87.0
2.27	140.5	97.5

Zero temperature extrapolated value $(LW)_o$=43±5

$NiSeO_4 \cdot 6H_2O$

T(°K)	LW (gauss)	$(LW)-(LW)_o$ (gauss)
1.30 0.01	46.6 0.06	7.1 5
1.48	53.2	13.7
1.74	73.2	33.7
1.76	74.5	35.0
1.86	83.8	44.3
2.04	117.7	78.2
2.25	135.7	96.2

Zero temperature extrapolation value $(LW)_o$-39.5±5

C. Results and Discussion

Along the γ axis the external field is perpendicular to the z axes of ions 1 and 3, and the perpendicular hyperfine splitting of the Cu^{2+} is less than 8 gauss. The line widths of the individual hyperfine lines are greater than the splittings, and a single inhomogeneous line with no structure is observed. Admittedly, this line is a poor choice for a line width measurement due to the hyperfine inhomogeneity, but all other sets of lines are also overlapped and show in general resolved structure. At the lowest temperatures an asymmetry of the line is detectable, but as the line broadens, this disappears. The line was treated as if it were a single Lorentz line. Table XII gives the widths as a function of temperature at ~9.5 GHz. The obvious short coming of the data is the very narrow temperature range over which line widths are available. In order to apply the previous equations, the line width in environment A, $1/T_{2A}$, is required. This would be the width at zero temperature and is obtainable by extrapolation. The extrapolation for the Cu^{2+} is very difficult to make with the present data since the curve is just beginning to bend over at the lowest temperature. Figure 11 plots peak-to-peak line width vs T and indicates the extrapolation to T = 0°K. Since the extrapolation is very uncertain, the values of $(1/T_2 - 1/T_{2A})$ become very uncertain especially at the lower temperatures.

No thorough study of the line width was made at frequencies other than X-band, but spectra taken at ~23 GHz indicate that there is no change in the line width with field. This eliminates the mechanism of Davidov and Baberscke (1975) since it should depend on the Larmor

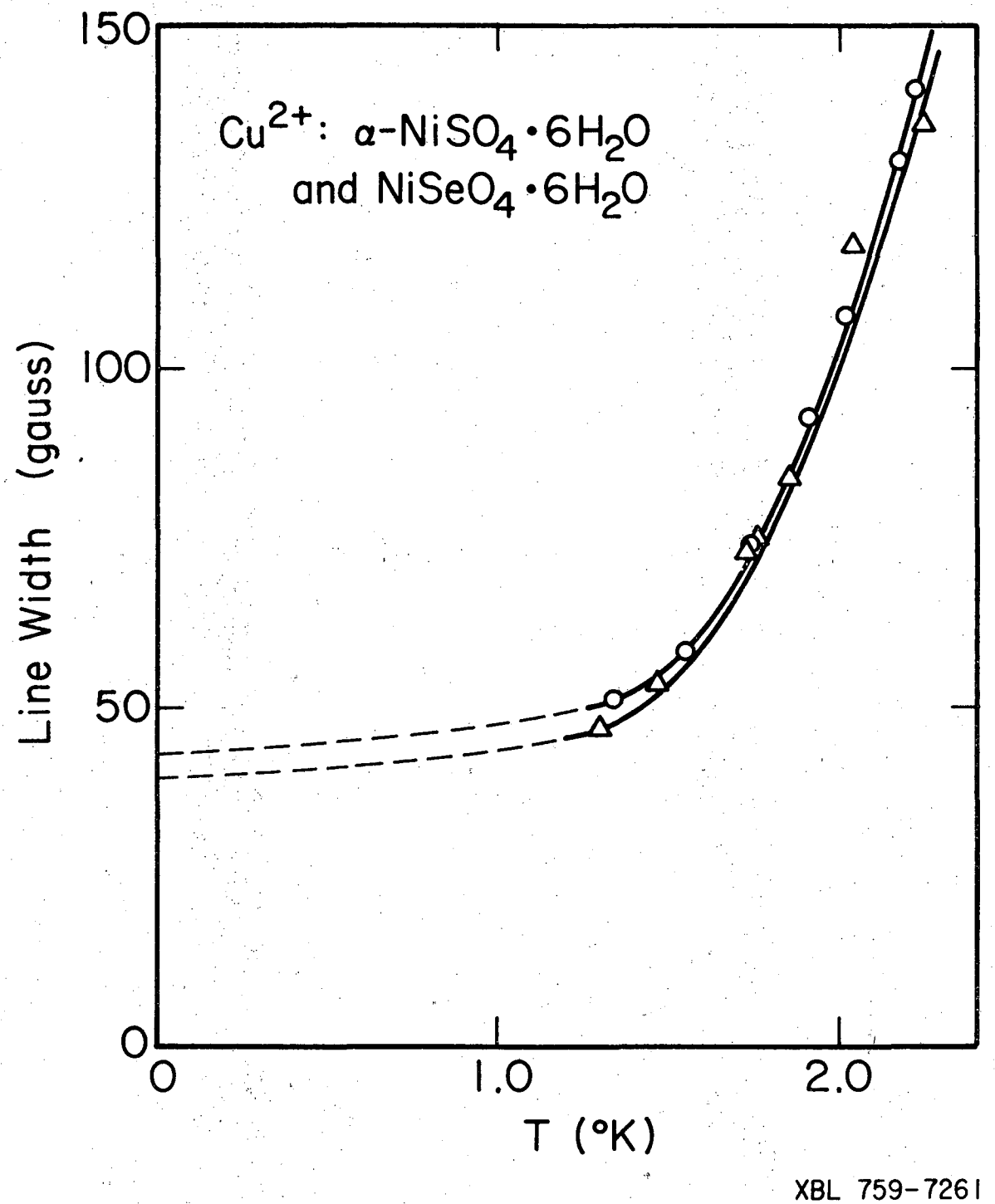

Fig. 11. A plot of line width vs temperature for Cu^{2+} in α-$NiSO_4 \cdot 6H_2O$ (□) and $NiSeO_4 \cdot 6H_2O$ (Δ) extrapolated to zero temperature. The solid line is not theoretical.

frequency. In addition, the lack of frequency dependence makes case 2 involving $\Delta\omega_B$ doubtful since from Section III the different molecular fields for the different environments causes different g-value shifts which would make $\Delta\omega_B$ frequency dependent.

To distinguish between the remaining cases, knowledge of the various rates and the temperature dependence can be employed. All three cases have a similar form, 1 and 3 being identical. Since for α-$NiSO_4 \cdot 6H_2O$ the zero-field splitting is known, the cases can be cast into a form where a single unknown quantity is solved for,

$$2P_B/(1/T_2 - 1/T_{2A}) = \tau_B \quad \text{or} \quad T_{2B} \tag{4-5}$$

A good estimate of τ_B can be made since the Ni^{2+} - Ni^{2+} isotropic exchange value is known to be between 0.1-0.2 cm^{-1} from thermodynamic work (Fisher and Hornung, 1968) and pair spectroscopy (St. John, 1974). Taking the lower limit leads to a value of 1.8×10^{-11} sec for τ_B using Eq. (III-3). Since the exchange interaction is not temperature dependent, the product in Eq. (4-5) should be a constant equal to approximately 1.8×10^{-11} sec if it is equal to T_B. Figure 12 plots the product, $2P_B/(1/T_2 - 1/T_{2A})$ vs T. As can be seen the product shows a slight temperature dependence and is much larger than the required value of 1.8×10^{-11} sec needed to be in the correct exchange range. The conclusion is that case 4 describes the situation best. On physical grounds case 4 sounds most plausible also since it requires that the environmental changes be the fastest process occurring, which is a very reasonable situation considering the estimates of the various quantities. The products in this case are equal to T_{2B} and indicate that T_{2B} has a slight temperature dependence. This conclusion is somewhat

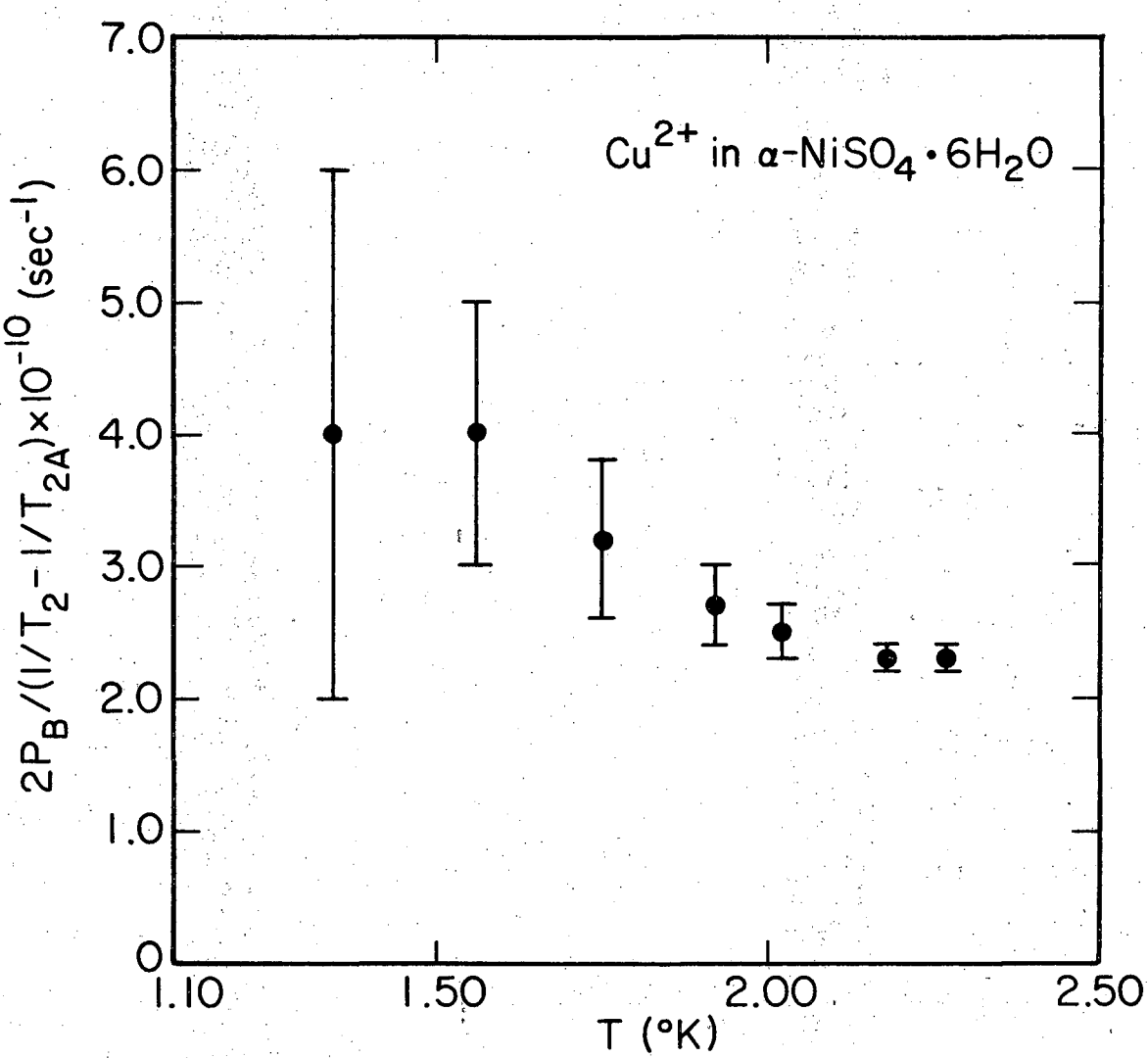

XBL 759-7260

Fig. 12. The product $2P_B/(1/T_2-1/T_{2A})$ is plotted vs temperature for Cu^{2+} in α-$NiSO_4 \cdot 6H_2O$ to indicate if a temperature dependence exists.

disappointing since the Ni^{2+} - Ni^{2+} exchange interaction is not extractable.

The presence of an apparent temperature dependence in T_{2B} thwarts the possibility of determining the D of the nickel. However, since the temperature dependence of T_{2B} is small, the determination of D would serve as an approximate check on the proposed mechanism. Rearranging Eq. (4-5) and taking the logarithm yields

$$\ln B = \ln\{(1/T_2 - 1/T_{2A})\ Z\} = -\ln(T_{2B}/2) - \frac{D}{k}\left(\frac{1}{T}\right) \qquad (4\text{-}6)$$

where the fact that $P_B = e^{-D/kT}/Z$ has been used. With T_{2B} assumed constant, a plot of ln B vs 1/T will yield a straight line with -D/k as the slope which should correspond to the known value of D for the α-$NiSO_4 \cdot 6H_2O$. Even though Z contains D, it is very insensitive to D over the temperature range used and was taken to be 4.74 cm^{-1} for the calculation. Figure 13 shows a plot of ln B vs 1/T and yields a value of 5.9 ± 1 cm^{-1} for the zero-field splitting. Comparing this with the known value of 4.74 cm^{-1} indicates that the agreement is poor but not entirely out of the limits of error.

The zero-field splitting in $NiSeO_4 \cdot 6H_2O$ is not known, but EPR spectra (Jindo, 1971) indicate that it is a little larger than that in α-$NiSO_4 \cdot 6H_2O$. Using the line width temperature data, the zero-field splitting in $NiSeO_4 \cdot 6H_2O$ will be estimated. Figure 14 gives the ln B vs 1/T plot which estimates D to be 5.9 ± 1 cm^{-1} in $NiSeO_4 \cdot 6H_2O$. The value of D used to calculate Z could be varied from 4.5 to 7.5 cm^{-1} without any change.

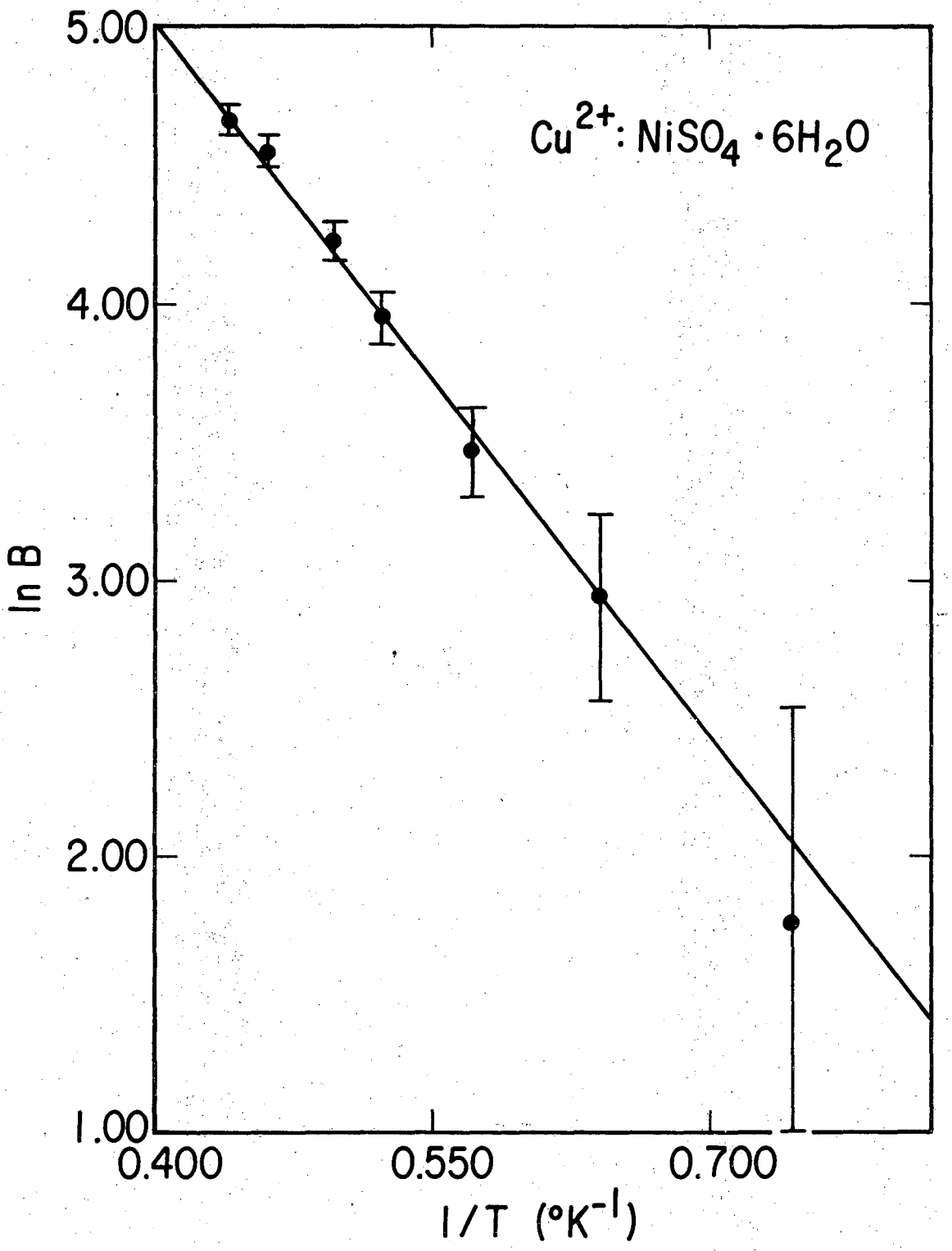

XBL 759-7259

Fig. 13. A plot of ln B, defined by Eq. (4-6), vs 1/T for Cu^{2+} in $NiSeO_4 \cdot 6H_2O$ is shown. The straight line is the best one drawn by eye. The slope yields a value of $D = 5.9 \pm 1$ cm^{-1}

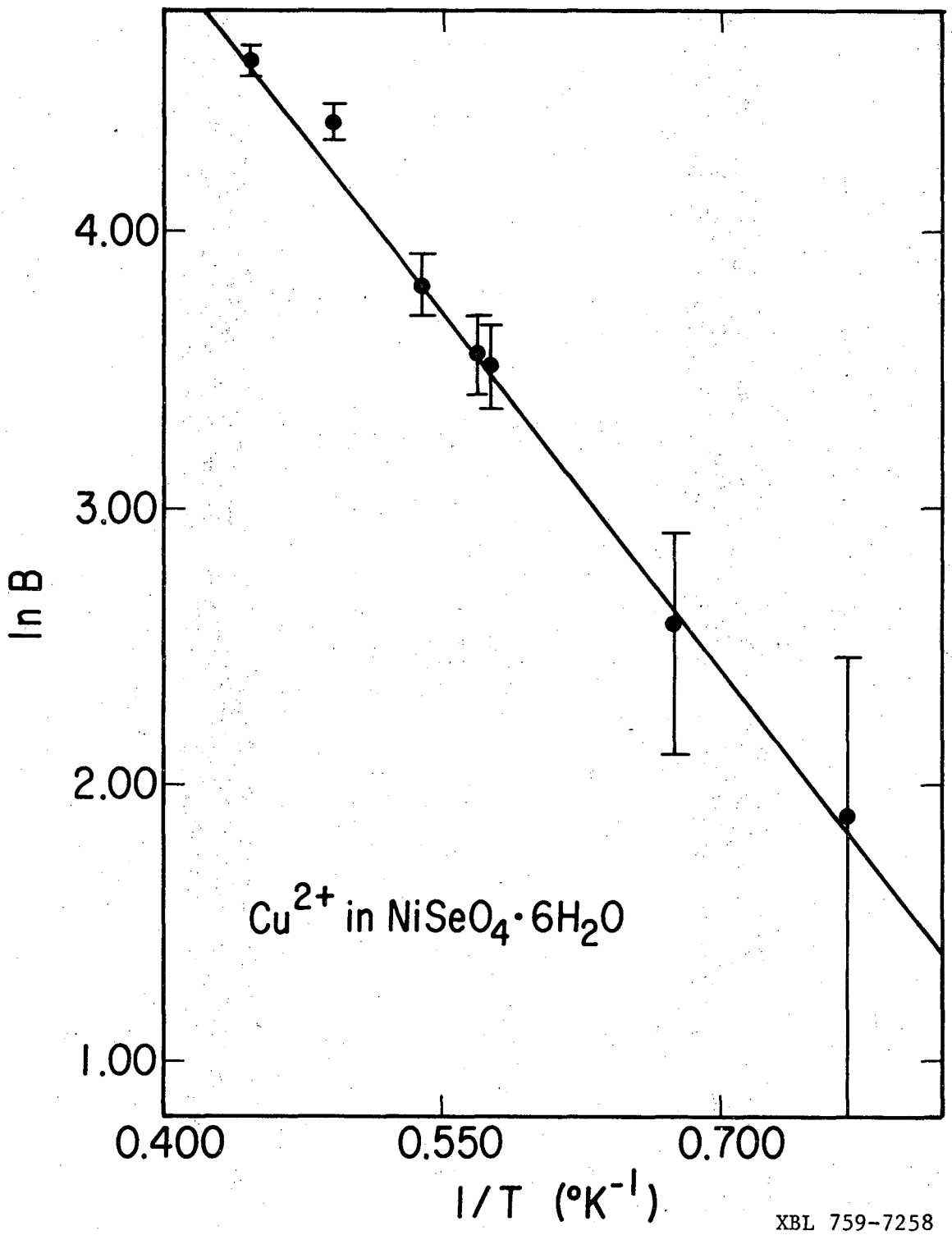

Fig. 14. A plot of ln B, defined by Eq. (4-6), vs 1/T for Cu^{2+} in $NiSeO_4 \cdot 6H_2O$ is shown. The straight line is the best one drawn by eye. The slope yields a value of $D = 5.9 \pm 1$ cm^{-1}.

Returning to Cu^{2+} in $(NH_4)_2Fe(SO_4)_2 \cdot 6H_2O$ (Gill and Ivey, 1974) of Section II-C, it is believed that the temperature dependence observed for the Cu^{2+} fits into the present framework. These workers observed the following sequence of spectra at various temperatures. At 1.3°K a fairly sharp four line Cu^{2+} spectra was observed in accordance with the fact that a singlet ground state exists and it is the only state populated at this temperature. The next state is 6.7 cm^{-1} above the ground state (Gill and Ivey, 1974). As the temperature rises to 4.2°K a satillite line appears which they attributed to a Cu^{2+} ion with one to its neighbors in the first excited state. On raising the temperature of 13°K, the lines broaden, and only a single line is observed. A maximum in the line width is obtained at 13°K, and further increases in temperature narrows the lines. Recapitulating, the sequence of events is (1) two lines observed, (2) broadening of the line widths, (3) a single broad line, and (4) narrowing of the line width. This sequence is in accord with the classical case of environmental exchange between two sites.

In this case, the exchange interaction between Fe^{2+}'s is not expected to be great, and the hopping rate will be less than in the previous nickel salts. The result is that spectra from two environments, Cu^{2+} surrounded by all ground state Fe^{2+} and Cu^{2+} with one of its Fe^{2+} neighbors in the first excited state, are observable at 4.2°K where few excitons are present, and thus the environmental exchange rate is slow. As the temperature increases the population of excitons increases which increases the rate of environmental exchange, and the lines broaden. At 13°K only a single broad line remains. The narrowing

after 13°K may either result from an increase of the environmental exchange to a point where $1/\tau_B \gg \Delta\omega_B$ or the host spin-lattice relaxation narrowing may take over.

ACKNOWLEDGEMENTS

I would like to thank Professor Rollie Myers for his patience in my early graduate career after my war experience and for his technical help, Rich Wilson for his computing aid and for putting up with lots of guff, Joyce Yarnell for the use of equipment built by her and for her pies, Duane Lindner for scientific discussions, and Aki Jindo whose thesis was an invaluable aid.

Also, one must graciously acknowledge the U. S. Energy Research and Development Administration, and the National Science Foundation (Grant GP 2139). I would in addition like to commend the Chemistry Department machine and wood shops for their courteous and helpful service.

APPENDIX I. OBSERVED IMPURITY IONS IN PARAMAGNETIC HOSTS

Transition Metal Hosts

Impurity Ion	Host	References
Mn^{2+}	$(NH_4)_2Co(SO_4)_2 \cdot 6H_2O$	Upreti, 1973
Mn^{2+}	$(NH_4)_2Co(SO_4)_3$	Chowdari, 1969
Mn^{2+}	$(NH_4)_2Ni(SO_4)_2 \cdot 6H_2O$	Upreti, 1974
Mn^{2+}	$(NH_4)_2Ni_2(SO_4)_3$	Chowdari, 1969
Mn^{2+}	$K_2Ni(SO_4)_2 \cdot 6H_2O$	Upreti, 1974
Mn^{2+}	$Ni(CH_3COO)_2 \cdot 4H_2O$	Janakiraman and Upreti, 1971a
Mn^{2+}	$NiSO_4 \cdot 7H_2O$	Janakiraman and Upreti, 1971a and 1971b
Mn^{2+}	$(NH_4)_2Fe(SO_4)_2 \cdot 6H_2O$	Janakiraman and Upreti, 1970
Cu^{2+}	$(NH_4)_2Fe(SO_4)_2 \cdot 6H_2O$	Gill and Ivey, 1974
Cu^{2+}	$K_2Co(SO_4)_2 \cdot 6H_2O$	Sastry and Sastry, 1973
Cr^{3+}	$K_3Fe(CN)_6$	Mitsuma, 1962
Ni^{2+}	$FeSiF_6 \cdot 6H_2O$	Rubins, 1974
V^{2+}, Mn^{2+}, Cu^{2+} and Co^{2+}	α-$NiSO_4 \cdot 6H_2O$	This work

Lanthanide Metal Hosts

Gd^{3+}	$Ce(C_2H_5SO_4)_3 \cdot 9H_2O$	Bleaney, Elli , and Scovil, 1951
Gd^{3+}	$Nd(NO_3)_3 \cdot 6H_2O$	Singh and Verkateswarlu, 1967
Gd^{3+}	$NdCl_3 \cdot 6H_2O$ and $PrCl_3 \cdot 7H_2O$	Singh, Upreti, and Verkateswarlu, 1967
Gd^{3+}	$M(C_2H_5SO_4)_3 \cdot 9H_2O$ ($M=Pr^{3+}$, Nd^{3+}, Sm^{3+}, Tb^{3+}, Dy^{3+}, Ho^{3+}, Er^{3+}, Yb^{3+}, and Lu^{3+})	Gerkin and Thorsell, 1972

Gd^{3+} and Fe^{3+}	EuGa Garnet	Hutchings, Windsor, and Wolf, 1966
Gd^{3+}, Eu^{3+} and Mn^{2+}	SmX (X=S,Se, and Te)	Birgeneau, Bucher, Rupp and Walsh, 1972
Fe^{3+}	TmGa Garnet	Rimai and Bierig, 1964
Gd^{3+}	TmX (X=Sb and Bi) PrX (X=Sb, Bi and Te)	Rettori, Davidov, Garevsky and Walsh, 1975
Gd^{3+}	TmX and PrX (X=P,As,Sb and Bi)	Sugawara, Huang and Cooper, 1975

APPENDIX II. THE EPR OF Mn^{2+} IN $ZnSeO_4 \cdot 6H_2O$ AND $ZnSeO_4 \cdot 6D_2O$

Introduction

The spectroscopy of Mn^{2+} substituted into $ZnSeO_4 \cdot 6H_2O$ had not been done previously, and so it was necessary to determine the g-values of Mn^{2+} in $ZnSeO_4 \cdot 6H_2O$ in order to make a comparison with Mn^{2+} substituted into the paramagnetic host $NiSeO_4 \cdot 6H_2O$. On observing the Mn^{2+} spectra, an exceptionally large zero-field splitting was detected, and for these reasons it seemed desirable to determine the Mn^{2+} spin Hamiltonian in the diamagnetic $ZnSeO_4 \cdot 6H_2O$.

Experimental Procedures and Results

Considering only $\Delta M_s = 1$, $\Delta m_s = 0$ transitions, the spectra of of Mn^{2+} should contain five sextets (30 lines) for each ion in the unit cell, assuming that $h\nu$ is greater than the zero-field splittings. The presence of four ions per unit cell in the $ZnSeO_4 \cdot 6H_2O$ lattice leads to an abundance of lines which naturally gives a complicated and highly overlapped spectra. In addition, the presence of a large zero-field splitting gives appreciable intensity to the "forbidden" transitions, both $\Delta M_s \neq 1$ and $\Delta m_s \neq 0$, which further complicates the observed spectra. In order to obtain the best possible resolution, host crystals of $ZnSeO_4 \cdot 6D_2O$ were prepared by repeated recrystallization from D_2O. The replacement of the protons by deuterons reduced the residual peak-to-peak line width caused by the water protons magnetic moments from ~10 gauss to ~6 gauss. Since better resolution could be obtained in the deuterated lattice, the majority of the work was conducted in it. However, even with the deuterated samples, it was not possible to follow the angular dependence of the lines due to the lack of resolution.

Previous work on Cu^{2+}, Ni^{2+} and Co^{2+} in the $ZnSeO_4 \cdot 6H_2O$ lattice indicated tetragonal symmetry around these ions, and they were fit nicely to an axial spin Hamiltonian (Jindo and Myers, 1972). Following the precedent set in these ions, the z axes of two of the ions in a unit cell should lie in a γc plane. When the magnetic field is rotated in the γc plane, a maximum spread in the fine structure pattern should occur with H_o along z. This maximum spread was observed and taken to be the z magnetic axis of the Mn^{2+}. The outer sextets ($M_s = \pm 3/2$ to $\pm 5/2$) were well separated from the main body of lines, the ($M_s = \pm 1/2$ to $M_s = \pm 3/2$) sextets were easily distinguishable on the outer edges of the main body, and the ($M_s = +1/2$ to $-1/2$) was indistinguishable in the complicated center of the main body of lines. A secondary relative maximum spread in the fine structure was also observed in the γc plane, and identified as the γ axis where H_o is along the x axis of two of the ions. The same spectra was also obtained in the ab plane confirming the assignment of the γ direction, and this was taken to be the x magnetic axis of the Mn^{2+}. Figure 15 shows the Mn^{2+} spectra along the γ axis and indicates that all five sextets are disernible for one pair of equivalent ions. Along the γ axis two spectra are expected, ions 1 and 3 being equivalent and 2 and 4 being equivalent here. The one set of five sextets is able to dominate the spectra here because the fine structure pattern of the other set is at a collapsed position causing overlap cancellation of intensity and the "forbidden" transitions also rob the collapsed set of intensity. It was not possible to distinguish a single set of five sextets either along the c or a axes where all the ions in the

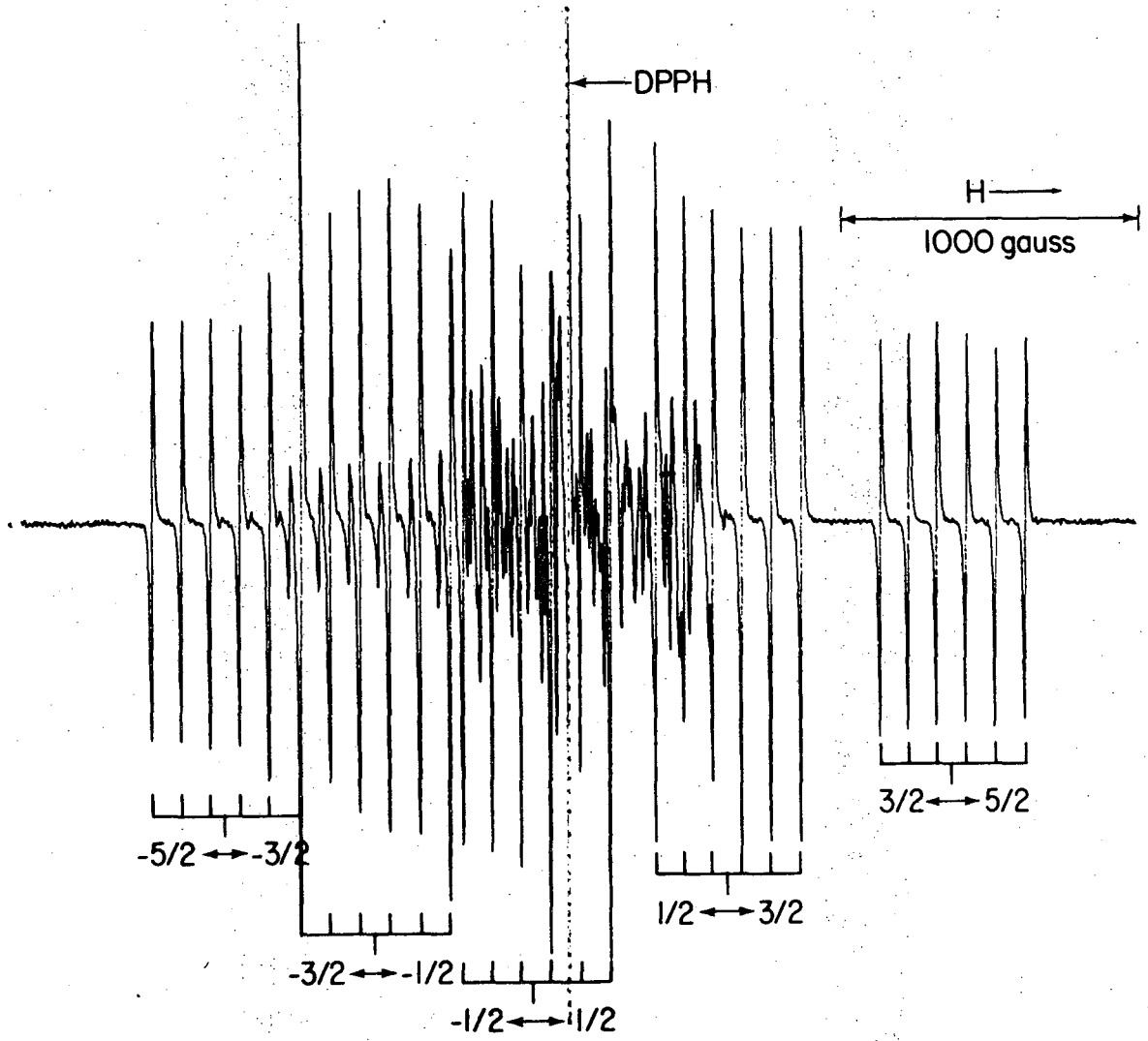

Fig. 15. A derivative spectra of Mn^{2+} in $ZnSeO_4 \cdot 6D_2O$ with the magnetic field along the γ axis. The five sextets belonging to the ions with the field perpendicular to their tetragonal field axes are identified. T = 77 K and ν = 23.2504 GHz.

cell should be magnetically equivalent. This may have been an alignment problem, a 1/4° rotation having very significant effects near these positions. Measurements with H_o along the z and x axes as defined above were the source of line position data used to determine the spin Hamiltonian. The angle ϕ was again taken to be the angle between the ion's z axis and the c crystal axis and was determined by subtracting the angle between the z axis maximum and the γ axis maximum from 90° since the angle between the γ axis and the c axis is 90°. Sextet centers were taken to be an average of the hyperfine $m_I = -1/2$ and $m_I = +1/2$ transitions within a sextet. The presence of very large zero-field splittings made the accuracy of the second-order perturbation equations (Abragam and Bleaney, 1970) suspect when applied at X-band (~9 GHz), and K-band (~23 GHz) measurements were employed when possible.

The Spin Hamiltonian

When a purely axial spin Hamiltonian was applied to the data, various inconsistencies arose, and so a Hamiltonian which included a small rhombic component was deemed necessary. This was, of course, a deviation from the previous ions. The spin Hamiltonian employed was taken to be

$$\mathcal{H} = \beta\vec{H}\cdot\overleftrightarrow{g}\cdot\vec{S} + D\left[S_z^2 - 1/3\ S(S+1)\right] + E\left(S_x^2 - S_y^2\right) \qquad \text{(A2-1)}$$
$$\frac{F}{180}\left[35S_z^4 - 30S(S+1)\ S_z^2 + 25S_z^2 - 6S(S+1) + 3S^2(S+1)^2\right]$$
$$+ \frac{a}{6}\left[S_x^4 + S_y^4 + S_z^4 - 1/5\ S(S+1)(3S^2 + 3S - 1)\right] + \vec{S}\cdot\overleftrightarrow{A}\cdot\vec{I}$$

The cubic field term, a, was assumed to have the same axis system as the other fine structure terms. With the cubic and higher order axial terms are

added to the second-order perturbation equations for the field positions given by Howling (1969), the transition fields are given by

$3/2 \rightarrow 5/2$

$$H1 = H_o - 2R - 64S/(8H_o) + 8T/(8H_o) - U/6 - 2pa \qquad \text{(A2-2a)}$$

$1/2 \rightarrow 3/2$

$$H2 = H_o - R + 8S/(8H_o) - 10T/(8H_o) + 5U/24 + 5/2\ pa \qquad \text{(A2-2b)}$$

$-1/2 \rightarrow 1/2$

$$H_3 = H_o + 32S/(8H_o) - 16T/(8H_o) \qquad \text{(A2-2c)}$$

$-3/2 \rightarrow -1/2$

$$H4 = H_o + R + 8S/(8H_o) - 10T/(8H_o) - 5U/24 - 5/2\ pa \qquad \text{(A2-2d)}$$

$-5/2 \rightarrow -3/2$

$$H5 = H_o + 2R - 64S/(8H_o) + 8T/(8H_o) + u/6 + 2pa \qquad \text{(A2-2e)}$$

The following definitions were used,

$$H_o = h\nu/g\beta$$

$$R = [D(3\cos^2\theta - 1) + 3D\cos\phi\sin^2\theta]$$

$$S = [(D - E\cos 2\phi)^2 \sin^2 2\theta + 4E^2\sin^2\theta\sin^2 2\phi]$$

$$T = \{[D\sin^2\theta + E\cos 2\phi(1 + \cos^2\theta)]^2 + 4E\cos^2\theta\sin^2 2\phi\}$$

$$U = F(35\cos^4\theta - 30\cos^2\theta + 3) \quad .$$

The rest of the symbols have their standard meanings (Abragam and Bleaney, 1970), and second order terms in a and F have been neglected.

Observing that the differences between Eqs. (A2-2a) and (A2-2e) as well as Eqs (A2-2b) and (A2-2d) eliminate all second order terms,

one can write these differences for H_o along the z and x axes as follows,

$$(H1 - H5)_z = 8D + 4(a + 2/3\ F) \qquad \text{(A2-3a)}$$

$$(H2 - H4)_z = 4D - 5(a + 2/3\ F) \qquad \text{(A2-3b)}$$

$$(H5 - H1)_x = -4D + 12E + 4(a + 1/4\ F) \qquad \text{(A2-4a)}$$

$$(H4 - H2)_x = -2D + 6E - 5(a + 1/4\ F) \qquad \text{(A2-4b)}$$

Equation (A2-3) indicates that measurements of the sextet centers along the z axis is sufficient to determine D with the sum (a + 2/3 F) thrown in. Coupling the results of Eq. (A2-3) with Eq. (A2-4), obtained from measurements of sextet centers along x, leads to the determination of the rest of the fine structure parameters, E, a, and F. The sign of D was obtained by observing the intensity disparity among sextets at low temperatures. At 1.3°K the $M_s = 3/2 \rightarrow 5/2$ transition is almost undetectable relative to the $M_s = -5/2 \rightarrow -3/2$ indicating a positive D value. It was not possible to determine $g_{\parallel}$ since the $M_s = -1/2 \rightarrow 1/2$ sextet could not be distinguished due to overlap. As noted earlier, all five sextets were distinguishable with H_o along x, and $g_{\perp}$ was calculated from the equation

$$g_{\perp} = \left[h\nu - \frac{2(D + E)^2}{h\nu} - \frac{17(A^2 + B^2)}{8h\nu} \right] / (\beta H) \qquad \text{(A2-5)}$$

The perpendicular hyperfine value was taken as the difference between the hyperfine $m_I = 1/2$ and the $m_I = -1/2$ transitions in the $M_s = -1/2$ 1/2 sextet. Since the hyperfine value is expected to be nearly isotropic for Mn^{2+}, A was set equal to B in the calculation of $g_{\perp}$. Using K-band (~23 GHz) data, the spin Hamiltonian parameters for Mn^{2+}

substituted into $ZnSeO_4 \cdot 6D_2O$ at 77°K were found to be

$$D = +600.0\times10^{-4}\ cm^{-1}\pm0.4$$

$$F = +34\times10^{-4}\ cm^{-1}\pm2$$

$$B = 90\times10^{-4}\ cm^{-1}\pm2$$

$$E = 18.6\times10^{-4}\ cm^{-1}\pm0.5$$

$$a = -13\times10^{-4}\ cm^{-1}\pm2$$

$$g_{\perp} = 1.997\pm0.003$$

As a test of these values, the field positions of the center of the sextets at X-band were calculated by direct diagonalization of the Hamiltonian. Table XIII compares the calculated and observed field positions with H_o parallel the z and x axes. For the calculations, $g_{\parallel}$ was taken equal to 2.00 when H_o was along z, and the second-order hyperfine shifts are not included. The absence of an E term effects the H_o parallel z positions only slightly, but its absence for the H_o parallel x positions results in an appreciable expansion in the fine structure pattern. The positions differ in the latter case by greater than 100 gauss. Data obtained with different samples were not as consistent as would have been liked. The reason for this is not known, but one obvious possibility is crystal alignment.

Other Dependences

Two interesting observations were made about the zero-field splitting, D. The first is that it appears to temperature dependent. Table XIV compares the observed splittings of the fine structure pattern along the γ axis (H_o parallel x) at 298°K and 77°K.

Table XIII. Comparison of experimental and calculated field positions (in gauss) for Mn^{2+} in $ZnSeO_4 \cdot 6D_2O$.*

	H_o along z		H_o along x	
Transition	Experimental	Calculated	Experimental	Calculated
3/2 → 5/2	833	837	4683	4693
1/2 → 3/2	2174	2169	3785	3783
-1/2 → 1/2	3431	3637	3166	3177
-3/2 → -1/2	4687	4684	2750	2778
-5/2 → -3/2	6006	6018	2414	2446

*ν = 9.5906 GHz.

Table XIV. Comparison of Mn^{2+} Splittings (in gauss) along the x axis at two temperatures.*

Splitting	298°K	77°K
$(H1-H5)_x$	2173	2363
$(H2-H4)_x$	1055	1147

*$\nu \sim 23$ GHz.

Also, the hydrated and deuterated samples had slightly different splittings. This is not too surprising when it is recalled that the large tetragonal component of the distortion was attributed to hydrogen bonding effects and that the proton hydrogen-bond is stronger than the dueteron hydrogen-bond (Novak, 1974). A similar observation was made recently by Berstein and Dobbs (1975) who observed changes in the zero-field splittings of the S-state ion Gd^{3+} when the water of hydration was deuterated in the ethylsulfates. Table XV compares the splittings of Mn^{2+} in $ZnSeO_4 \cdot 6H_2O$ and $ZnSeO_4 \cdot 6D_2O$. Since the D value is by far the largest splitting factor, these observed changes in observed splittings with temperature and deuteration are attributed to changes in D.

Table XV. Comparison of Mn^{2+} splittings (in gauss) along the z and x axes in $ZnSeO_4 \cdot 6H_2O$ and $ZnSeO_4 \cdot 6D_2O$.*

Splitting	$ZnSeO_4 \cdot 6H_2O$	$ZnSeO_4 \cdot 6D_2O$
$(H1-H5)_z$	5098	5206
$(H5-H1)_x$	2325	2363

*T = 77°K and $\nu \sim 23$ GHz.

APPENDIX III. COPPER(II) AND NICKEL(II) PAIR SPECTRA IN $ZnSeO_4 \cdot 6H_2O$

Introduction

A standard scientific procedure for understanding a system is to first understand its component parts. In magnetic insulators, the component parts are the individual transition metal ions and their surrounding array of ligands. As previously noted, the individual isolated ions have been the object of considerable study, as the comprehensive treatise of Abragam and Bleaney (1970) can attest. The next more complicated unit is a pair of ions which are able to interact with one another. Study of the interactions between the ions can then lead to an understanding of the properties of magnetically concentrated systems. EPR, when observable, is the most sensitive probe of the details of the exchange interaction between transition metal ions in insulators, and a number of reviews exist on the subject (e.g., Kokozka and Gordon, 1969; Smith and Pilbrow, 1974). Work along these lines has concentrated on pairs of ions in unique dimer units, particularly the copper pairs formed by carboxylic acids and other organic ligands.

Pairs of ions can also be prepared by substituting magnetic ions into isostructural diamagnetic lattices at a high enough percentage where a significant number of pairs exist. Unlike the dimers, the EPR of these statistical pairs suffer from having the single ion spectra as the largest feature which often obscures the pair spectra. On the other hand, this type of pair is directly related to a magnetically concentrated material which would occur at 100% substitution.

EPR is an especially good technique for probing the exchange interaction when the interaction is of the order of magnitude of the Zeeman energy or less, i.e., small exchange interactions. Relatively small interactions are expected for hydrated salts of transition metals. With these things in mind a study of the pair spectra of Cu^{2+}-Cu^{2+} and Ni^{2+}-Ni^{2+} pairs in the $ZnSeO_4 \cdot 6H_2O$ lattice was undertaken with the aim of interpreting more complicated pair systems and to aid in the understanding of previous work (Batchelder, 1970) on the EPR of pure α-$NiSO_4 \cdot 6H_2O$.

The Hamiltonian to be used for the interpretation of the pair spectra is a sum of the single ion Hamiltonians plus an interaction term

$$\mathcal{H} = \mathcal{H}_1 + \mathcal{H}_2 + \mathcal{H}_{int} \qquad (3A\text{-}1)$$

For ions with orbital singlet ground states, $\mathcal{H}_1$ and $\mathcal{H}_2$ are just the normal spin Hamiltonians for ions 1 and 2, and $\mathcal{H}_{int}$ is the dipolar and exchange interactions. The single ion spin Hamiltonian can be gotten from the EPR of the ions at low percentages in a diamagnetic host. This assumes that the exchange interaction does not effect the single ion paramaters which is a reasonable assumption for small exchange. The dipolar interaction is well known and can be accurately calculated with aid of appropriate crystallographic data. The form of the exchange interaction is not known and is the quantity of interest to be determined from the experimental data.

There have been two approaches to the determination of the exchange interaction. The approach which has been used almost exclusively is to guess a particular form of the interaction (usually

isotropic) and then see if it reproduces the observed spectra. This is surely the easiest procedure, but it is hard to acquire all the details of the interaction. The other approach, used for example by Culvahouse and Schinke (1969) and Dixon and Culvahouse (1971), is to start with the general bilinear form of the exchange interaction and determine all the components by using symmetry arguments and experimental data such as line splittings. This method determines the details of the exchange interaction very well but is also the most difficult to do experimentally. Very detailed spectra are needed for this method, and these are often times not available due to overlap problems. The work on the pairs in the $ZnSeO_4 \cdot 6H_2O$ used the first approach and as such is not very complete. Before proceding a caveat is in order. In the work to be presented many problems and inconsistencies exist; so that the conclusions drawn are to be viewed with some suspect. It is for this reason given as an appendix and not a chapter.

Cu^{2+}-Cu^{2+} Pairs in $ZnSeO_4 \cdot 6H_2O$

The Spin Hamiltonian

The simplest exchange pair consists of two ions each with a single unpaired electron as is found in the Cu^{2+}-Cu^{2+}. The coupling of the two spin 1/2 ions results in the familiar singlet-triplet problem, and this is usually the most convenient representation to work in since in many cases the isotropic exchange and Zeeman energies can be simultaneously diagonal. Nearly all the copper pair work done has been with what will be called similar pairs. Similar means that the g-tensors of the two ions are equal and parallel. This situation is accompanied by at least inversion symmetry in the pair unit which

simplifies the form of the exchange interaction. A dissimilar pair is one where either the g-tensors are different (not very common) or the g-tensors of the two ions are not parallel. The presence of non-parallel g-tensors introduces angular properties into the exchange interaction. It will be shown later that the $ZnSeO_4 \cdot 6H_2O$ lattice has both similar and dissimilar pairs, and for this reason, the more general form of the interaction Hamiltonian will be developed to account for both types of pairs.

For ions which have their orbital momentum well quenched, isotropic exchange has been shown to be a good approximation (Moriya, 1963; Anderson, 1963). This is true of Cu^{2+} in a tetragonal ligand field, as is found in $ZnSeO_4 \cdot 6H_2O$ (Jindo and Myers, 1972), and isotropic exchange has been almost exclusively used for Cu^{2+}. However, Moriya (1963) has shown that in the orbital singlet case the anisotropy in the exchange interaction should be of the order $\left(\frac{\Delta g}{g}\right)J$ where Δg is the deviation from the free electron value and J is the isotropic exchange value. For Cu^{2+} this should run around 5-10% which will certainly not be negligible except for very small exchange interactions. Regrettable as it is, isotropic exchange will be assumed in what follows since deviations from it rapidly increases the complexity of the problem.

The review by Smith and Pilbrow (1974) gives an excellent treatment of Cu^{2+}-Cu^{2+} pairs which takes all the anisotropy in the Hamiltonian into account exactly. The exchange interaction is taken by them to be

$$\mathcal{H}_{ex} = -J\vec{S}_1 \cdot \vec{S}_2 \qquad \text{(A3-2)}$$

(This is probably not the most common form, unfortunately. The interaction is written more frequently with either -2J or +J). When the

g-tensor axes of the two ions are not parallel the dipolar interaction becomes quite complicated and when written in the coordinate system of on of the ions, in this case ion 1, is given by

$$\mathcal{H}_{dip} = \sum_{\alpha,\gamma=x_1,y_1,z_1} R_{\alpha\gamma} S_{1\alpha} S_{2\gamma} \tag{A3-3}$$

where

$$R_{\alpha\gamma} = g_{1\alpha} \left\{ \sum_{\xi=x_2,y_2,z_2} g_{2\xi} d_{\gamma\xi} \left(d_{\alpha\xi} - 3\sigma_\alpha \sum_{\zeta=x_1,y_1,z_1} d_{\zeta\xi} \sigma_\zeta \right) \right\} \beta^2/r^3 \,. \tag{A3-4}$$

in Eq. (A3-4) the $d_{\zeta\xi}$ are direction cosines connecting the ζ axis (x_1,y_1 or z_1) and the ξ axis (x_2,y_2 or z_2), and the σ_α are the direction cosines of $\vec{r}$, the vector from ion 1 to ion 2, and the coordinate system of ion 1 (x_1,y_1 or z_1).

The most convenient representation to work in is one that diagonalizes the Zeeman interaction of the two ions. For similar pairs the isotropic exchange will also be diagonal in this representation. For a dissimilar pair the exchange will not in general be diagonal in this representation, and if J is large enough, the Zeeman representation may not be the most convenient. For an exchange interaction smaller than the Zeeman interaction, the Zeeman representation remains convenient. By the standard rotation of the spin operators to diagonalize the Zeeman energy (Abragam and Bleaney, 1970), the single ion Hamiltonian including hyperfine becomes

$$\begin{aligned} \mathcal{H}_i = {} & g_i \beta H S_{iz_i'} + K_i S_{iz_i'} I_{iz_i''} + \tau_{i1} S_{ix_i'} I_{ix_i''} + \tau_{i2} S_{iy_i'} I_{iy_i''} \\ & + \tau_{i3} S_{iy_i'} I_{ix_i''} + \tau_{i4} S_{ix_i'} I_{iz_i''} + \tau_{i5} S_{iy_i'} I_{iz_i''} \end{aligned} \tag{A3-5}$$

The quantities in Eq. (A3-5) are defined as

$$g_i^2 = \sum_{j=x_i,y_i,z_i} g_j^2 \ell_j^2$$

$$K_j^2 = \left(\sum_{j=x_i,y_i,z_i} A_j^2 g_j^2 \ell_j^2 \right) / g_i^2$$

$$\tau_{i1} = g_i A_{z_i} \left[\left(\alpha_{x_i}^2 + \alpha_{y_i}^2 \right) / \left(g_{x_i}^2 \ell_{x_i}^2 + g_{y_i}^2 \ell_{y_i}^2 \right) \right]^{1/2}$$

$$\tau_{i2} = A_{x_i} A_{y_i} \left[\left(g_{x_i}^2 \ell_{x_i}^2 + g_{y_i}^2 \ell_{y_i}^2 \right) / \left(\alpha_{x_i}^2 + \alpha_{y_i}^2 \right) \right]^{1/2} / (K_i g_i)$$

$$\tau_{i3} = \frac{\alpha_{x_i} g_{x_i} \ell_{x_i} g_{y_i} \ell_{y_i} \left[A_{y_i}^2 - A_{x_i}^2 \right]}{\left\{ \left[\left(\alpha_{x_i}^2 + \alpha_{y_i}^2 \right) \left(g_{x_i}^2 \ell_{x_i}^2 + g_{y_i}^2 \ell_{y_i}^2 \right) \right]^{1/2} K_i g_i \right\}}$$

$$\tau_{i4} = g_{z_i} \ell_{z_i} \left(K_i^2 - A_{z_i}^2 \right) / \left\{ K_i \left[g_{x_i}^2 \ell_{x_i}^2 + g_{y_i}^2 \ell_{y_i}^2 \right]^{1/2} \right\}$$

$$\tau_{i5} = \left(A_{y_i}^2 - A_{x_i}^2 \right) g_{x_i} \ell_{x_i} g_{y_i} \ell_{y_i} / \left\{ K_i g_i \left[g_{x_i}^2 \ell_{x_i}^2 + g_{x_i}^2 \ell_{y_i}^2 \right]^{1/2} \right\}$$

$$\alpha_k = A_k g_k \ell_k / k_i g_i$$

where the subscript $k = x_i, y_i, z_i$. The direction cosines ℓ_{x_i}, ℓ_{y_i} and ℓ_{x_i} are between the external field H and the x_i, y_i and z_i axes, i.e., the g-tensor axes. The unprimed coordinates are those of the g-tensor. The single primed coordinates refer to the electron spin axes and the double primed refer to the nuclear spin axes.

After the rotation of the spins, the interaction Hamiltonian is transformed to

$$\mathcal{H}_{int} = \sum_{\substack{P_1'=x_1',y_1',z_1' \\ P_2'=x_2',y_2',z_2'}} (D_{P_1'P_2'} + J_{P_1',P_2'}) S_{1P_1'} S_{2P_2'} \qquad \text{(A3-6)}$$

The spin coefficients have the following definitions

$$D_{P_1'P_2'} = \sum_{\substack{\alpha,\gamma=x_1,y_1,z_1 \\ r=x_2,y_2,z_2}} R_{\alpha\gamma} \ell^1_{\alpha P_1'} \ell^2_{rP_2'} d_{\gamma r} \qquad \text{(A3-7)}$$

and

$$J_{P_1'P_2'} = -J \sum_{\substack{q_1=x_1,y_1,z_1 \\ q_2=x_2,y_2,z_3}} \ell^1_{q_1P_1'} \ell^2_{q_2P_2'} d_{q_1q_2} \qquad \text{(A3-8)}$$

The direction cosines $\ell^1_{q_1P_1'}$ and $\ell^2_{q_2P_2'}$ are those connecting the g-tensor axes to the spin axes defined by the conditions which diagonalize the Zeeman energies of ions 1 and 2. The direction cosines $d_{q_1q_2}$ or $d_{\gamma r}$ are again those that connect the g-tensor coordinate system of ion 2 with that of ion 1. For similar pairs $d_{q_1q_2} = \delta q_1 q_2$, and the exchange term is isotropic. For non-parallel g-tensors, the isotropic exchange will appear as anisotropic in this representation.

Types of Cu^{2+}-Cu^{2+} Pairs in the $ZnSeO_4 \cdot 6H_2O$ Lattice

As noted in Section III-B, an ion in the $ZnSeO_4 \cdot 6H_2O$ lattice has nearest neighbors at four spatially equivalent positions arranged approximately at the apices of a tetrahedron. When a pair consists of an ion and one of its nearest neighbors, it will be designated as (1-2) or (3-2) pair. The numbering refers to the fact that the unit cell has four ions which are stacked in layers which are numbered consecutively as in Fig. 3. The (1-2) or (3-2) pair is a dissimilar one because the ions composing it have differently oriented g-tensors. The four possible pair arrangements with the nearest neighbors are not in general equivalent. Four an arbitrary direction of the magnetic field, the Zeeman energy for a (3-2) pair will be different than a (1-2) pair which would make them inequivalent. With the magnetic field in the ac or ab planes, both pairs have the same Zeeman energy. Since the exchange is isotropic, only one type of pair is found in these planes if the dipolar interaction is neglected. When the dipolar interaction is taken into account, the equivalence of the four nearest neighbor type pairs is broken. With the magnetic field along the crystal c axis, even the dipolar interaction energies for all nearest neighbor pairs are the same, and only one type of nearest neighbor pair exists. This direction of external field should yield the simplest spectra.

The next nearest neighbors are situated at the corners of a square surrounding the ion of interest. Referring to Fig. 3 and picking ion 2 as the reference ion, a pair may be formed with an ion found by translating along ±X or ±Y by a distance a. These pairs are similar

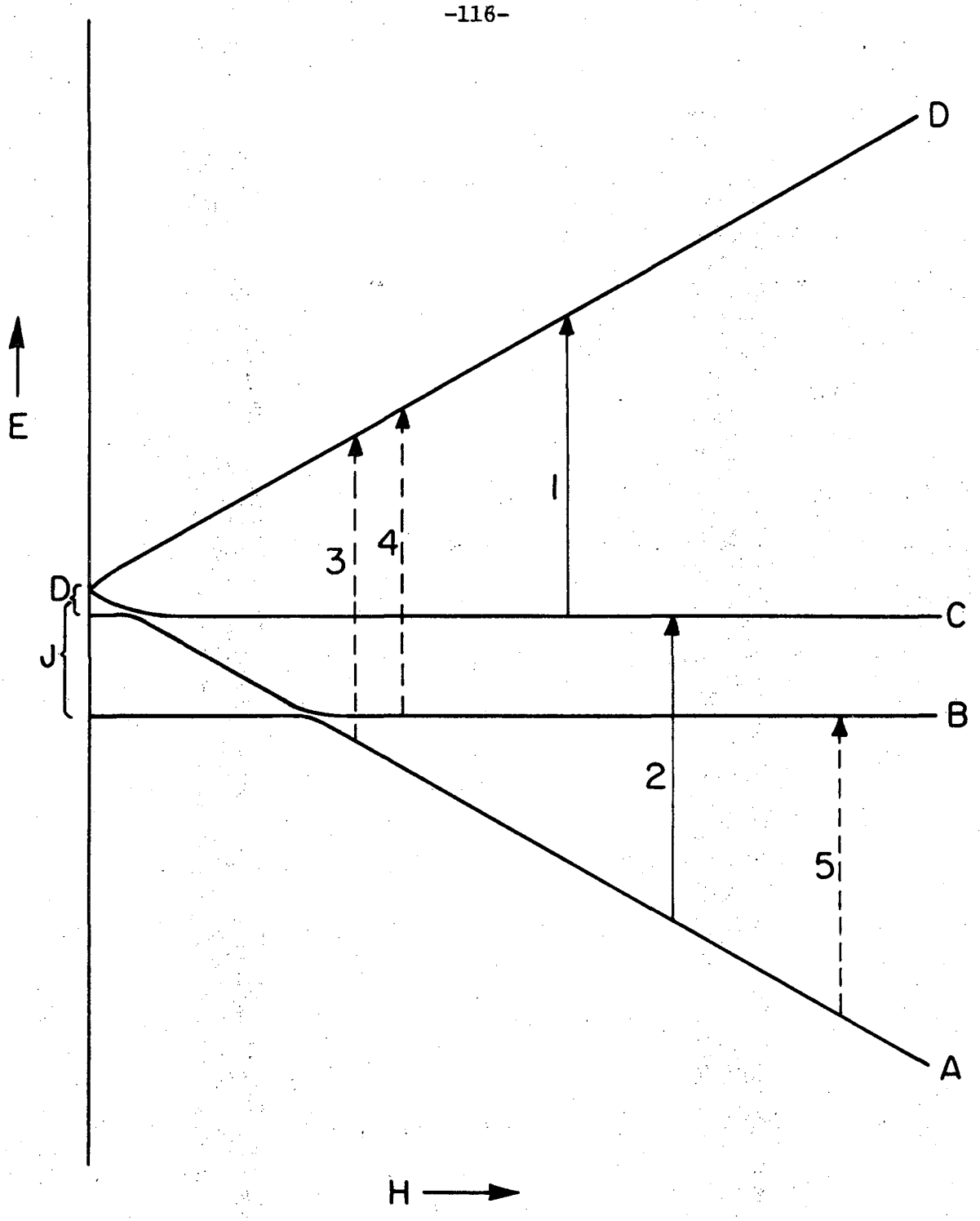

XBL 7510-7422

Fig. 16. A typical energy level pattern for a Cu^{2+}-Cu^{2+} pair as function of magnetic field. Antiferromagnetic exchange has been assumed with $h\nu > |J|$. Solid arrows indicate "allowed" transitions and dashed arrows "forbidden" transitions.

pairs since the two ions making up the pair have parallel axis systems and the same g-tensor. These pairs, which will be denoted 2-2 pairs, are all equivalent for a given layer of ions at all angles of the external magnetic field if the dipolar interaction is neglected. Pairs formed by translation along X will be called 2_x-2 and if found by a translation along Y as 2_y-2. However, next nearest neighbor pairs in different layers may be different when the Zeeman energies differ between layers. The dipolar interaction splits the four next nearest neighbors into two sets. One set arises from 2_x-2 pairs and the other from 2_y-2 pairs. Then for an arbitrary field direction, there will be two closely spaced 2-2 pairs in a given layer of ions. With the magnetic field along the c axis, all 2-2 pairs are equivalent, and the simplest spectra should again occur with this orientation. All other possible pairs are considered to be so far apart as to have a non-measurable interaction.

Experimental Results and Discussion

As previously stated the orientation of magnetic field which is expected to yield the simplest pair spectra is that when the field is along the c axis. In this orientation only one type of nearest neighbor pair (1-2 and 3-2) as well as only one type of next nearest neighbor pair (2-2) exists. In order to assign the observed lines, it is helpful to refer to a typical energy level scheme for a pair of coupled spin 1/2 ions as in Fig. 16. In Fig. 16, it has been assumed that $h\nu > |J|$. The dashed arrows indicate the transition is "forbidden" and the solid a-rows indicate an "allowed" transition. The exchange has been arbitrarily assumed to be antiferromagnetic. If

the exchange was ferromagnetic, the singlet and triplet would have their order inverted, but the qualitative features of the transitions would remain the same. This fact points out that it is difficult to obtain the sign of the exchange interaction from the line positions. For isotropic exchange the splitting D arises soley from the dipolar interaction and is, therefore, relatively small for the distances involved, $<0.01\ cm^{-1}$. Because of this, transitions 1 and 2 should lie very close to the single ion transitions, and only the outer lines of these transition's hyperfine patterns are expected to be observable. Transitions 1 and 2 are also the "allowed" ones and will be the strongest of the pair transitions. Transitions 4 and 5 are the called singlet-triplet transitions and are most direct measure of $|J|$. However, they are also "forbidden" and are expected to be weak. Transition 3 is the $\Delta M_s = 2$ transition within the triplet and as such is expected also to be very weak. With this preface of what might be expected for the Cu^{2+}-Cu^{2+} pair, the observed spectra will be discussed in terms of the transitions enumerated in this paragraph.

The c Axis Spectral Features. Feature 1. Just outside the single ion quartet on both sides, one and a half lines with about 1/100 the intensity of the single ion lines are found. The separation between the outer line and the half line as measured from the observable feature of the half line to the equivalent position of the outer line is $A_c/2$. The outer lines are at 3127±5 gauss and 2682±5 gauss at 9.55133 GHz and 77°K. These are by far the strongest non-single ion lines.

Feature 2. Outside of and apparently partially overlapping the features of 1, a jumble of lines occur. No measurements were made on these lines. The intensity of these lines are down by at least a factor of 10 from feature 1.

Feature 3. The third feature is the most striking. It is a well defined septet structure of lines. The center of the septet as measured from the center line is at 1450±1 gauss (9.24182 GHz and 4.2°K) and 1420±10 gauss (9.01109 GHz and 1.3°K). The intensity is very small, approximately 1/100 of feature 1. The spacing between the individual septet lines is $\sim A_c/2$. The intensity ratios of the septet are about 1.00:2.07:3.00:3.54:3.07:2.46:1.23.

An electron in contact with two nuclei of spin 3/2 and with the same coupling constant produces a pattern of seven lines in the ratio 1:2:3:4:3:2:1 if the ratio of the exchange to the coupling constant (J/A) is 100 or greater (Culvahouse, Schinke and Pfortmiller, 1969). Thus, the septet described as feature 3 certainly arises from a pair of copper ions. On the assumption $h\nu > |J|$, the position of the septet below the single ion lines and its low intensity suggest that it is either transition 3 or 4. These may be distinguished by the hyperfine splitting. Transition 3 is expected to have the same splitting as the single ion, A_c, and 4 should have half of this, $A_c/2$. The latter is observed and the septet is assigned to transition 4. The observation of the septet center at the two frequencies show an increase of the transition field with frequency which supports the assumption the $h\nu > |J|$. A search for the other singlet-triplet transition, 5, was unsuccessful. This may be explained by realizing that the transition

probability will have the Zeeman energy in the denominator to first order and will, therefore, decrease as the field is increased.

The lines of feature 1 are assumed to be the outer lines of transitions 1 and 2 which have been slightly shifted away from the single ion resonances by the dipolar interaction. The fact that the separation of the lines is $A_c/2$ implies that the total pattern is a septet. These two satellites described as feature 1 are, therefore, assigned to transitions 1 and 2 associated with the septet of feature 3. The jumble of lines called feature 2 were not investigated along the c axis and their origin will be postponed until discussion of the a axis.

Since the ab plane orientation is experimentally the simplest to work in, the most detailed information was obtained in this direction. The a axis is qualitatively the same as the c axis.

The a Axis Spectral Features. Feature 1. Strong satellites were found on either side of the single ion hyperfine pattern. As along the c axis, only the outer 1-1/2 lines of an apparent septet are observable. Measurements of the outer lines are

3268±5 gauss at 9.43012 GHz and 77°K

2883±5 gauss

3393±1 gauss at 9.7656 GHz and 77°K

3010±1 gauss

3184±1 gauss at 9.1266 GHz and 77°K

2804±1 gauss

Where observable, the splitting between the outer line and the next line is $\sim A_a/2$.

Feature 2. Outside of the strong satellites appears a jumble of many overlapping lines. On the low field side of the single ion spectra, the complex hyperfine pattern begins at 2500 gauss (top of the 1st peak and at 9.12604 GHz and 77°K) and extends into the strong satellite lines at ~2704 gauss. This must be nearly all of a hyperfine pattern since the width along the a axis will be ~210 gauss. An average of the high and low value yields a center at 2602 gauss. A similar feature occurs on the high field side of the single ion resonance. Here, the pattern begins at 3497 gauss and continues down to 3265 gauss (at 9.1259 GHz and 77°K) with an average of 3381 gauss.

Feature 3. At approximately half the single ion resonance field, a weak septet with a hyperfine spacing $\sim A_a/2$ is seen. Measurements of the center are

1493±1 gauss at 9.1254 GHz and 77°K

1483±1 gauss at 9.01109 GHz and 1.3°K

The interpretation of features 1 and 3 along the a axis is the same as features 1 and 3 along the c axis previously given. However, a problem exists here. The dipole interaction is expected to break the degeneracy of the 1-2 and 3-2 pairs along the a axis, and because of this, a clean septet is not expected. Calculations indicate that the dipolar interaction of these two pairs is significantly different to cause problems. This aspect is not yet understood.

As pointed out by Culvahouse, Schinke, and Pfortmiller (1969), when the exchange interaction is of the order of magnitude of the hyperfine interaction, the hyperfine pattern is no longer simple and in general, can be very complex. For this

reason, the weak satellites are attributed to the 4 and 5 transitions of a pair with a much smaller exchange than the pair which presumably gives rise to features 1 and 3. The intensities of these 4 and 5 transitions are weak as they should be, and the 1 and 2 lines of this weak exchange pair are not shifted enough from the single ion lines to be observable.

On the basis of distance, the strong satellites and the septet (features 1 and 3) are assigned to the 1-2 and 3-2 pairs, and the weak satellites (feature 2) are assigned to 2-2 pairs. As the field is rotated in the ab plane from the a axis to a γ axis, the strong satellites disappear under the two single ion hyperfine patterns which move apart. This would be the case if they were due to 1-2 and 3-2 pairs and not to 2-2 pairs which would remain as satellites to the single ion lines. The 1-2 and 3-2 pairs remain fairly stationary because the Zeeman interaction of one of the ions of the pair increases as the other decreases on rotation in the ab plane away from the a axis. As a result, little change in the Zeeman interaction of the 1-2 or 3-2 pair occurs. Measurements at higher frequencies (e.g., K-band) should split the single ion sets of lines apart far enough to observe the feature 1 when the magnetic field is along the γ axis. Also, the septet breaks up and along the γ axis is nearly a four line pattern. This type of behavior is expected for transition 4 of a 1-2 or 3-2 pair. The weak satellites remain outside both single ion hyperfine patterns as a 2-2 pair should do. These angular dependences reinforce the assignment of the various lines given earlier.

With the field along the γ axis, the low field weak satellite loses its jumbled appearance and is observed as set of three well resolved lines. At 9.1265 GHz and 77°K, their centers are at 2500, 2574 and 2640 gauss and are in the intensity ratio 3:2:1. This behavior is also not understood.

Cu^{2+}-Cu^{2+} Pair Calculations

From a qualitative view point the line assignment seems fairly reasonable. However, when put to the test of matching calculated spectrum with the observed spectra for a quantitative determination of parameters, the results are less satisfactory.

1-2 and 3-2 Pairs. A reasonable estimation of the magnitude of the exchange for 1-2 and 3-2 pairs can be obtained directly from the singlet-triplet transition by subtracting out the Zeeman interaction. Neglecting the dipolar interaction, the exchange value may be estimated along the a and c axes as

$$|J| = h\nu - g_{a \text{ or } c}\beta H \qquad \text{(A3-9)}$$

Table XVI gives the value of J calculated in this way. The magnitude of J calculated for the two directions support the assumption of isotropic exchange.

From Table XVI it can be seen that the exchange interaction is of the order of magnitude of the Zeeman energy for X-band measurements. This necessitated finding the transition fields by direct diagonalization of the energy matrix. For economy the hyperfine terms were neglected and only the center of the hyperfine pattern was calculated. Table XVII gives the energy matrix in the singlet-triplet representation. The

Table XVI. The magnitude of J for 1-2 or 3-2 pairs calculated by Eq. (A3-9).*

Axis	Septet Center (gauss)	g	ν (GHz)	(J) (cm^{-1})
c	1450±1	2.279	9.2418	0.154
a	1493±1	2.179	9.1254	0.153

* In most places we shall refer to -J as -2J so that we follow the convention of the previous sections.

Table XVII. Energy matrix for two dissimilar spin 1/2 ions in the singlet triplet representation.

	$\|11\rangle$	$\|1\text{-}1\rangle$	$\|10\rangle$	$\|00\rangle$
$\|11\rangle$	$1/2(g_1+g_2)\beta H$ $+1/4(D_{z_1z_2}+J_{z_1z_2})$	$1/4(D_{x_1x_2}+J_{x_1x_2})$ $-1/4(D_{y_1y_2}+J_{y_1y_2})$ $-i/4(D_{x_1y_2}+J_{x_1y_2})$ $-i/4(D_{y_1x_2}+J_{y_1x_2})$	$(D_{z_1x_2}+J_{z_1x_2})/4\sqrt{2}$ $+(D_{x_1z_2}+J_{x_1z_2})/4\sqrt{2}$ $-i(D_{z_1y_2}+J_{z_1y_2})/4\sqrt{2}$ $-i(D_{y_1z_2}+J_{y_1z_2})/4\sqrt{2}$	$(D_{z_1x_2}+J_{z_1x_2})/4\sqrt{2}$ $-(D_{x_1z_2}+J_{x_1z_2})/4\sqrt{2}$ $-i(D_{z_1y_2}+J_{z_1y_2})/4\sqrt{2}$ $+i(D_{y_1z_2}+J_{y_1z_2})/4\sqrt{2}$
$\|1\text{-}1\rangle$	C.C.	$-1/2(g_1+g_2)\beta H$ $+1/4(D_{z_1z_2}+J_{z_1z_2})$	$-(D_{z_1x_2}+J_{z_1x_2})/4\sqrt{2}$ $-(D_{x_1z_2}+J_{x_1z_2})/4\sqrt{2}$ $-i(D_{y_1z_2}+J_{y_1z_2})/4\sqrt{2}$ $-i(D_{z_iy_2}+J_{z_1y_2})/4\sqrt{2}$	$(D_{z_1x_2}+J_{z_1x_2})/4\sqrt{2}$ $-(D_{x_1z_2}+J_{x_1z_2})/4\sqrt{2}$ $-i(D_{y_1z_2}+J_{y_1z_2})/4\sqrt{2}$ $+i(D_{z_1y_2}+J_{z_1y_2})/4\sqrt{2}$
$\|10\rangle$	C.C.	C.C.	$-1/4(D_{z_1z_2}+J_{z_1z_2})$ $+1/4(D_{x_1x_2}+J_{x_1x_2})$ $+1/4(D_{y_1y_2}+J_{y_1y_2})$	$1/2(g_1-g_2)\beta H$ $-i/4(D_{x_1y_2}+J_{x_1y_2})$ $+i/4(D_{y_1x_2}+J_{y_1x_2})$

Table XVII. Continued.

	|11⟩	|1-1⟩	|10⟩	|00⟩
|00⟩	C.C.	C.C.	C.C.	$-1/4(D_{z_1z_2}+J_{z_1z_2})$ $-1/4(D_{x_1x_2}+J_{x_1x_2})$ $-1/4(D_{y_1y_2}+J_{y_1y_2})$

D's are defined by Eq. (A3-7) and the J's by Eq. (A3-8). A multitude of direction cosines have been generated and require explicit definition. In order to specify the direction cosines, a precise labeling scheme for the ions is necessary. Table XVIII gives the position of the ions and their designations. Ion 2 is the reference ion and can form a pair with any of the other four ions. The direction cosines labeled by d connect the g-tensor axis systems of the various ions to that of ion 2 and are given in Table XIX.

Some comments on notation are necessary for these direction cosines. In the previous discussion of the Hamiltonian, the reference ion was designated as ion 1, and the other member of the pair was ion 2. Thus, to use the direction cosines in the Hamiltonian equations ion 1 changes to ion 2 and ion 2 to either 1 or 3 depending on which neighbor is the other member of the pair. For the calculations of the dipolar interaction, the direction cosines of the vector connecting ion 2 to its neighbors 1 or 3 are necessary. These are given in Table XX.

The ℓ direction cosines used in Eqs. (A3-7) and (A3-8) are those connecting the g-tensor axes with the electron spin axes which diagonalize the Zeeman energy. These are given by Smith and Pilbrow (1974), p. 188. A computer program to calculate the transition fields by directly diagonalizing the energy matrix was written. Figures 17 and 18 give the calculated transition fields as function of the exchange parameter for the 3(1)-2 pair and with the magnetic field along the a axis. Figure 17 is for ferromagnetic exchange, and Fig. 18 is for antiferromagnetic exchange. The transitions are labelled according to Fig. 19 which shows the energy level pattern and transitions

Table XVIII. Nearest neighbor ion designation in the crystal (Beevers and Lipson, 1932).

Ion	X(Å)	Y(Å)	Z(Å)
2	5.498	1.462	4.623
1(1)	4.942	4.942	0.0
1(2)	4.942	-2.018	0.0
3(1)	2.018	2.018	9.245
3(2)	8.978	2.018	9.245

Table XIX. The d direction cosines for nearest neighbor pairs.*

1(1)-2 and 1(2)-2 Pairs

$d_{x_2x_1} = \sin^2\phi$	$d_{x_2y_1} = \cos\phi$	$d_{x_2z_1} = -\sin\phi\cos\phi$
$d_{y_2x_1} = -\cos\phi$	$d_{y_2y_1} = 0$	$d_{y_2z_1} = -\sin\phi$
$d_{z_2x_1} = -\sin\phi\cos\phi$	$d_{z_2y_1} = \sin\phi$	$d_{z_2z_1} = \cos^2\phi$

3(1)-2 and 3(2)-2 Pairs

$d_{x_2x_3} = \sin^2\phi$	$d_{x_2y_3} = -\cos\phi$	$d_{x_2z_3} = -\sin\phi\cos\phi$
$d_{y_2x_3} = \cos\phi$	$d_{y_2y_3} = 0$	$d_{y_2y_3} = \sin\phi$
$d_{z_2x_3} = -\sin\phi\cos\phi$	$d_{z_2y_3} = -\sin\phi$	$d_{z_2z_3} = \cos^2\phi$

*The angle ϕ is the angle between the crystal c axis and the tetragonal axis of the ions. The angle $\phi = 43.3°$ for Cu^{2+} in $ZnSeO_4 \cdot 6H_2O$ (Jindo and Myers, 1972).

Table XX. Direction cosines of the vector connecting ion 2 with its nearest neighbors (referenced to ion 2).

Pair	σ_x	σ_y	σ_z
1(1)-2	0.2865	-0.4909	-0.8227
1(2)-2	0.9026	0.3558	-0.2422
3(1)-2	-0.2865	-0.4909	0.8227
3(2)-2	-0.9026	0.3558	0.2422

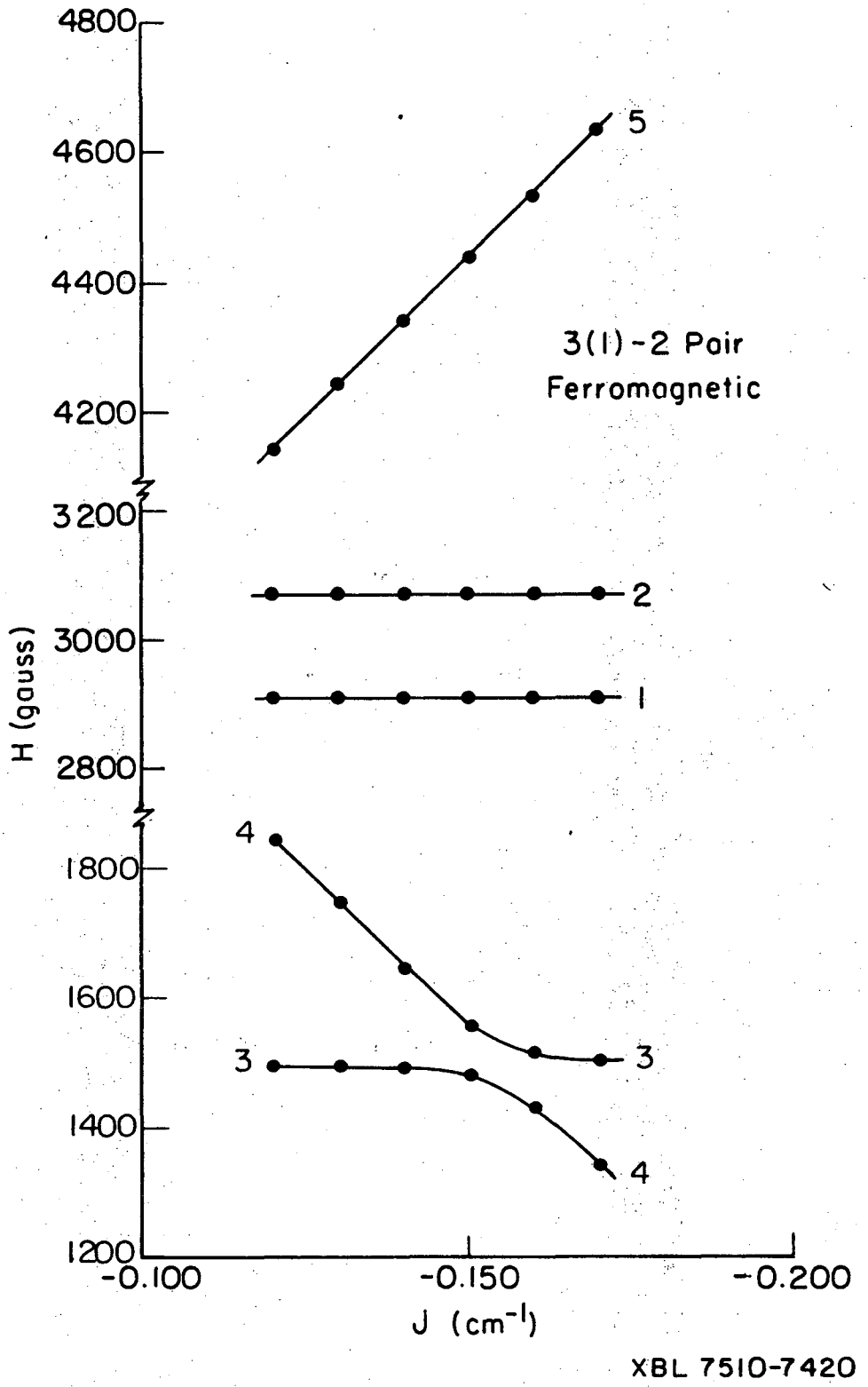

Fig. 17. The transition field for a 3(1)-2 Cu^{2+}-Cu^{2+} pair are plotted as a function of a ferromagnetic exchange parameter. The numbering is from Fig. 19. The exchange value J is from the Hamiltonian $J(S_1 \cdot S_2)$, and $\nu = 9.1260$ GHz.

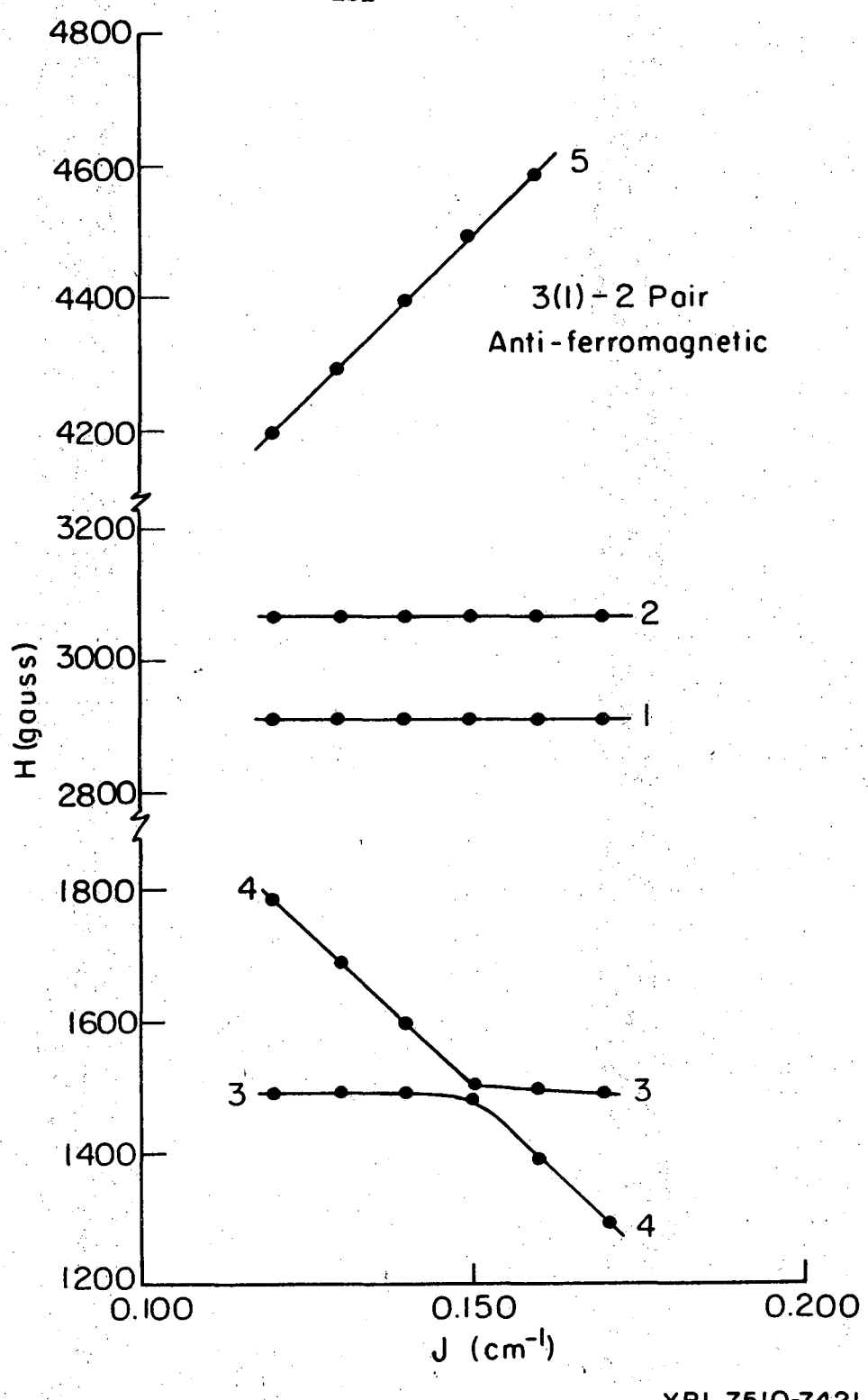

Fig. 18. The transition fields for a 3(1)-2 Cu^{2+}-Cu^{2+} pair are plotted as a function of an antiferromegnetic exchange parameter. The numbering of the transitions is from Fig. 19. The exchange value J is from the Hamiltonian $J(S_1 \cdot S_2)$, and ν = 9.1260 GHz.

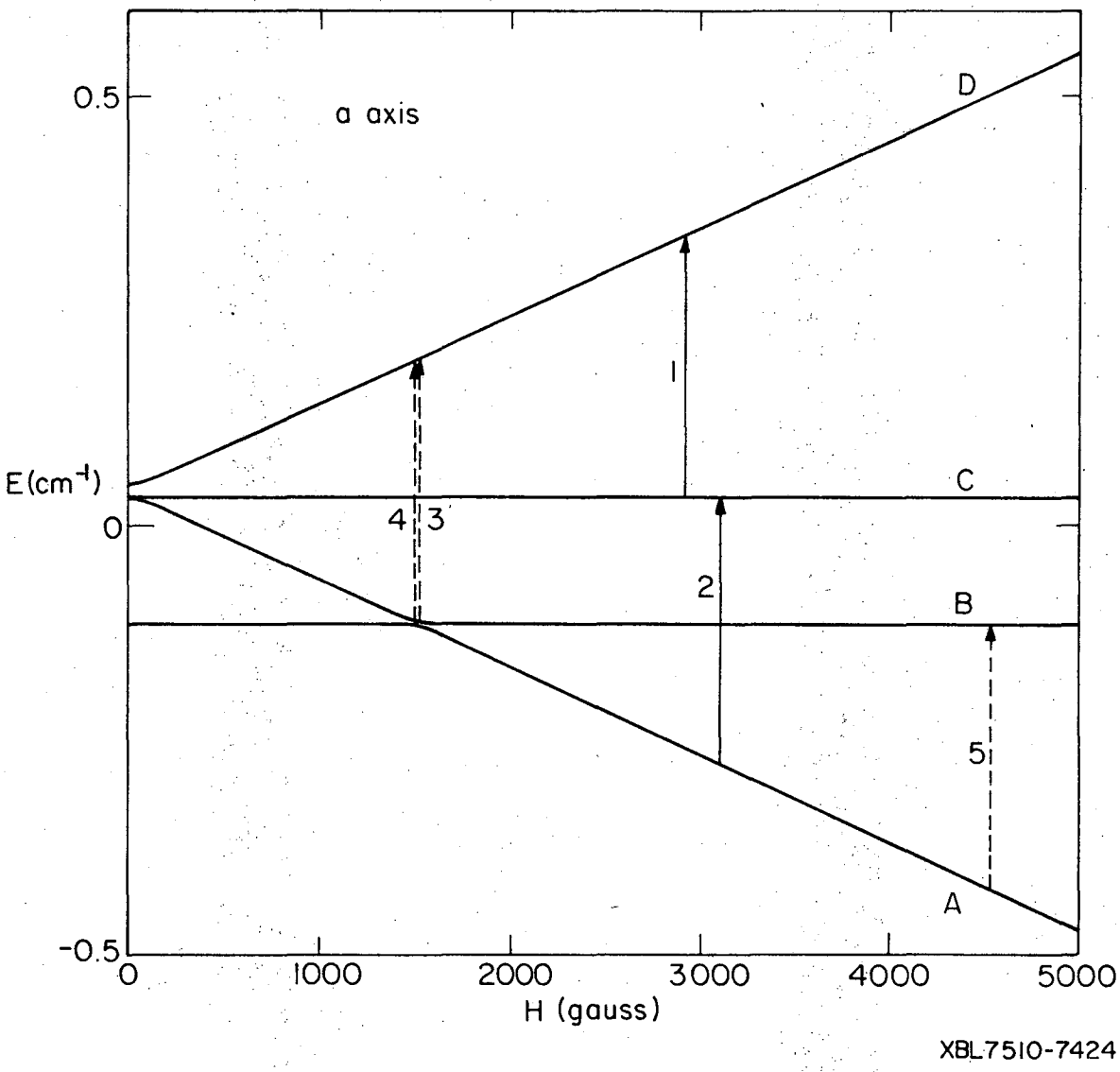

Fig. 19. The calculated energy level pattern for a Cu^{2+}-Cu^{2+} 3(1)-2 pair as a function of magnetic field. The field is oriented along the a axis. The plot is calculated with $-2J = +0.150\ cm^{-1}$. The transitions are shown for $\nu = 9.1260$ GHz. The dashed arrows are "forbidden" transitions and the solid arrows are "allowed" ones.

calculated for an exchange of $-2J = +0.150\ cm^{-1}$. Due to the non-crossing of energy levels, the lowest field transition in Figs. 17 and 18 begins as transition 3 and then becomes transition 4. Likewise, the next transition starts as 4 and transforms into 3. As can be seen from the figures, the only transitions which are strongly effected by the size of the exchange are the singlet-triplet transitions, 4 and 5. This implies that the transitions 1 and 2 are shifted from the single ion resonance only by the dipolar interaction. It was hoped that the exchange parameter could be read off the graph by taking the J which corresponded to observed singlet-triplet transition, 4. However, the appropriate observed transition field occurs right in the cross over region and makes the value of J less certain. Transition 5 would be amendable to this procedure, but it was never observed.

All the above calculations apply to 3-2 pairs. The 1-2 pairs have a different dipolar interaction with the magnetic field along the a axis. Their 1 and 2 transitions are calculated to be almost exactly on top of the single ion spectra and are not expected to be observable. Because of the difference in the dipolar energy between the 1-2 and 3-2 pairs, the clean septet which is observed is somewhat unexpected. The calculation would indicate that two septets slightly displaced from one another would result, most likely in complicated hyperfine pattern. One could imagine that the singlet-triplet transition draws in intensity from the dipolar interaction mixing small amounts of wavefunctions. This would allow the 3-2 pairs some intensity but not the 1-2 pairs resulting in only a spectra from the 3-2 pairs.

The fact that the septet hyperfine spacing is $A_a/2$ rather than A_a definitely means that the transition arises from the singlet-triplet transition. Therefore, the position on graph chosen for transition 4 in the cross over region must be strongly sloping. On this basis, the antiferromagnetic exchange gives the best fit. This is the only indication of the sign of J since equally good agreement is obtained for transitions 1 and 2 for both antiferromagnetic and ferromagnetic exchange. Table XXI gives the best values calculated along with the observed line centers.

Similar results are obtained from the spectra obtained with the magnetic field along the c axis. Measurements at a significantly different frequency are needed to avoid the crossover problem. To summarize, the most consistent behavior is found for an antiferromagnetic nearest neighbor exchange interaction of magnitude $-2J = 0.150\ cm^{-1}$ between two neighbor Cu^{2+} ions in $ZnSeO_4 \cdot 6H_2O$.

2-2 Pairs. The complicated structure lying outside the strong satellites which have been denoted as the weak satellites cannot be attributed to any of the 1-2 or 3-2 pair transitions. Their complicated structure is typical of hyperfine structures resulting when the exchange is of the order of magnitude of the hyperfine coupling constant. The most likely origin of these lines are the 4 and 5 transitions of a 2-2 pair. The 2-2 pairs are similar pairs, and the indication from the hyperfine pattern is that the exchange value is smaller than the 1-2 pairs as expected on distance and superexchange pathways grounds. Under these conditions the second order equations derived by Smith and Pilbrow (1974) are directly applicable. Their

Table XXI. Comparison of calculated and observed transitions for 3(1)-2 pair with the magnetic field along the a axis and an isotropic exchange of $-2J = +0.150\ cm^{-1}$.

Transition	Observed (gauss)*	Calculated
1	2909±5	2914
2	3079±5	3069
3	------	1480
4	1493±3	1507
5	------	4489

procedure is to take the energy matrix in the simple product representation and diagonalize the nearly degenerate $|+1/2,-1/2\rangle$ and $|-1/2,+1/2\rangle$ states exactly. Once this is done second order perturbation theory can be safely employed.

The transition fields using the basic form of Smith and Pilbrow are as follows

Transition 1

$$H_1 = H_o + \left\{-D'_{zz}/2 - K(m_1 + m_2)/2 + \Phi - \left[2\left(S_1^2 + S_2^2\right)\right.\right. \qquad \text{(A3-10)}$$
$$\left.\left. + 1/2\left(S_3^2 + S_4^2\right) + \left(S_7^2 + S_8^2\right) - \left(S_5^2 + S_6^2\right)\right] /h\nu\right\}/g\beta$$

Transition 2

$$H_2 = H_o + \left\{D'_{zz}/2 - K(m_1 + m_2)/2 - \Phi - \left[-\left(S_1^2 + S_2^2\right)\right.\right. \qquad \text{(A3-11)}$$
$$\left.\left. + 1/2\left(S_3^2 + S_4^2\right) + 2\left(S_5^2 + S_6^2\right) + \left(S_9^2 + S_{10}^2\right)\right] /h\nu\right\}/g\beta$$

Transition 3

$$H_3 = H_o + \left\{-D'_{zz}/2 - K(m_1 + m_2)/2 - \phi - \left[\left(S_1^2 + S_2^2\right)\right.\right. \qquad \text{(A3-12)}$$
$$\left.\left. + 1/2\left(S_3^2 + S_4^2\right) + 2\left(S_7^2 + S_8^2\right) - \left(S_9^2 + S_{10}^2\right)\right] /h\nu\right\}/g\beta$$

Transition 4

$$H_4 + H_o + \left\{D'_{zz}/2 - K(m_1 + m_2)/2 + \Phi - \left[-\left(S_7^2 + S_8^2\right)\right.\right. \qquad \text{(A3-;3)}$$
$$\left.\left. + 1/2\left(S_3^2 + S_4^2\right) + \left(S_5^2 + S_6^2\right) + 2\left(S_9^2 + S_{10}^2\right)\right] /h\nu\right\}/g\beta$$

For axial symmetry and similar ions the symbols have these definitions.

$$H_o = h\nu/g\beta \; ; \; g^2 = g_{\parallel}^2\cos^2\theta + g_{\perp}\sin^2\theta$$

$$K^2 = (A_{\parallel}^2 g_{\parallel}^2\cos^2\theta + A_{\perp}^2 g_{\perp}^2\sin^2\theta)/g^2$$

$$D'_{zz} = D_{zz} - J$$

$$\Phi = \{[1/4(D_{xx} + D_{yy}) - 1/2\ J]^2 + 1/4\ k^2(m_1 - m_2)^2\}^{1/2}$$

$$S_1 = (UD_{zx} + bD_{xz})/4 + (U\tau_4 m_2 + b\tau_4 m_1)/2$$

$$S_2 = (-UD_{zy} - bD_{yz})/4$$

$$S_3 = (D_{xx} - D_{yy})/_4$$

$$S_4 = -(D_{xy} + D_{yx})/4$$

$$S_5 = (-UD_{xz} - bD_{zx})/4 + (U\tau_1 m_1 + b\tau_4 m_2)/2$$

$$S_6 = (UD_{yz} + bD_{zy})/4$$

$$S_7 = (WD_{zx} + dD_{xz})/4 + (W\tau_4 m_2 + d\tau_4 m_1)/2$$

$$S_8 = (-WD_{zy} - dD_{yz})/4$$

$$S_9 = (-WD_{xz} - dD_{zx})/4 + (W\tau_4 m_1 + d\tau_4 m_2)/2$$

$$S_{10} = (-WD_{yz} - dD_{zy})/4$$

$$U = [1/4(D_{xx} + D_{yy}) - 1/2\ J]/f_1$$

$$W = [1/4(D_{xx} + D_{yy}) - 1/2\ J]\ f_2$$

$$b = [\Phi - 1/2\ K(m_1 - m_2)]/f_1$$

$$d = [-\Phi - 1/2\ K(m_1 - m_2)]/f_2$$

$$f_1 = \{[1/4(D_{xx} + D_{yy}) - 1/2\ J]^2 + [\Phi - 1/2\ K(m_1 - m_2)]^2\}^{1/2}$$

$$f_2 = \{[1/4(D_{xx} + D_{yy}) - 1/2\ J]^2 + [-\Phi - 1/2\ K(m_1 - m_2)]^2\}^{1/2}$$

The D's are defined as in Eq. (A3-7) with the direction cosines of $\vec{r}$ given in Table XXII. The complex hyperfine pattern can be seen to be the result of the term Φ. For large J, Φ is not effected by the hyperfine term, and the pattern is determined by the term $-K(m_1 + m_2)/2$. This leads to a pattern derived as if it arose from a total nuclear spin of $m_1 + m_2$ and a hyperfine splitting 1/2 as large as the single ion splitting. For copper with m = 3/2, a septet is produced. If $J << A$, the Φ term is due almost entirely to the hyperfine energy which may be added to the first order term $-K(m_1 + m_2)/2$. This yields a sum only in one of the m's (1 or 2) resulting in a four line hyperfine pattern. When J and A are of comparable magnitude, the hyperfine pattern is changing from the quartet to the septet, and a complicated pattern results which is very sensitive to the exchange parameter. Thus, the center of the pattern as well as the structure of the hyperfine pattern are indicative of the exchange interaction.

Along the a axis, their are two types of 2-2 pairs by virtue of the fact that there are two different dipolar energies possible. Because of this, the already complicated hyperfine pattern is further complicated by the overlap of two nearly equivalent spectra slightly displaced from one another by the slightly different dipolar interactions. This makes it very difficult to determine a center for the weak satellite lines. The centers were taken as an average of the start and finish of the observed pattern for the a axis spectra. Table XXIII gives the calculated and observed centers for both ferromagnetic and antiferromagnetic exchange. Figure 20 gives the energy vs field plot and transitions for representative values of a 2-2 pair.

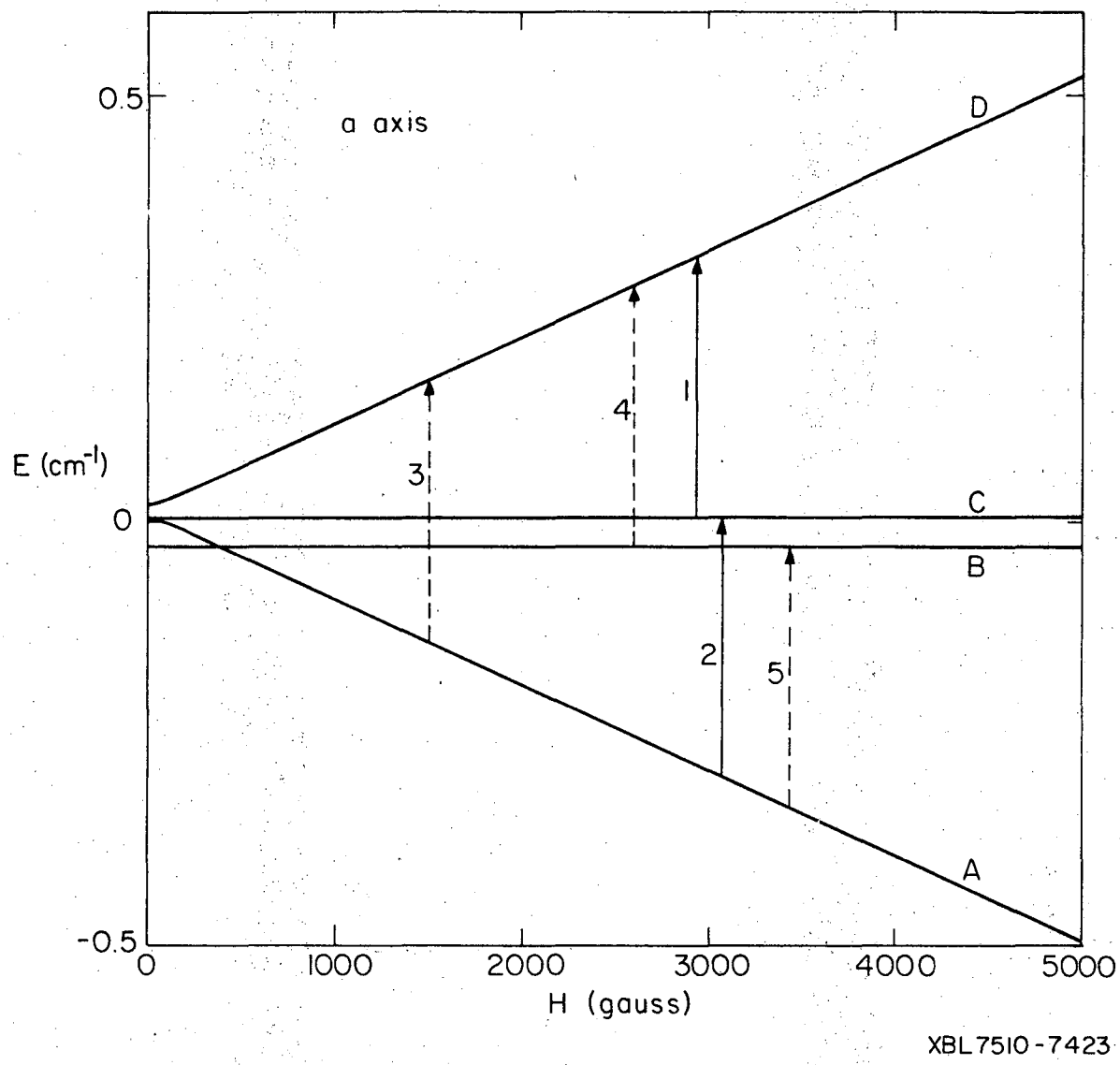

Fig. 20. The calculated energy level pattern for a Cu^{2+}-Cu^{2+} 2_x-2 pair as a function of magnetic field. The field is oriented along the a axis. The plot is calculated for $-2J = +0.038$ cm^{-1}, and the transitions are shown for = 9.1260 GHz. The dashed arrows are "forbidden" transitions and the solid arrows are "allowed" ones.

Table XXII. The direction cosines of the vector connecting ion 2 with its next nearest neighbors (referenced to ion 2).

Pair	σ_x	σ_y	σ_z
2_x-2	-0.5146	0.7071	-0.4849
2_y-2	-0.5146	-0.7071	-0.4849
2_{-x}-2	0.5146	-0.7071	0.4849
2_{-y}-2	0.5146	0.7071	0.4849

Table XXIII. Calculated and observed centers for 2-2 pairs for the a axis spectra.

	Observed**	Calc. (ferro)	Calc. (Antiferro)
Transition 4 (gauss)*	2602±20	2602	2601
Transition 5 (gauss)	3381±20	3372	3377
-2J (cm^{-1})	-------	-0.042	+0.038

*Labeled according to Fig. 20.

**ν = 9.126 GHz and T = 77°K.

With the magnetic field along the γ axis, only one type of 2-2 pair exists for each single ion of which there are two. As stated previously, the weak satellite on the low field side of the low field single ion (γ ion) appears as a very clear set of 3 lines in the ratio 3:2:1. Taking these to be three of the four lines, the center can be determined. Table XXIV gives the best calculated and the observed values for this satellite.

Equally good agreement can be gotten for all the above lines centers using either ferromagnetic or antiferromagnetic exchange. Because of this, the sign of J is indeterminate for the 2-2 pairs. Several problems still exist. The first is that the exchange value determined by the center calculations does not give the observed hyperfine pattern when a simulation is preformed. For the γ axis satellite given in Table XXIV, the hyperfine pattern is reproduced if J << K which cannot give the correct pattern center. Also, a different J is needed for the two directions studied. Both these problems could theoretically be taken care of by a highly anisotropic exchange interaction, but no progress along these lines was made. The problem of the 2-2 pairs is still not fully understood.

$\underline{Ni^{2+}\text{-}Ni^{2+}\ \text{Pairs in}\ ZnSeO_4\cdot 6H_2O}$

The spectroscopy of pairs of ions with spins greater than 1/2 is fairly sparse. Only two reports of Ni^{2+}-Ni^{2+} pairs have been made (Dixon and Culvahouse, 1971; Altshuler and Valishev, 1965). The reason for the sparsity is the complexity in the number of lines accompanying the larger spin degeneracy and specifically for Ni^{2+}, the large zero-field splittings which are common. Also, additional higher order exchange

Table XXIV. Calculated and observed center for the low field weak satellite lines along the γ axis.

	Observed**	Calc. (ferro)	Calc. (Antiferro)
Transition 4 (gauss)*	2607±4	2612	2607
$-2J$ (cm^{-1})	------	-0.028	+0.030

*Labeled according to Fig. 20.

**ν = 9.126 GHz and 77°K

terms are sometimes found necessary which adds additional parameters to be determined. The work on the Ni^{2+}-Ni^{2+} pairs in $ZnSeO_4 \cdot 6H_2O$ to be presented is quite imcomplete and only tentative assignment of the lines will be given.

The Spin Hamiltonian

As with the Cu^{2+}-Cu^{2+} pairs, the spin Hamiltonian will be assumed to be the sum of the single ion Hamiltonians, as determined from dilute spectroscopy, and the exchange and dipolar interactions. The single ion Hamiltonians are given as usual by

$$\mathcal{H}_i = \beta \vec{H} \cdot \overleftrightarrow{g}_i \cdot \vec{S}_i + D S_{zi}^2 \qquad \text{(A3-14)}$$

Ni^{2+} also has an orbital singlet ground state which should again make the assumption of isotropic exchange reasonable. Apologizing for the inconsistency in nomenclature, which also exists in the literature, the exchange Hamiltonian for the pair calculations is taken in this case as

$$\mathcal{H}_{ex} = J \vec{S}_1 \cdot \vec{S}_2 \qquad \text{(A3-15)}$$

and the dipolar Hamiltonian as

$$\mathcal{H}_d = \frac{g^2 \beta^2}{r^3} \left[(\vec{S}_1 \cdot \vec{S}_2) - 3 \frac{(\vec{S}_1 \cdot \vec{r})(\vec{S}_2 \cdot \vec{r})}{r^2} \right] \qquad \text{(A3-16)}$$

The value of g for Ni^{2+} is nearly isotropic and is taken as such for the dipolar term. The tact to be followed is to express the Hamiltonian in an appropriate representation and to computer diagonalize the Hamiltonian to find the transition fields. The exchange value can then be varied until agreement is found for the line positions.

From the work of the previous sections and the thermodynamic work of Fisher and Hornung (1960), the exchange interaction is expected to be of the order of a few tenths of a wavenumber. On this basis, the predominate term in the spin Hamiltonian will be the zero-field splitting, D, which is 4.20 cm^{-1} (Jindo and Myers, 1972). To a good approximation the spins will remain quantized along the tetragonal crystal field axis and will remain almost fixed for all orientations of the magnetic field due to the large size of D. This approximation will be assumed valid from this point on.

The fact that the spins remain essentially quantized along the tetragonal crystal field axis has a major effect on the pair situation. Since the spin axis is fixed in this approximation, the dipolar and exchange terms remain fixed for all directions of the magnetic field. This quite unlike the copper case where the spins essentially follow the field and change their orientation with respect to $\vec{r}$. Because of the spin axis fixed nature, only one type of nearest neighbor pair exists which will be designated a 1-2 pair. This is true for the ac and ab planes where the Zeeman energy of the 1-2 and 3-2 pairs remains the same.

Because of the size of D, it is desirable to choose wavefunctions for the single ion parts of the Hamiltonian which are quantized along the tetragonal axes. The pair wavefunctions can then be chosen as product functions of these single ion wavefunctions. The single ion Hamiltonians for the pair are given by

$$\mathcal{H} = g_{\parallel}\beta H_{z1}S_{z1} + g_{\perp}\beta[H_{x1}S_{x1} + H_{y1}S_{y1}] + DS_{z1}^2 + g_{\parallel}\beta H_{z2}S_{z2} + g_{\perp}\beta[H_{x2}S_{x2} + H_{y2}S_{y2}] + DS_{z2}^2 \qquad \text{(A3-17)}$$

which is given in the product representation by Table XXV.

To express the isotropic exchange interaction in the product representation necessitates specifying the coordinate system in which it is written. The exchange Hamiltonian is chosen to be written in the crystal coordinate system as defined by previously by Batchelder (1970). To express the spin operators of the exchange interaction in terms of the ion coordinate systems requires the following rotations

$$\begin{pmatrix} S'_{x1} \\ S'_{y1} \\ S'_{z1} \end{pmatrix} = \begin{pmatrix} \cos\phi & 0 & -\sin\phi \\ 0 & 1 & 0 \\ \sin\phi & 0 & \cos\phi \end{pmatrix} \begin{pmatrix} S_{x1} \\ S_{y1} \\ S_{z1} \end{pmatrix}$$

$$\begin{pmatrix} S'_{x2} \\ S'_{y2} \\ S'_{z2} \end{pmatrix} = \begin{pmatrix} 0 & 1 & 0 \\ 0 & -\cos\phi & -\sin\phi \\ 0 & -\sin\phi & \cos\phi \end{pmatrix} \begin{pmatrix} S_{x2} \\ S_{y2} \\ S_{z2} \end{pmatrix}$$

The angle ϕ is the angle between the tetragonal crystal field axis and the crystal c axis. The primed operators are in the crystal coordinate system and the unprimed are in either the crystal field coordinate system of ion 1 or 2. Having preformed these rotations, the exchange Hamiltonian, Eq. (A3-15), becomes using the lowering and raising operators

Table XXV. 1-2 nickel pair zeeman and zero-field Hamiltonian in the product representation.

	$\|11\rangle$	$\|10\rangle$	$\|01\rangle$	$\|1\text{-}1\rangle$	$\|00\rangle$	$\|\text{-}11\rangle$	$\|\text{-}10\rangle$	$\|0\text{-}1\rangle$	$\|\text{-}1\text{-}1\rangle$
$\|11\rangle$	$2D+G_{z1}+G_{z2}$	$G_{x2}-iG_{y2}$	$G_{x1}-iG_{y1}$	0	0	0	0	0	0
$\|10\rangle$	C.C.	$D+G_{z1}$	0	$G_{x2}-iG_{y2}$	$G_{x1}-iG_{y1}$	0	0	0	0
$\|01\rangle$	C.C.	C.C.	$D+G_{z2}$	C.C.	$G_{x2}-iG_{y2}$	$G_{x1}-iG_{y1}$	0	0	0
$\|1\text{-}1\rangle$	C.C.	C.C.	C.C.	$2D+G_{z1}-G_{z2}$	0	0	0	$G_{x1}-iG_{y1}$	0
$\|00\rangle$	C.C.	C.C.	C.C.	C.C.	0	0	$G_{x1}-iG_{y1}$	$G_{x2}-iG_{y2}$	0
$\|\text{-}11\rangle$	C.C.	C.C.	C.C.	C.C.	C.C.	$2D-G_{z1}+G_{z2}$	$G_{x2}-iG_{y2}$	0	0
$\|\text{-}10\rangle$	C.C.	C.C.	C.C.	C.C.	C.C.	C.C.	$D-G_{x1}$	0	$G_{x2}-iG_{y2}$
$\|0\text{-}1\rangle$	C.C.	C.C.	C.C.	C.C.	C.C.	C.C.	C.C.	$D-G_{2z}$	$G_{x1}-iG_{y2}$
$\|\text{-}1\text{-}1\rangle$	C.C.	C.C.	C.C.	C.C.	C.C.	C.C.	C.C.	C.C.	$2D-G_{z1}-G_{z2}$

C.C. ≡ Complex $G_{z1} = g_{\|}\beta H_{z1}$ $G_{x1} = g_{\perp}\beta H_{x1}/\sqrt{2}$ $G_{y1} = g_{\perp}\beta H_{y1}/\sqrt{2}$

Conjugate $G_{z2} = g_{\|}\beta H_{z2}$ $G_{x2} = g_{\perp}\beta H_{x2}/\sqrt{2}$ $G_{y2} = g_{\perp}\beta H_{y2}/\sqrt{2}$

$$\mathcal{H}_{ex} = J\Big[S_{z1}S_{z2}\cos^2\phi + S_1^+S_2^+(1/4\ \sin^2\phi) + S_1^-S_2^-(1/4\ \sin^2\phi) \qquad \text{(A3-12)}$$

$$+ S_1^+S_2^-(1/4\ \sin^2\phi + i/2\ \cos\phi) + S_1^-S_2^+(1/4\ \sin^2\phi - i/2\ \cos\phi)$$

$$+ S_{1z}S_2^+(-1/2\ \cos\phi\sin\phi - i/2\ \sin\phi) + S_{1z}S_2^-(-1/2\ \cos\phi\sin\phi + i/2\ \sin\phi)$$

$$+ S_1^+S_{z2}(-1/2\ \cos\phi\sin\phi + i/2\ \sin\phi) + S_1^-S_{z2}(-1/2\ \cos\phi\sin\phi - i/2\ \sin\phi)$$

In the product representation Eq. (A3-18) is given in Table XXVI.

Expressing the dipolar interaction in the crystal coordinates requires the same rotations of the spin operators into the ion coordinate systems. The first part of the dipolar interaction is analogous to the exchange interaction and may be incorporated into it. The second part is best handled by expressing $\vec{r}$ in polar coordinates.

$$x = r\sin\alpha\cos\beta$$

$$y = r\sin\alpha\sin\beta$$

$$z = r\cos\alpha$$

The angles α and β are polar coordinate angle of r in the crystal coordinate system. This allows the r dependence to cancel leaving only the angular factors. The second part of the dipolar interaction may then be written in the ion coordinates as

$$\frac{(\vec{S}_1'\cdot\vec{r})(\vec{S}_2'\cdot\vec{r})}{r^2} = \vec{S}_1\cdot\overleftrightarrow{C}\cdot\vec{S}_2 \qquad \text{(A3-19)}$$

The components of the C tensor are as follows

Table XXVI. 1-2 nickel pair isotropic exchange Hamiltonian in the product representation.

	$\|11\rangle$	$\|10\rangle$	$\|01\rangle$	$\|1\text{-}1\rangle$	$\|00\rangle$	$\|\text{-}11\rangle$	$\|\text{-}10\rangle$	$\|0\text{-}1\rangle$	$\|\text{-}1\text{-}1\rangle$
$\|11\rangle$	$J\cos^2\phi$	$-J\cos\phi\sin\phi/\sqrt{2}$ $-iJ\sin\phi/\sqrt{2}$	$-J\cos\phi\sin\phi/\sqrt{2}$ $+iJ\sin\phi/\sqrt{2}$	0	$J\sin^2\phi/2$	0	0	0	0
$\|10\rangle$	C.C.	0	$J\sin^2\phi/2$ $+iJ\cos\phi$	$-J\cos\phi\sin\phi/\sqrt{2}$ $-iJ\sin\phi/\sqrt{2}$	0	0	0	0	0
$\|01\rangle$	C.C.	C.C.	0	0	0	$-J\cos\phi\sin\phi/\sqrt{2}$ $+iJ\sin\phi/\sqrt{2}$	$J\sin^2\phi/2$	0	0
$\|1\text{-}1\rangle$	C.C.	C.C.	C.C.	$-J\cos^2\phi$	$J\sin^2\phi/2$ $+iJ\cos\phi$	0	0	$-J\cos\phi\sin\phi/\sqrt{2}$ $-iJ\sin\phi/\sqrt{2}$	0
$\|00\rangle$	C.C.	C.C.	C.C.	C.C.	0	$J\sin^2\phi/2$ $+iJ\cos\phi$	0	0	$J\sin^2\phi/2$
$\|\text{-}11\rangle$	C.C.	C.C.	C.C.	C.C.	C.C.	$-J\cos^2\phi$	$J\cos\phi\sin\phi/\sqrt{2}$ $+iJ\sin\phi/\sqrt{2}$	0	0
$\|\text{-}10\rangle$	C.C.	C.C.	C.C.	C.C.	C.C.	C.C.	0	$J\sin^2\phi/2$ $-iJ\cos\phi$	$J\cos\phi\sin\phi/\sqrt{2}$ $+iJ\sin\phi/\sqrt{2}$
$\|0\text{-}1\rangle$	C.C.	C.C.	C.C.	C.C.	C.C.	C.C.	C.C.	0	$J\cos\phi\sin\phi/\sqrt{2}$ $-iJ\sin\phi/\sqrt{2}$
$\|\text{-}1\text{-}1\rangle$	C.C.	C.C.	C.C.	C.C.	C.C.	C.C.	C.C.	C.C.	$J\cos^2\phi$

C.C. ≡ Complex conjugate.

$$C_{11} = -\cos^2\phi\sin^2\alpha\cos\beta\sin\beta - \cos\phi\sin\phi\cos\alpha\sin\alpha\cos\beta + \cos\phi\sin\phi\cos\alpha\sin\alpha\sin\beta + \sin^2\phi\cos^2\alpha$$

$$C_{12} = \cos\phi\sin^2\alpha\cos^2\beta - \sin\phi\cos\alpha\sin\alpha\cos\beta$$

$$C_{13} = -\cos\phi\sin\phi\sin^2\alpha\cos\beta\sin\beta + \cos^2\phi\cos\alpha\sin\alpha\cos\beta + \sin^2\phi\cos\alpha\sin\alpha\sin\beta - \cos\phi\sin\phi\cos^2\alpha$$

$$C_{21} = -\cos\phi\sin^2\alpha\sin^2\beta - \sin\phi\cos\alpha\sin\alpha\sin\beta$$

$$C_{22} = \sin^2\alpha\cos\beta\sin\beta$$

$$C_{23} = -\sin\phi\sin^2\alpha\sin^2\beta + \cos\phi\cos\alpha\sin\alpha\sin\beta$$

$$C_{31} = -\cos\phi\sin\phi\sin^2\alpha\cos\beta\sin\beta - \sin^2\phi\cos\alpha\sin\alpha\cos\beta - \cos^2\phi\cos\alpha\sin\alpha\sin\beta - \cos\phi\sin\phi\cos^2\alpha$$

$$C_{32} = \sin\phi\sin^2\alpha\cos^2\beta + \cos\phi\cos\alpha\sin\alpha\cos\beta$$

$$C_{33} = -\sin^2\phi\sin^2\alpha\cos\beta\sin\beta + \cos^2\phi\cos^2\alpha + \cos\phi\sin\phi\cos\alpha\sin\alpha\cos\beta - \cos\phi\sin\phi\cos\alpha\sin\alpha\sin\beta$$

In the product representation Eq. (A3-19) becomes as shown in Table XXVII.

A computer program was written to determine the transition fields which utilized direct diagonalization of the energy matrix made up of Tables XXV to XXVII. The $g_{\parallel}$, $g_{\perp}$, and D were taken from the single ion data (Jondo and Myers, 1972), and $\vec{r}$ was gotten from the $ZnSeO_4 \cdot 6H_2O$ crystallographic data (Hajek and Cepelak, 1965). The exchange value J was left as the only adjustable parameter. With the Hamiltonian specified, the next section will discuss the assignment of the observed lines along the principal crystal axis in terms of it.

Table XXVII. Equation (A3-19) in the product representation.

	$\|11\rangle$	$\|10\rangle$	$\|01\rangle$	$\|1\text{-}1\rangle$	$\|00\rangle$	$\|\text{-}11\rangle$	$\|\text{-}10\rangle$	$\|0\text{-}1\rangle$	$\|\text{-}1\text{-}1\rangle$
$\|11\rangle$	C_{33}	$C_{31}/\sqrt{2}$ $-iC_{32}/\sqrt{2}$	$C_{13}/\sqrt{2}$ $-iC_{23}/\sqrt{2}$	0	$(C_{11}-C_{22})/2$ $-i(C_{12}+C_{21})/2$	0	0	0	0
$\|10\rangle$	C.C.	0	$(C_{11}+C_{22})/2$ $+i(C_{12}-C_{21})/2$	$C_{31}/\sqrt{2}$ $-iC_{32}/\sqrt{2}$	0	0	0	$(C_{11}+C_{22})/2$ $-i(C_{12}+C_{21})/2$	0
$\|01\rangle$	C.C.	C.C.	0	0	0	$C_{13}/\sqrt{2}$ $-iC_{23}/\sqrt{2}$	$(C_{11}-C_{22})/2$ $-i(C_{12}+C_{21})/2$	0	0
$\|1\text{-}1\rangle$	C.C.	C.C.	C.C.	$-C_{33}$	$(C_{11}+C_{22})/2$ $+i(C_{12}-C_{21})/2$	0	0	$-C_{13}/\sqrt{2}$ $+iC_{23}/\sqrt{2}$	0
$\|00\rangle$	C.C.	C.C.	C.C.	C.C.	0	$(C_{11}+C_{22})/2$ $+i(C_{12}-C_{21})/2$	0	0	$(C_{11}-C_{22})/2$ $-i(C_{12}+C_{21})/2$
$\|\text{-}11\rangle$	C.C.	C.C.	C.C.	C.C.	C.C.	$-C_{33}$	$-C_{31}/\sqrt{2}$ $+iC_{32}/\sqrt{2}$	0	0
$\|\text{-}10\rangle$	C.C.	C.C.	C.C.	C.C.	C.C.	C.C.	0	$(C_{11}+C_{22})/2$ $-i(C_{12}-C_{21})/2$	$C_{31}/\sqrt{2}$ $+iC_{32}/\sqrt{2}$
$\|0\text{-}1\rangle$	C.C.	C.C.	C.C.	C.C.	C.C.	C.C.	C.C.	0	$-C_{13}/\sqrt{2}$ $+iC_{23}/\sqrt{2}$
$\|\text{-}1\text{-}1\rangle$	C.C.	C.C.	C.C.	C.C.	C.C.	C.C.	C.C.	C.C.	C_{33}

C.C. = Complex Conjugate

C_{ij}'s as previously defined

Experimental Results and Discussion

Under the expected conditions that $D > g\beta H$ and J, the energy level scheme of the Ni^{2+}-Ni^{2+} pairs will consist of a singlet and two quartets. For a positive D, as is observed for the single ion, the singlet will lie lowest. In zero-field the wavefunctions to a first approximation are

$$\text{singlet} \qquad |00\rangle$$

$$\text{quartet(1)} \begin{cases} \frac{1}{\sqrt{2}}\left[|01\rangle + |10\rangle\right] \\ \frac{1}{\sqrt{2}}\left[|01\rangle - |10\rangle\right] \\ \frac{1}{\sqrt{2}}\left[|0\text{-}1\rangle + |\text{-}10\rangle\right] \\ \frac{1}{\sqrt{2}}\left[|0\text{-}1\rangle - |\text{-}10\rangle\right] \end{cases}$$

$$\text{quartet(2)} \begin{cases} |11\rangle \\ |\text{-}1\text{-}1\rangle \\ \frac{1}{\sqrt{2}}\left[|\text{-}11\rangle + |1\text{-}1\rangle\right] \\ \frac{1}{\sqrt{2}}\left[|\text{-}11\rangle - |1\text{-}1\rangle\right] \end{cases}$$

If these were the true wavefunctions, no transitions would be allowed because conventional microwave frequencies are not large enough to cross the zero-field splitting. The mixing of the functions by the Zeeman and exchange interactions makes transitions within the quartets allowable. Transitions between the levels of quartet(2) can be distinguished from those between levels of quartet(1) by observing the

relative intensity variation as function of temperature. At liquid nitrogen temperatures (77°K) the pair spectra are easily observable, and all levels are virtually equally populated. On lowering the temperature to liquid helium (4.2°K), the size of D is sufficiently large to begin an appreciable decrease in the population of the quartet(2) relative to quartet(1). At 1.3°K transitions within quartet(2) are no longer observable and transitions within quartet(1) become very weak since even quartet(1) is significantly depopulated at this temperature.

Ni^{2+}-Ni^{2+} Pair Spectra Along the c Axis. Under any circumstances when the magnetic field is along the crystal c axis, only one type of 1-2 pair exists. Figure 21 shows a spectra with orientation at 4.2°K. At 77°K the lines labeled (5,6) and (8,9) are much more intense than those labeled 1, (2,3), and 4. This intensity variation indicates that the 1, (2,3), and 4 lines are transitions between the levels of quartet(1). Figure 22 shows a plot of energy vs magnetic field calculated from the Hamiltonian given in the last section with a ferromagnetic exchange $-2J = -0.14\ cm^{-1}$. For a typical microwave frequency of 9.6520 GHz, the energy vs field plot indicates that within quartet(1) three lines are likely to occur if 2 and 3 are suitably overlapped. Therefore, lines 1, (2,3), and 4 are assigned to the transitions in Fig. 22 with the same number. Other spectra gave a splitting of the (2,3) line indicating that it is composed of two lines and thus reinforce the assignment. The assignment of the two lines (5,6) and (8,9) is not as clear since there are more possible transitions within quartet(2) than are observed. Levels H and G are so close together that transitions from them to the I and F levels

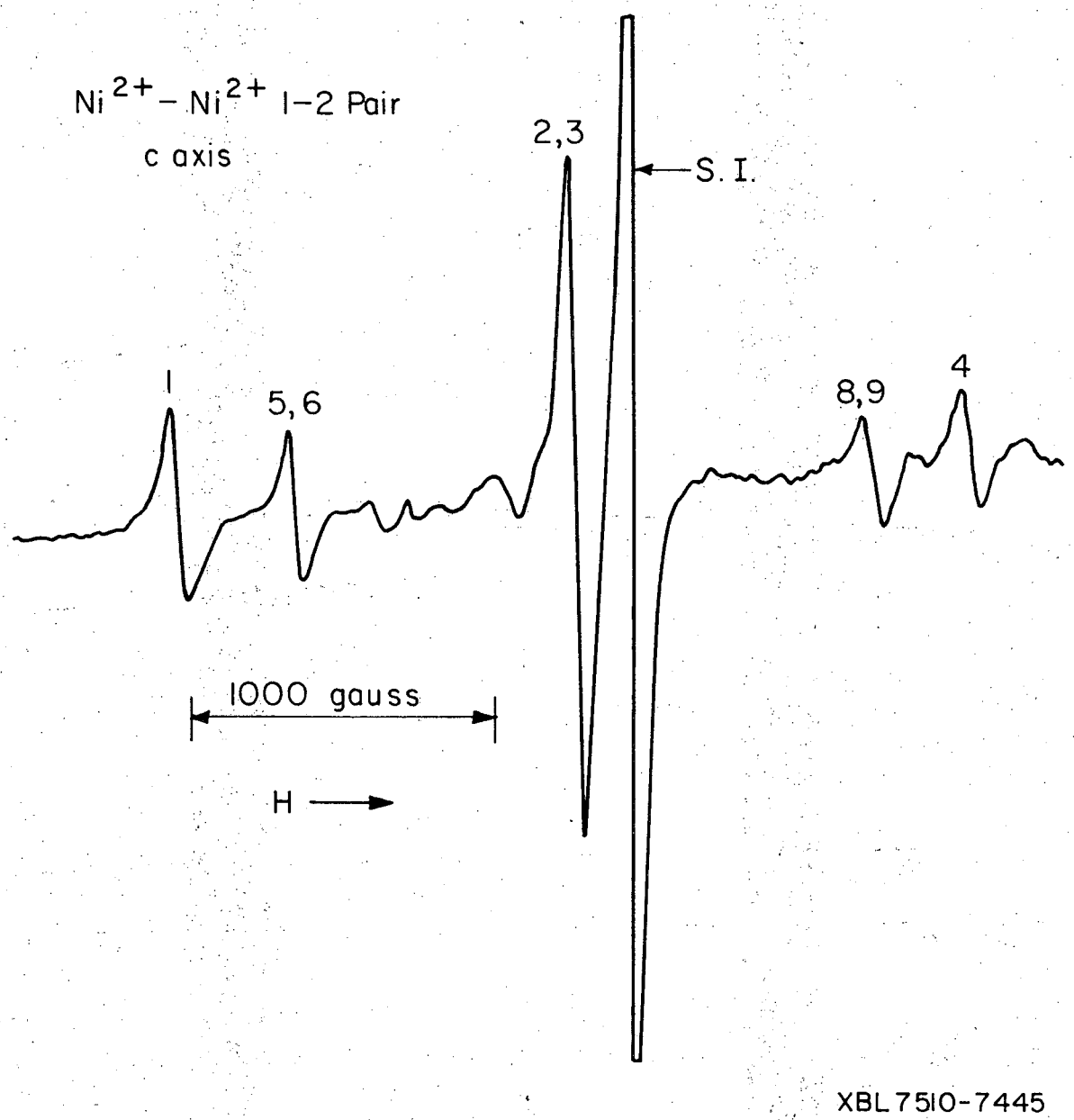

Fig. 21. A spectra of ~5% Ni^{2+} substituted into $ZnSeO_4 \cdot 6H_2O$ at 4.2°K and 9.6520 GHz. The magnetic field is oriented along the c axis. The line labeled S.I. indicates the single ion line, and the numbered lines are due to pairs. The single ion line is at 1909 gauss.

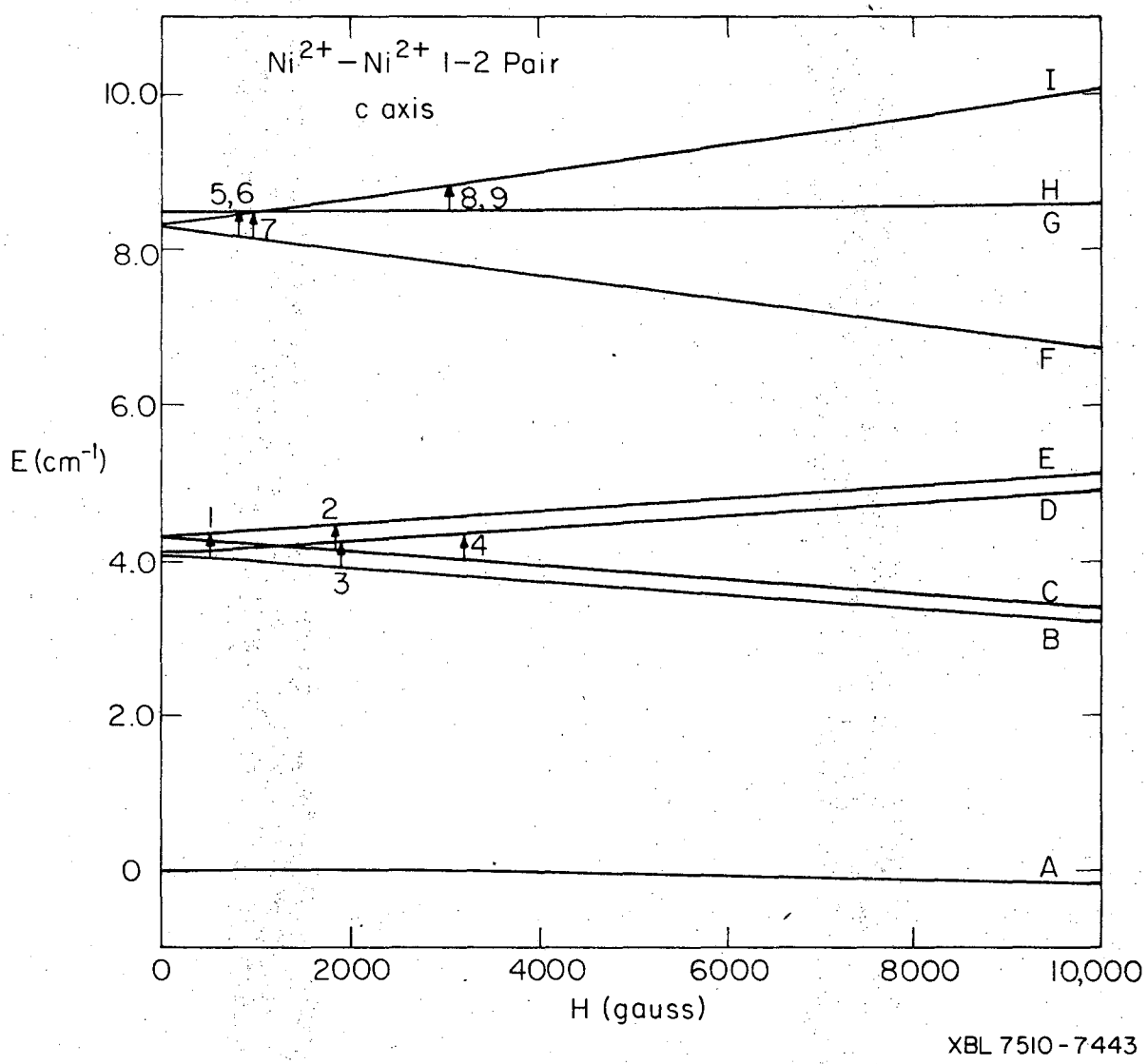

Fig. 22. A calculated plot of the Ni^{2+}-Ni^{2+} pair energy levels vs magnetic field with the field along the c axis and a value of $-2J = -0.14\ cm^{-1}$. The arrows are drawn for transitions which would take place for $\nu = 9.6520$ GHz.

will be overlapped. The high field line can then be assigned to the (8,9) transition. The low field line (5,6) could arise from either transition 7 or (5,6). To match the (8,9) transition, the (5,6) line is assigned to the (5,6) transition, and transition 7 is assumed to be too weak to be observed. Table XXVIII gives the line positions with the magnetic field along the c axis.

Calculations of the line positions using the Hamiltonian from Tables XXV to XXVII have very unsatisfactory results. Taking the exchange interaction to be ferromagnetic as determined by thermodynamic work (Fisher and Hornung, 1968), a tabulation of the line positions as function of J can be made and is given in Table XXIX. The observed field positions at ν = 9.6520 GHz from Table XXVIII should be compared with the calculated values of Table XXIX. Fitting transition 1 which measures the splitting within quartet(1) most directly yields a value of $-2J = -0.142\ cm^{-1}$, but fitting transition 4 yields $-2J = -0.120\ cm^{-1}$. The 2 and 3 transitions cannot be fitted in this range which is disturbing. Thus, the calculations are not very definitive. They yield a rough determination of the exchange of $-2J = -0.13 \pm 0.02\ cm^{-1}$. The poor agreement between the calculated and observed values, if the calculation is correct, implies that a modification of the exchange Hamiltonian used is necessary. Perhaps anisotropy in the exchange interaction is required, or since Ni^{2+} has a spin 1, the biquadratic exchange, $J'(\vec{S}_1 \cdot \vec{S}_2)^2$, may be necessary. Also, the assumption of a fixed spin may not be good enough.

Table XXVIII. Ni^{2+}-Ni^{2+} pair line positions with the magnetic field along the c axis at 4.2°K.

Transition	Line Position (gauss) ν = 9.6520 GHz	Line Position (gauss) ν = 8.6166 GHz
1	464±6	--
(5,6)	844	614±20
(2,3)	1740	1483 & 1536
(8,9)	2678	2740
4	2984	2800

Table XXIX. Calculated Ni^{2+}-Ni^{2+} 1-2 pair line positions as a function of J (ν = 9.6520 GHz).

$-2J(cm^{-1})$	4*	8	9	2	3	6	7	5	1
-0.10	2805	2685	2675	1889	1855	1173	1163	962	927
-0.12	2982	2851	2838	1882	1841	1017	1003	963	718
-0.14	3156	3019	3001	1874	1826	860	841	966	497
-0.16	3328	3188	4164	1866	1811	703	678	967	226
-0.18	3498	3358	3328	1856	1793	546	513	969	---

*Numbers refer to transitions as in Fig. 22.

Ni^{2+}-Ni^{2+} Pair Spectra Along the a Axis. Figure 23 shows the spectra obtained with the magnetic field pointing along the crystal a axis, and Fig. 24 shows the accompanying energy vs field plot calculated with $-2J = -0.14\ cm^{-1}$. As may be seen, a similar line pattern to that found along the c axis is expected even though the energy levels behave differently. Changing the temperature from 77°K to 4.2°K shows that the lines 1, (2,3), and 4 of Fig. 23 increase in intensity relative to the other marked lines (6,7), 8 and 9. The assignment of the 1, (2,3), and 4 lines is, therefore, given to the transitions within quartet(1). Lines 8 and 9 are assigned to the transitions 8 and 9 and are split due to their appearance at higher field where levels H and G become sufficiently split. The (6,7) line is assigned to the two transitions 6 and 7 which are assumed to be overlapped. On rotating the field away from the a axis, the lines (6,7), 1, 8, 4 and 9 all split into two lines. How this fits into the assignment is not known. The origin of the lines at the lowest field positions is also not known. Table XXX gives the line positions at two frequencies.

Ni^{2+}-Ni^{2+} Pair Spectra Along the γ Axis. The spectra observed with the magnetic field along the γ axis is substantially different from the other axes and is shown in Fig. 25 for 4.2°K. This figure does not show the entire spectra. A single ion line appears beyond the 11,000 gauss capability of the magnetic, and 1-1/2 pair lines appear between 10,000 and 11,000 gauss. Figure 26 gives the corresponding energy vs magnetic field plot, again with $-2J = -0.14\ cm^{-1}$. Temperature variation from 77°K to 4.2°K indicates that the relative intensities of lines 6, 7, 8 and 9 decreases with respect to lines 1, 2 or 3, and

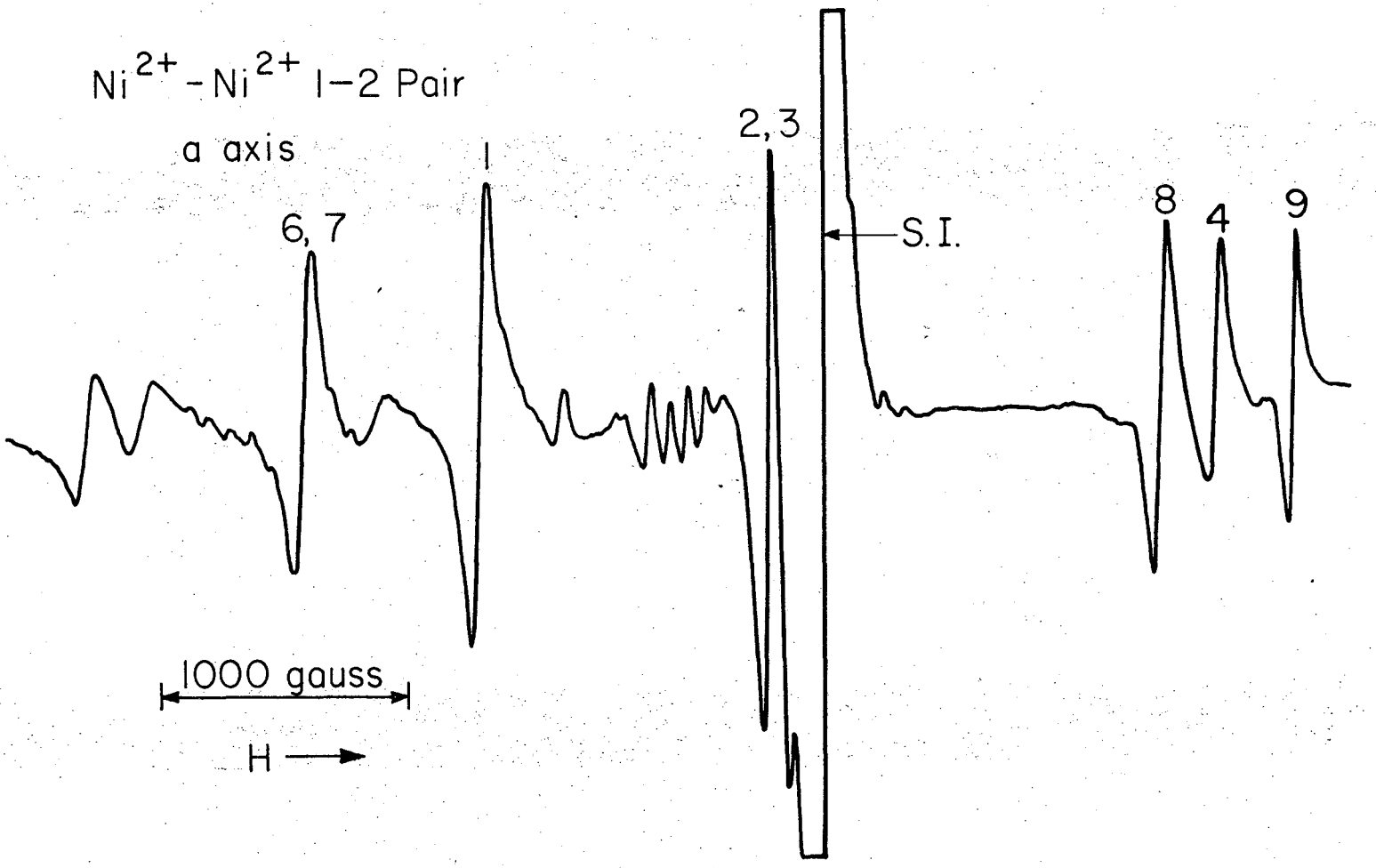

Fig. 23. A spectra of ~5% Ni^{2+} substituted into $ZnSeO_4 \cdot 6H_2O$ at 4.2°K and 9.3313 GHz. The magnetic field is oriented along the a axis. S.I. indicates the single ion line, and the numbered lines are due to pairs. The single ion line is at 3662 gauss. The weak set of lines between lines 1 and 2,3 are due to Cu^{2+} impurities.

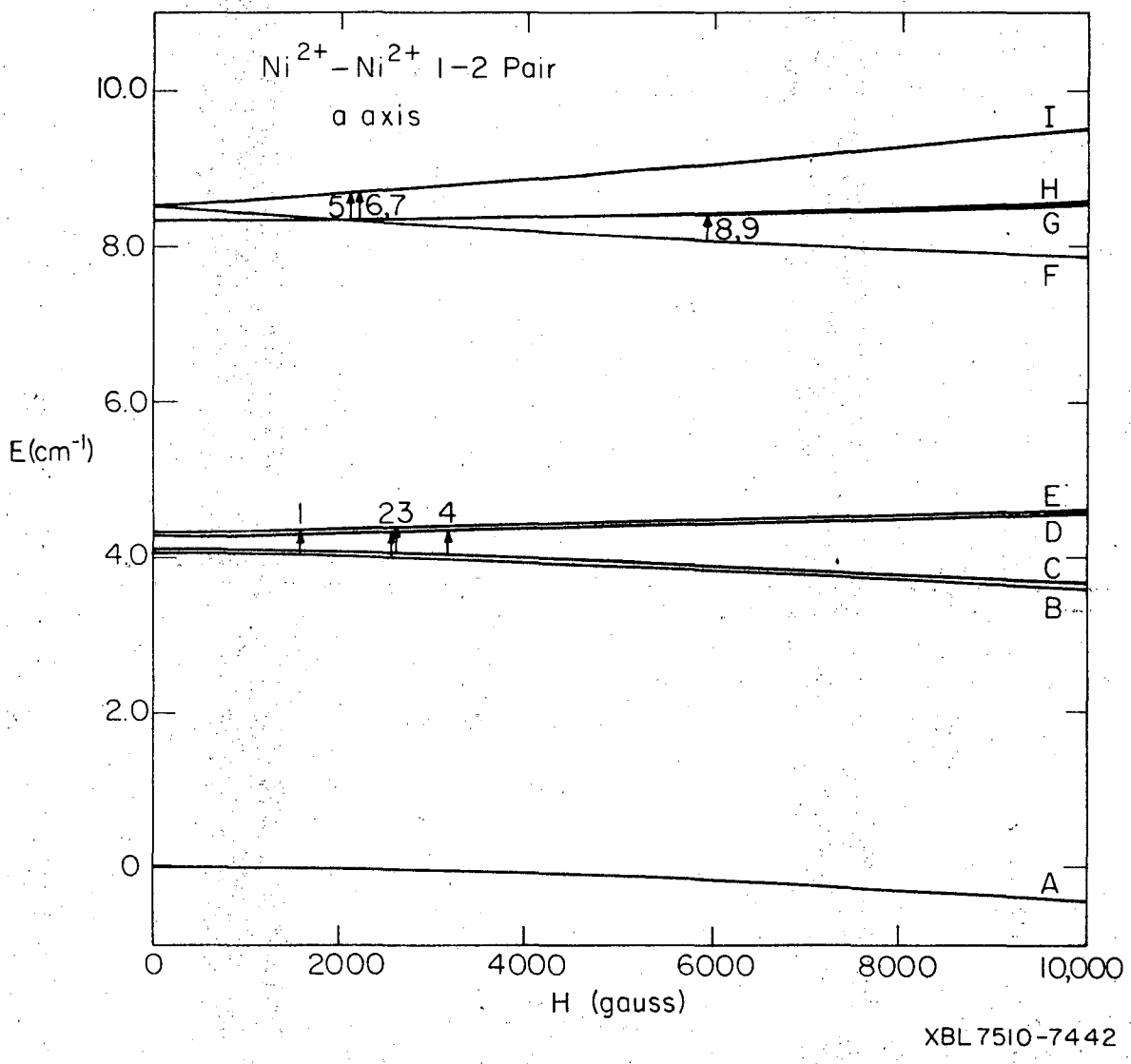

Fig. 24. A calculated plot of the Ni^{2+}-Ni^{2+} pair energy levels vs magnetic field with the field along the a axis and a value of $-2J = -0.14\ cm^{-1}$. The arrows are drawn for transitions which would take place for $\nu = 9.3313$ GHz.

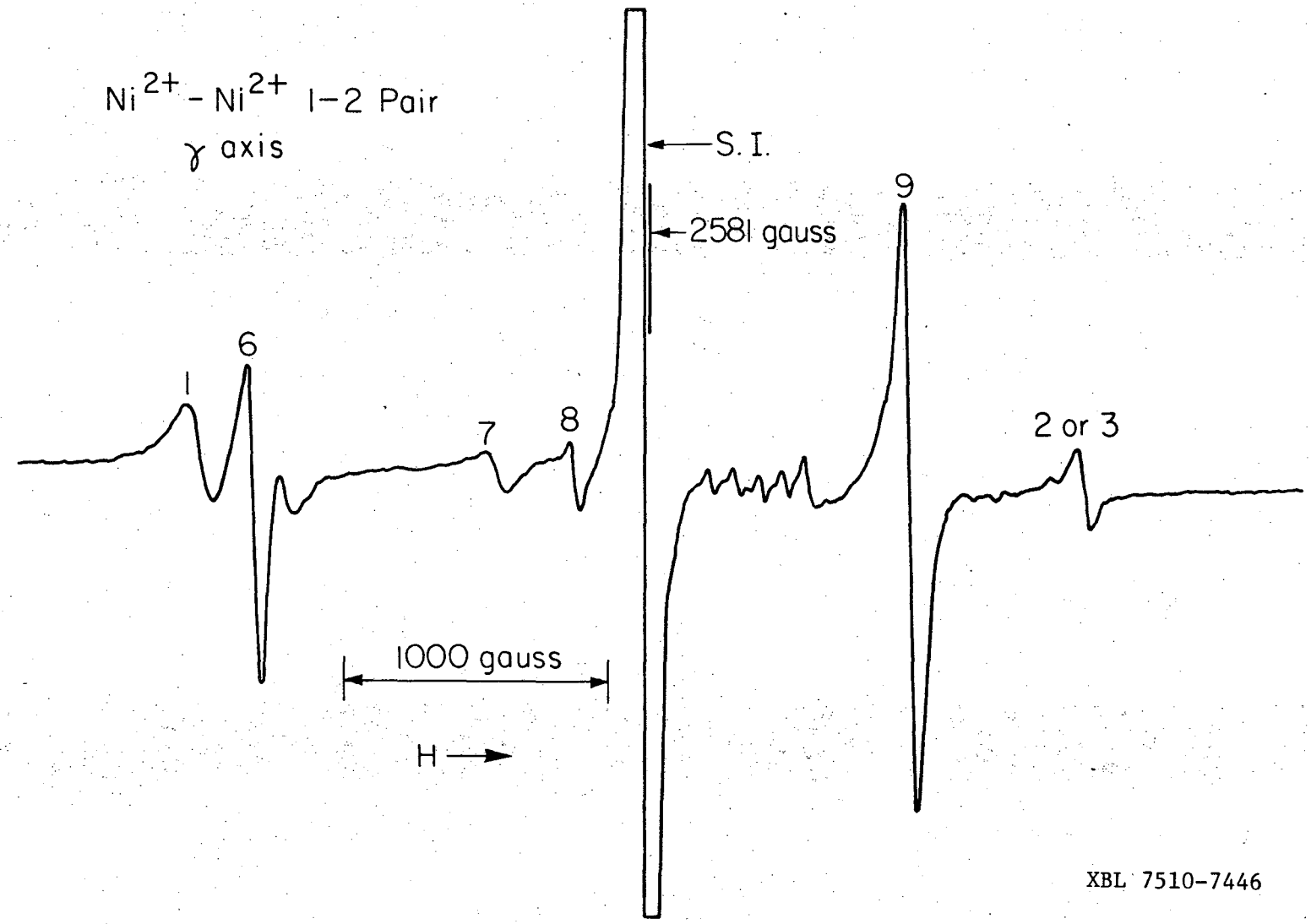

Fig. 25. A spectra of ~5% Ni^{2+} substituted into $ZnSeO_4 \cdot 6H_2O$ at 77°K and 9.2666 GHz. The magnetic field is oriented along the axis. The mark at 2581 is an NMR field marker. S.I. indicates the single ion line, and the numbered lines are due to pairs. The set of weak lines between the S.I. line and line 9 are due to Cu^{2+} impurities.

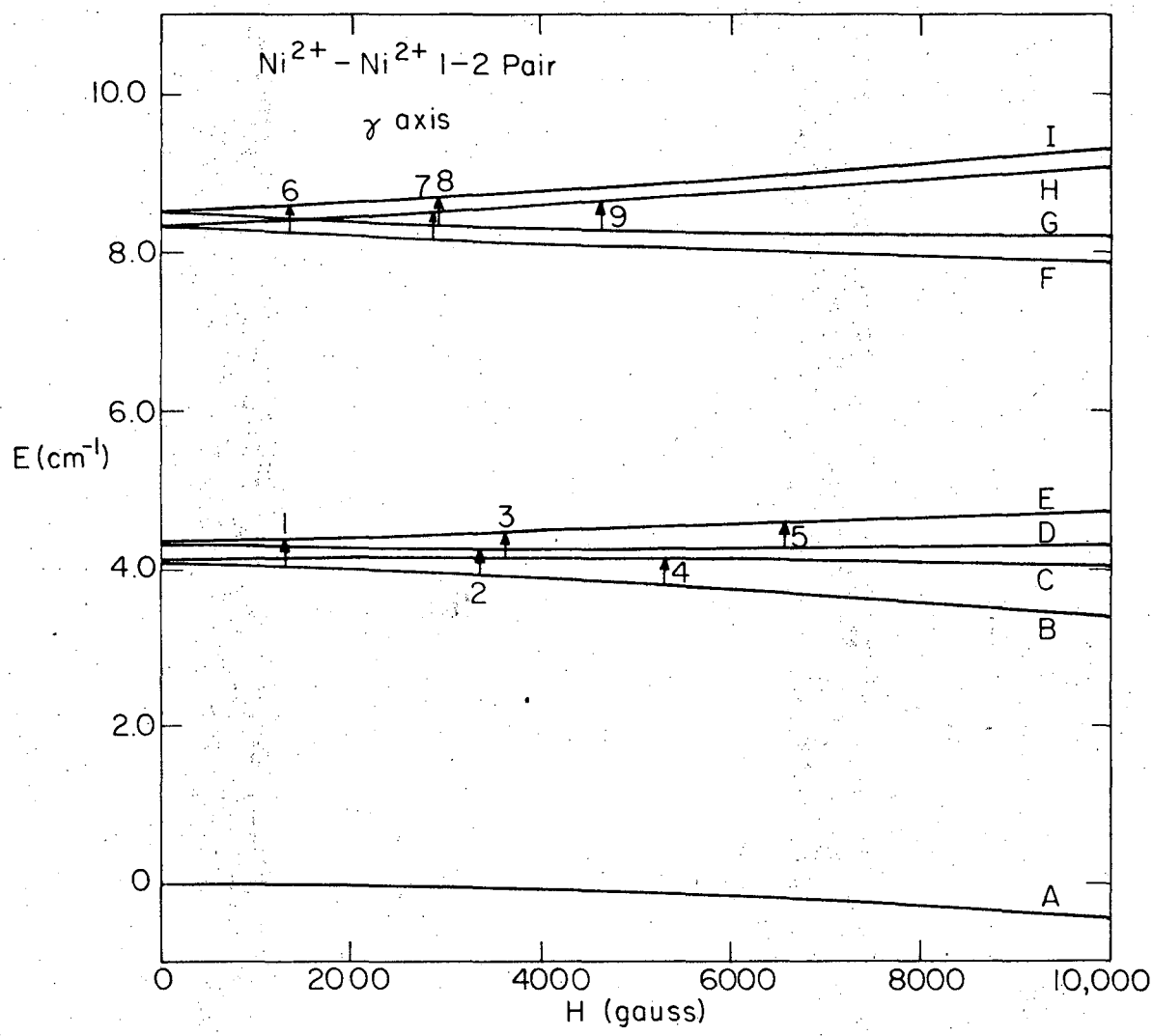

XBL 7510-7444

Fig. 26. A calculated plot of the Ni^{2+}-Ni^{2+} pair energy levels vs magnetic field with the field along the γ axis and a value of $-2J = -0.14\ cm^{-1}$. The arrows are drawn for transitions which would take place for $\nu = 9.2666$ GHz.

Table XXX. Ni^{2+}-Ni^{2+} pair line positions with the magnetic field along the a axis.

Transition	Line Position (gauss) ν = 9.2642 GHz and 77°K	Line Position (gauss) ν = 9.3311 GHz and 4.2°K
(6,7)	6101±6	1584±6
1	2327	2286
(2,3)	---	3423
8	4914	4963
4	5112	5182
9	5413	5485

those lines at high field. In this case, the four lines in quartet(2) are most easily assigned and are taken to be transitions 6, 7, 8 and 9 as shown in Fig. 26. The assignment of the transitions between levels in quartet(1) is less certain. Presumably the lowest field line which increases its intensity at the lower temperature is due to transition 1. The 1-1/2 lines seen at high field, >10,000 gauss, could possibly be those labeled 4 and 5. The line above line 9 could possibly be due to transition 2 or 3. It might be supposed that this line is transition 3 and that transition 2 is overlapped and hidden by the other lines at lower field than the line (2 or 3). In Table XXXI are given the transition fields of the observed lines.

To conclude, the problem of the Ni^{2+}-Ni^{2+} pairs in $ZnSeO_4 \cdot 6H_2O$ is far from a satisfactory solution, and further work is required to sort out the details.

Table XXXI. Ni^{2+}-Ni^{2+} pair line positions with the magnetic field along the γ axis.

Transition	Line Position (gauss) ν = 9.2645 GHz and 77°K	Line Position (gauss) ν = 9.3311 GHz and 4.2°K
1	897±6	816±6
6	1098	1079
7	2004	---
8	2294	---
9	3532	3575
3	4164	4227
4	10331	10228

REFERENCES

A. Abragam, The Principles of Nuclear Magnetism (Clarendon Press, Oxford, 1961).

A. Abragam and M. L. H. Pryce, Proc. Roy. Soc. A205, 135 (1951).

S. A. Al'tshuler, S. A. and R. M. Valishev, Soviet Physics JETP 25, 309 (1965).

P. W. Anderson and P. R. Weiss, Rev. Mod. Phys. 25, 269 (1953).

P. W. Anderson in Solid State Physics, F. Seitz and D. Turnbull, Eds., (Academic Press, New York, NY, 1963) Vol. 14, pp. 99-214.

W. T. Batchelder, The Electron Paramagnetic Resonance Spectra of α-$NiSo_4 \cdot 6H_2O$ at Liquid Helium (Ph. D. Thesis), UCRL-19157, May 1970.

C. A. Beevers and H. Lipson, Z. Kristallogr. 83, 123 (1932).

E. R. Bernstein and G. M. Dobbs, Phys. Rev. B 11, 4623 (1975).

R. J. Birgeneau, E. Bucher, L. W. Rupp, Jr, and W. M. Walsch, Jr. Phys. Rev. B. 148, 444 (1972).

B. Bleaney, R. J. Elliot and H. E. D. Scovil, Proc. Phys. Soc. (London) A64, 933 (1951).

B. Bleaney and D. J. E. Ingram, Proc. Phys. Soc. (London) A65, 953 (1952).

N. Bloembergen, E. M. Purcell, and R. V. Pound, Phys. Rev. 73, 679 (1948).

G. Brauer, ed., Handbook of Preparative Inorganic Chemistry (Academic Press, NY, 1963), Vol. 2 pp. 1047-1087.

B. V. R. Chowdari, J. Phys. Chem. Sol. 30, 2747 (1969).

J. W. Culvahouse and D. P. Schinke, Phys. Rev. 187, 671 (1969).

J. W. Culvahouse, D. P. Schinke, and L. G. Pfortmiller, Phys. Rev. 177, 454 (1969).

D. Davidov and K. Baberschke, Phys. Lett. 51A, 144 (1975).

D. Davidov, C. Rettori, and V. Zevin, Sol. Stat. Comm. 16, 247 (1975).

R. T. Dixon and J. W. Culvahouse, Phys. Rev. B. 3, 2279 (1971).

R. A. Fisher and E. W. Hornung, J. Chem. Phys. 48, 4284 (1968).

R. E. Gerkin and D. L. Thorsell, J. Chem. Phys. 57, 2665 (1972).

J. C. Gill and P. A. Ivey, J. Phys. Chem. 7, 1536 (1974).

Gmelins Handbuch der Anorganischen Chemie Verlag Chemie, GMDH, Weinhein, Bergstrasse, System No. 32, p. 946 (1956).

Gmelins, Teil B-Lieferung 2, pp. 685-689 (1966).

J. B. Goodenough, Magnetism and the Chemical Bond (Interscience, NY, 1963).

J. H. E. Griffiths and J. Owen, Proc. Roy. Soc. (London) A213, 459 (1952).

B. Hajek and V. Cepelak, Z. Chem. 5, 234 (1965).

M. T. Hutchings, C. G. Windsor and W. P. Wolf, Phys. Rev. 148, 444 (1966).

D. H. Howling, J. Mag. Res. 1, 339 (1969)

R. Janakiraman and G. C. Upreti, Chem. Phys. Lett. 4, 550 (1970).

R. Janakiraman and G. C. Upreti, J. Chem. Phys. 54, 2336 (1971a).

R. Janakiraman and G. C. Upreti, Phys. Stat. Sol. (b) 47, 679 (1971b).

A. Jindo, Single Crystal Studies of Hydrated Transition Metal Ions by Electron Paramagnetic Resonance (Ph. D. Thesis), UCRL-20386, Jan. 1971.

A. Jindo and R. J. Myers, J. Mag. Res. 6, 633 (1972).

J. Kanamori, J. Phys. Chem. Sol. 10, 87 (1959).

C. Kittel, Introduction to Solid State Physics (John Wiley & Sons, Inc., NY, 1971), 4th ed., pp. 596-599.

A. Klein, Annales de Chemie 14, 263 (1940).

G. F. Kokoszka and G. Gordon, Transition Metal Chemistry 5, 181 (1969).

R. Kubo and K. Tomita, J. Phys. Soc. Japan 9, 888 (1954).

Landolt-Bornstein, Magnetic Properties of Coordination and Organo-Metallic Transition Metal Compounds (Springer-Verlag, Berlin, 1966), Vol. 2, pp. 4-63 to 4-66.

B. R. McGarvey in Transition Metal Chemistry, Richard L. Carlin, ed. (Marcel Dekker, Inc., NY, 1966), Vol. 3.

F. Mehran, K. W. H. Stevens, R. S. Title, and F. Holtzberg, Phys. Lett. 27, 1368 (1971).

D. J. Meredith and J. C. Gill, Phys. Lett. 25A, 429 (1967).

T. Mitsuma, J. Phys. Soc. Japan 17, 128 (1962).

T. Moriya and Y. Obata, J. Phys. Soc. Japan 13, 1333 (1958).

T. Moriya in Magnetism, G. T. Rado and H. Suhl, ed. (Academic Press, NY, 1963), Chapter 3.

R. J. Myers, Pure and Appl. Chem. 4, 263 (1973).

A. Novak, Structure and Bonding 18, 177 (1974).

B. H. O'Conner and D. H. Dale, Acta Cryst. 21, 705 (1966).

D. W. Pratt, Magnetic Resonance Spectra of VCl_4 and Other Paramagnetic Species (Ph. D. Thesis), UCRL-17406, April 1967.

M. Pryce, Proc. Roy. Soc. (London) A283, 443 (1965).

L. Rimai and R. W. Bierig, Phys. Rev. Lett. 12, 284 (1964).

C. Rettori, D. Davidov, A. Grayevsky and W. M. Walsh, Phys. Rev. B. 11, 4450 (1975).

R. S. Rubins, J. Chem. Phys. 60, 4189 (1974).

B. A. Sastry and G. S. Sastry, J. Chem. Phys. 59, 6419 (1973).

M. W. Scoggins, Anal. Chem. 42, 301 (1970).

G. B. Singh, G. C. Upreti and Putcha Verkateswarlu, J. Chem. Phys. 46, 2885 (1967).

G. B. Singh and Putcha Verkateswarlu, J. Chem. Phys. 46, 4765 (1967).

J. S. Smart, Effective Field Theories of Magnetism, (Saunders, Philadelphia, 1966).

T. D. Smith and J. R. Pilbrow, Coord. Chem. Rev. 13, 173 (1974).

K. Sugawara, C. Y. Huang and B. R. Cooper, Phys. Rev. B. 11, 4455 (1975).

I. Svare and G. Seidel, Phys. Rev. 134, A172 (1964).

T. J. Swift and R. E. Connick, J. Chem. Phys. 37, 307 (1962).

G. C. Upreti, Chem. Phys. Lett. 18, 120 (1973).

G. C. Upreti, J. Mag. Res. 14, 274 (1974).

H. Van Dijk, M. Durieux, J. R. Clement and J. K. Lógan, Physica 24, S129 (1958).

J. H. Van Vleck, Phys. Rev. 74, 1168 (1948).

R. M. White, Quantum Theory of Magnetism (McGraw Hill, NY, 1970).

R. W. G. Wyckoff, ed., Crystal Structures (Interscience Publishers, NY, 1965), Vol. 3, p. 824.

G. Zverev and N. Petelina, Soviet Phys. JETP 15, 820 (1962).

TECHNICAL INFORMATION DIVISION
LAWRENCE BERKELEY LABORATORY
UNIVERSITY OF CALIFORNIA
BERKELEY, CALIFORNIA 94720